INVESTIGATION OF A REVERSE ENGINEERING METHOD FOR DETERMINATION OF MATERIAL PROPERTIES OF DAMAGED OR COLLAPSED REINFORCED CONCRETE BUILDING

Halmat Ahmed AWLA

MSc Thesis
Department of Civil Engineering
Program: Structural Engineering
Supervisor: Associate Prof. Dr. Muhammet KARATON

September-2019

T.C.

FIRAT ÜNİVERSİTESİ

FEN BİLİMLERİ ENSTİTÜSÜ

INVESTIGATION OF A REVERSE ENGINEERING METHOT FOR DETERMINATION OF MATRERIAL PROPERTIES OF DAMAGED OR COLLAPSED OR REINFORCED CONCRETE BUILDING

Yüksek Lisans Tezi

Halmat Ahmed AWLA

171115108

Tezin Enstitüye Verildiği Tarih : 08.10.2019

Tezin Savunulduğu Tarih: 11.11.2019

Anabilim Dalı: İnşaat Mühendisliği

Programı: Mekanik

Danışman: Doç.Dr.Muhammet KARATON

Doç.Dr.Erkut SAYIN

Doç.Dr.Burak YÖN

KASIM-2019

ACKNOWLEDGEMENT

First and foremost praises and thanks to Allah, the Almighty, the greatest of all, on whom ultimately we depend for sustenance and guidance.

I would like to express my sincere gratitude to my supervisor Associate Prof. Dr. Muhammet Karaton for his continuous academic guidance and endless help. His guidance helped me in all the time of research and writing of this thesis. I couldn't have imagined having a better advisor for my research work. It was a great honor and privilege to study and work under his guidance.

I would also like to express my deepest gratitude to my dear parents and to my whole family for their continuous support and encouragement.

I would like to exhibit my special thanks to my beloved wife, this thesis would not have been possible without her support and patience.

Lastly, I wish to thank all my colleagues in Firat University with whom I shared a wonderful time.

Halmat Ahmed AWLA

September-2019

TABLE OF CONTENTS

SUMMARY

Investigation of a Reverse Engineering Method for Determination of Material Properties of Damaged or Collapsed Reinforced Concrete Building

In this thesis, a reverse engineering technique is investigated to predict the real properties of materials of collapsed or damaged reinforced concrete structures caused by severe earthquakes. For this purpose, two full scale laboratory tested structures were used for verifying of the technique. First structure is a two dimension three bay and four story reinforced concrete bare frame that tested in European Laboratory for Structural Assessment. Other structure is also reinforced concrete tall bridge pier that tested in Pacific Earthquake Engineering Research Center. The numerical solutions are obtained by using Fiber Element Approaches based on displacement and force. The material properties for the reinforced concrete elements are defined according to American Concrete Institute code (ACI-318) and Turkish Standard 500 (TS500). The comparisons are evaluated in terms of story displacement and damaged regions obtained from experimental and numerical results. The material classes of the structures are determined by numerical solution the best compatible with experimental response.

Keywords: Reverse engineering method, Reinforced concrete structures, Material classes, Fiber element approaches based on displacement and force.

ÖZET

Hasar Görmüş Veya Yıkılmış Betonarme Binaların Malzeme Özelliklerinin Belirlenmesi İçin Bir Tersine Mühendislik Metodunun İncelenmesi

Bu tezde, şiddetli depremlerden dolayı yıkılmış veya hasar görmüş betonarme yapıların gerçek malzeme özelliklerinin tahmini için tersine bir mühendislik tekniği incelenmiştir. Bu amaçla, tekniğin doğrulamasının yapılması için laboratuvarda testleri yapılmış iki tam ölçekli yapı kullanılmıştır. İlk yapı Avrupa Yapısal Değerlendirme Laboratuvarında test edilmiş olup iki boyutlu üç açıklıklı ve dört katlı sadece betonarme çerçevelerden oluşmaktadır. Diğer yapı ise Pasifik Deprem Araştırma Merkezinde test edilmiş olup betonarme uzun bir köprü ayağıdır. Nümerik sonuçlar yer değiştirmeye ve kuvvete dayalı Fiber eleman yaklaşımları kullanılarak elde edilmiştir. Betonarme elemanların malzeme özellikleri Amerikan Beton Enstitüsü 318 ve Türk Standartları 500 standartlarına göre belirlenmiştir. Karşılaştırmalar, deney ve nümerik sonuçlardan elde edilen kat yer değiştirmeleri ve hasar bölgeleri açısından değerlendirilmiştir. Yapıların malzeme sınıfları deney sonuçlarıyla en uyumlu olan numerik sonuçlar yardımıyla belirlenmiştir.

Anahtar Kelimeler: Tersine mühendislik metodu, Betonarme yapılar, Malzeme sınıfları, Yer değiştirme ve kuvvete dayalı Fiber eleman yaklaşımları

LIST OF FIGURES

LIST OF TABLES

LIST OF SYMBOLS

$a_d(x)$	Linear interpolation function matrix
$\{a\}$	Relative acceleration vector
α_c	Mass matrix coefficient for Rayleigh damping
$b(x)$	Force interpolation function matrix
β_c	Mass matrix coefficient for Rayleigh damping
$[C]$	Damping matrix
$D(x)$	Section force
$d(x)$	Section deformation
$D_R(x)$	Section resisting force
E_c	Elasticity modulus of concrete
E_s	Elasticity modulus of steel
$\varepsilon(x)$	Axial strain
F	Element flexibility matrix
f_{cc}	Uniaxial compressive strength
f_{ct}	Uniaxial tensile strength
f_y	Yield strength of steel
$f(x)$	Section flexibility
$\{F_g\}$	External load vector due to ground acceleration
$[K]$	Stiffness matrix
$k(x)$	Section stiffness
$\overline{K}$	Element stiffness matrix
L_p	Plastic hinge length
$[M]$	Mass matrix
$M_z(x)$	Bending moment at section x
$N(x)$	Axial force at section x
Q	Element forces
q	Element deformations
$\overline{Q}_R$	Element resisting force
$u(x)$	Axial displacement
$\{u\}$	Relative displacement vector

$\{v\}$	Relative velocity vector
$v(x)$	Transverse displacement
$\chi_z(x)$	Curvature about z-axis

LIST OF ABBREVIATIONS

ACI	American concrete institute
DB	Displacement based
FB	Force based
FEA	Fiber element approach
RC	Reinforced Concrete
RE	Reverse engineering

1.INTRODUCTION

Engineering is widely used in manufacturing, maintaining, constructing and designing of structures, products and systems. Generally engineering can be divided in two main types: Forward engineering (conventional engineering) and Reverse engineering Figure 1.1. Forward engineering is the process or journey starting from an idea then ending with a physical implementation of a system. Reverse engineering (RE) is known as the process of copying of an object, sub assembly of a product without any documentation, technical drawings. The RE method is not only a copy of a product, but it is an analysis in order to deduce some features of the product when sufficient information and enough documentations involved in the original production process are not available [4]. Reverse engineering method is widely used in many engineering disciplines as mechanical designs, entertainment automotive, microchips, electronics, software and chemical engineering [5-9]. For instance, competing manufacturers learn how a new device was built and works, when a new device comes to market, they buy and disassemble one to research on it [8]. The reverse engineering may be employed by chemical companies to win a manufacturing process patent on their competitor's, furthermore catastrophic failure can be decreased and prevented in civil engineering projects, when a specific design copied from previous successes [7, 9].

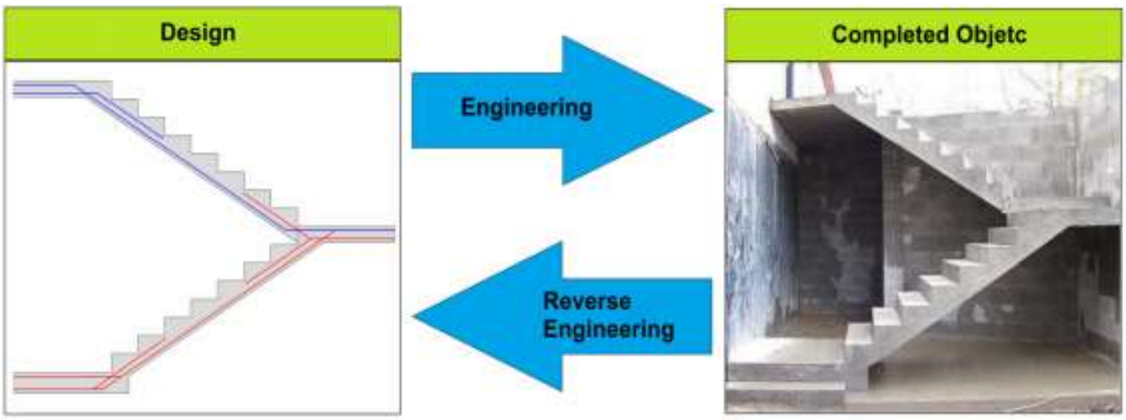

Figure 1.1. Reverse engineering concept

For the first time, term of the reverse engineering was used by Miriam Webster in 1973 [10], RE was defined as the process of disassembling and analyzing a device or a product for understanding the concepts involved in the manufacturing process in order to making improvement in the original product or to produce something similar [10].

Reverse engineering of buildings (from historical castles, churches to villas and modern palaces) as well as weapons, furniture, clothes and vehicles has a long history. Political leaders and professional military are always trying to reverse engineer opponent plans and plots, rhetoric, diplomacy and arming programs of the allies. Engineers can learn by reading publication, attending conference, working on projects, as well as by reverse engineering products. RE and copying from the past is a preferable action as Newton saying “If I have seen further it is by standing on the shoulders of giants”. Publication, patenting and the method almost equally contribute to the progress of science and knowledge [10].

RE sometime called re-engineering, retro-engineering or reverse analysis, the produced object by using RE is detail studied of its construction, function and operation aspects, the process can be of software program, mechanical or electrical device, cultural monument or buildings [11]. The method is an operating procedure to revealing the principals of how devices and systems are working, as opposed to the concept of design engineering [12].

In this study a novel reverse engineering method was proposed for determination of material properties of damaged structures. Two full scale laboratory tested structures were used for performing the process, first; a two dimension three bay four story bare frame that tested in (European Laboratory for Structural Assessment-ELSA) [1], second; a 7.32m tall bridge pier that was tested in (Pacific Earthquake Engineering Research Center-PEER) [2]. The structures were tested up to collapse limit and their responses in terms of story displacements, base shear and damage regions were observed step by step. The above mentioned structures were modelled numerically based on fiber element approach FEA and using both displacement based and force based formulations, they were analyzed under several nonlinear dynamic time history analysis trails, in the numerical cases analysis all material properties treated constant, but elasticity modulus, tensile strength and compressive strength gradually increased according to ACI-318 and TS 500 codes. By using a reverse engineering technique, top displacements and damage region results of the experimental tests and numerical model cases are compared then a calibration study was obtained to determine best numerical case modelling, which its results showed better agreement with the experimental studies.

Older analysis and design procedures based on equivalent elastic methods showed insufficient approximation to describe the behavior of structures during earthquakes, the necessity for using more accurate methods, which explicitly account for geometrical nonlinearity and material inelasticity to evaluate seismic demand on structures became evident [13]. FEA is a widely used method to performing nonlinear analysis, two nonlinear algorithms are currently being used with different level of complexity and computational efforts; nonlinear static analysis and nonlinear dynamic analysis. It is widely recognized that the latter one is the most accurate method to represent the response of a building subjected to a strong earthquake. Nonlinear analysis of reinforced concrete frames by using of solid finite elements is the most accurate and versatile method. However, it becomes too expensive, in the computational sense. In this case, the most economical models are lumped plasticity and distributed plasticity methods, in the first type two zero length nonlinear rotation springs are connected by an elastic beam/column element that the spring computes nonlinearity, the second type discretizes the element section into fibers and the length into integration points. FEA method has two main principle formulations, displacement based (DB) stiffness approach and force based (FB) flexibility approach [14]. In the current work also a comparison study was presented between displacement based and force based modelling approaches, to evaluating their suitability and to determine that which of them responds more realistically to the real life structures under earthquake excitations.

2.NUMERICAL MODELLING OF THE RC STRUCTURAL ELEMENTS

Structures are experience different level of damage under earthquake excitations in their usable life, because they will not respond elastically to moderate and strong earthquakes. For evaluating the response of reinforced concrete (RC) structures to an earthquake, determination of the structural properties is first step. However, soil interaction and earthquake characteristics are complementary steps. Due to the complexity of interaction between various components of the structures, several models for the nonlinear response analysis of RC structures have been proposed to date. According to the degree of freedom and complexity these models are divided in to three categories: Global models, Discrete finite element models and Microscopic finite element models[15].

Global models; the structure which consist of several members and multi degree of freedom is idealized to very few of degree of freedoms. The nonlinear response and hysteretic behavior are concentrated at these degrees of freedoms of the idealized structure. Such models are only used to predict the response of structures approximately because an accurate prediction of global displacements with this limited degree of freedom is impossible [15]. Discrete finite element models; the structure consists of interconnected elements that are able to represent the hysteretic behavior, constitutive nonlinearity can be defined at the section state or at the element state in an average manner. In this type of modelling, there are two formulations procedures as lumped plasticity and distributed plasticity method [15].

Microscopic finite element models; structural members and joints are meshed into a large number of finite elements, constitutive and geometric nonlinearity are introduced. Analysis of reinforced concrete structures by means of this modelling method is most versatile approach. Moreover, bond deterioration between concrete and steel, creep, thermal phenomena are physical nonlinearities can be defined with this modelling type. Since this method is computationally expensive for nonlinear analysis, it could be limited only to the research for critical parts of large frames and structures [15].

Best compromise between accuracy and simplicity among models is the discrete finite element model for evaluating the inelastic seismic response for the structures. A survey of existing researches on discrete finite element models is presented in the following sections.

2.1. Lumped Models

Based on the fact that the inelastic behavior of RC structures often concentrated at the end of structural elements Thus, the first method to analyzing nonlinear problems is by using of zero length plastic hinges, that located at the end of elements [16]. Lumped plasticity models are widely proposed in the most design codes and guide lines [17]. The earliest model that introduced by Clough and Johnston [18] was consist of two parallel components, one elastic perfectly plastic to represent yielding and the other perfectly elastic to represent strain hardening. The model allowed a bilinear moment-rotation relation. The stiffness matrix of the member is the sum of stiffness values of the components. A series model was proosed by Giberson [19] although it had been reportedly used earlier. The model original form consists of two zero nonlinear rotational spring connected by an elastic beam/column element that the spring computes nonlinear behavior of the structure [14]. This model is more capable than the Clough's model since it represents more complex hysteretic behavior of reinforced concrete members. Takizawa [20] developed the Clough's model to allowing for the effect of cracking. Lumped plasticity models which include cyclic stiffness degradation in shear and flexure were proposed by Clough and Benuska, Takida et al., Brancaleoni et al. [21-23]. Banon et al. and Brancaleoni et al. developed a model which including "pinching effect" under reversal loads [22, 24]. Otani, Filippou and Issa [25, 26] proposed a model that takes into account fixed end rotations at the beam column joining point due to the pull out effect between the reinforcing steel and concrete.

Multi linear constitutive models that include cracking and cyclic stiffness degradation were suggested by Takayanagi and Schnobrich [27]. Advantages in lumped plasticity models are reduce storage requirements and computational costs because of its simplicity which improves numerical stability to the mathematical model. However, it has some limitation and deficiencies. Propagation of inelasticity deformation region into the member is defined as a function of loading in lumped plasticity models to simplify and overcome the actual complex behavior of reinforced concrete structures. This case is a source of inaccuracy [28, 29]. Various researchers studied plastic hinge length calibrated from experimental data, the researchers have agreed that plastic hinge length L_p is a function of the members length, reinforcement ratio and/or axial force [30]. A comprehensive survey of plastic hinge developments was covered by Fedak et al. and Hines et al. [30, 31]. Moreover, lumped plasticity models has another defect, it is their inability to describe completely the deformation softening behavior of RC members. Lai et al. [32] proposed a fiber hinge model which consists of an elastic element extending over the entire length of the RC member and has one inelastic element at each end, each inelastic elements is made up of one inelastic spring at each corner that represent the reinforcement and one another spring at the center which represent the concrete that is effective in compression only.

2.2. Distributed nonlinearity Models

Distributed model is a more accurate method for modelling and analyzing of inelastic for RC structures. In this approach, the nonlinear behavior of structural element is distributed along its length Figure 2.1. Therefore, material inelasticity can occur at any point [33]. The constitutive behavior of the cross-section is either derived from the stress-strain which formulated by using classical plasticity theory or is explicitly derived by subdividing the cross-section into fibers. In the Fiber Element Analysis FEA, the length of the element is discretized into cross sections which located on element integration points and cross-sections are also divided into fibers.

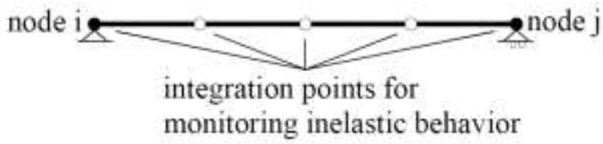

Figure 2.1. Distributed Plasticity Approach Schematic of a typical Element [30].

A beam-column element model was introduced by Otani [26] the model consist of two cantilever beams fixed at point of contra flexure of the member. The interaction of bending moment and axial force was neglected. The global behavior of the model was derived by integration of the curvatures along the two cantilever components Figure 2.2. The deficiency of the proposed model is the assumption of a fixed point of contra flexure in the element.

Soleimani et al. [34] introduced a model which include an inelastic zone of deformation, the zone gradually spread from the beam-column contact as the load increased. This deformations are depending on loading history. A hinge was added at the ends of the member to describe the fixed-end rotations. The rest of the structural element behaviors as elastic. These hinge points were related to the curvature through an “Effective

Length" factor which remains constant during the analysis. A similar model was introduced by Meyer et al. [35]. Takeda et al. [21] proposed a model for calculating the stiffness of the plastic zone during reloading and for describing the hysteretic moment-curvature relation. Empirical rules of this model was extended by Roufaiel and Meyer [36] for calculate the effect of axial force on the flexural hysteretic behavior. However, no it concerned with variation of the axial load due to overturning moments. A simpler and similar model that calculates end inelastic deformations by means of a trilinear moment-curvature relation was proposed by Darvall and Mendis [37].

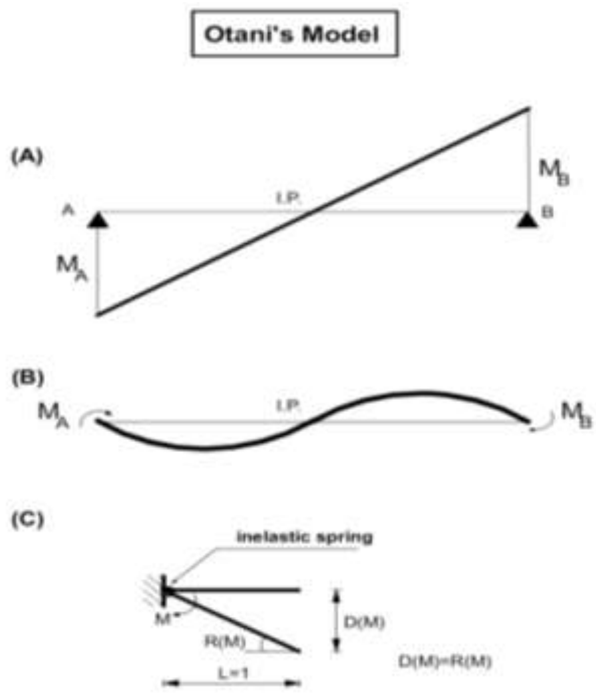

Figure 2.2. Otani's model, a) moment distribution, b) element deformation, c) equivalent inelastic rotational spring [15].

Takayanagi and Schnobrich [27] proposed a model which divides the member into several numbers of short segments. Each element was idealized with a nonlinear rotational spring which depending on the bending moment at midpoint of segment. It was assumed that the segment length to be constant. The multi-spring model was reduced to a single beam-column element by using static condensation techniques. The model is shown in Figure 2.3. To consider for the interaction between bending moment and axial force, the model was first employed in the study of the seismic analysis of coupled shear walls. In the model, it was observed that significant variation of axial force. The model belongs to the family of distributed nonlinearity and it has ability to consider inelasticity that takes place at any point.

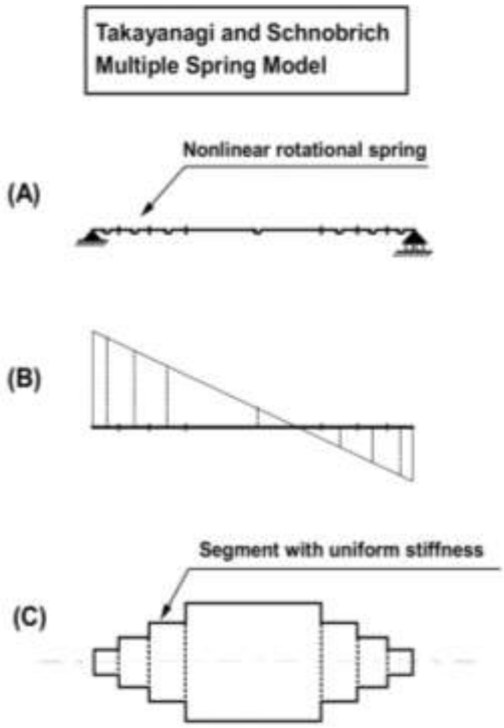

Figure 2.3. Takayanagi and Schnobrich multiple spring representation, a) structural element, b) diagram of the distributed moment and c) distribution of section stiffness [15].

Filippou and Issa [25] subdivided the structural member into sub-elements. Each sub-element represents that effects such as inelastic behavior to bending, shear and bond-slip behavior at the beam-column joint. The model allows the hysteretic behavior of the individual sub-element to be simpler. The structural members exhibit a complex hysteretic behavior due to the interaction of the different sub-elements. Many researchers have successfully formulated the distribute nonlinearity method for modelling RC structures in the nonlinear analysis based on Timoshenko and Euler –Bernoulli beam theory [38-48]. Other studies [49-58] focused on taking into account the axial force – bending moment – shear force interaction.

2.3.Fiber Element Approach (FEA)

FEA has been widely employed in the past two decades for the nonlinear analysis of framed structures. In the method, the element length is divided into segments or integration points and the cross-section is discretized into fibers. The geometric characteristics of the fibers are their area and the position in *y, z* coordination system as seen Figure 2.4. A uniaxial constitutive relation is assigned to each fiber and sectional stress-strain state is obtained by the integration of the nonlinear response of each fiber [3, 15, 59]. Most popular material models for steel are the selected one of bilinear, the Menegotto-Pinto [60] and Monti-Nuti [61], whilst concrete may be defined by tri-linear, Scott et al. [62] and Mander et al. [63]. In the literature there are many other material constitutive laws [59].

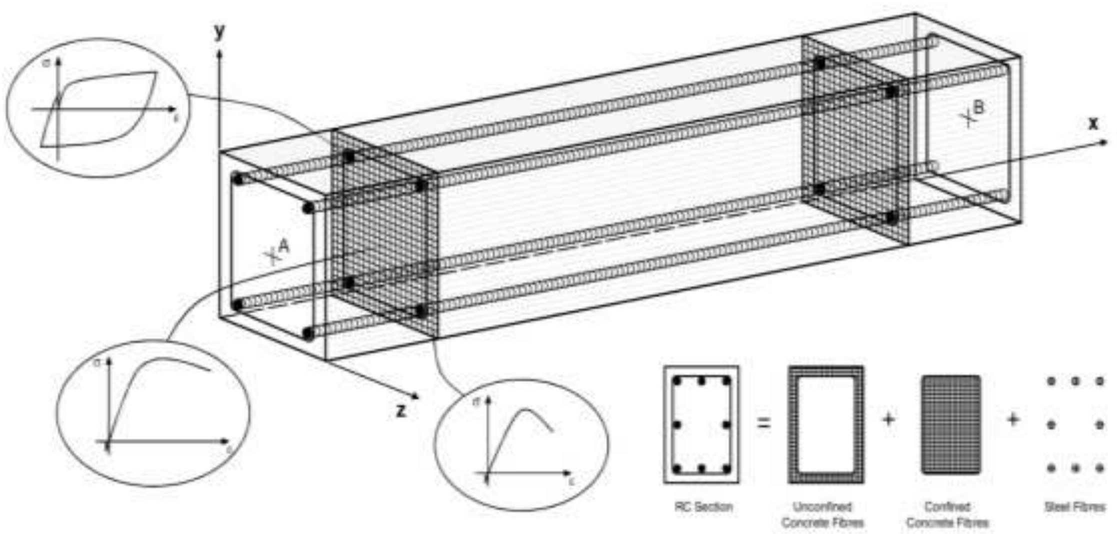

Figure 2.4. Fiber element schematic of a typical RC member [59].

Fiber element method is subdivided into two approaches as “Displacement Based” and “Force Based”. The first model of fiber element modelling based on flexibility was introduced by Kaba and Mahin [41]. These researchers used the flexibility that it based on only uniaxial bending. Fiber strains are determined by using section deformations based on the assumption of the plane sections remain plane. The stresses and stiffness of each fiber were established from the stress-strain relation of each fiber.

Zeris and Mahin (1988 and 1991) [43, 64] improved the formulation of Kaba-Mahin model for the biaxial case. Softening behavior of a cantilever beam which observed in Figure 2.5 was investigated by Zeris and Mahin (1988) [43]. When the cantilever was displaced beyond the point of ultimate resistance, Section 1 at the fixed base entered into softening region. Sections 2 to 5 were in the elastic region. Classical stiffness-based models failed to represent the real behavior of the member, due to the assumption of the linear curvature distribution. The actual curvature distribution during the element softening was deviated from the distributed curvature assumption. In the formulations of FEA which are based on Euler-Bernoulli hypothesis the effect of shear is neglected as in Taucer et al. [15]. Contrary in the formulations based on the Timoshenko beam theory the effect of shear included as in Ceresa et al. and Mullapudi et al. [65, 66].

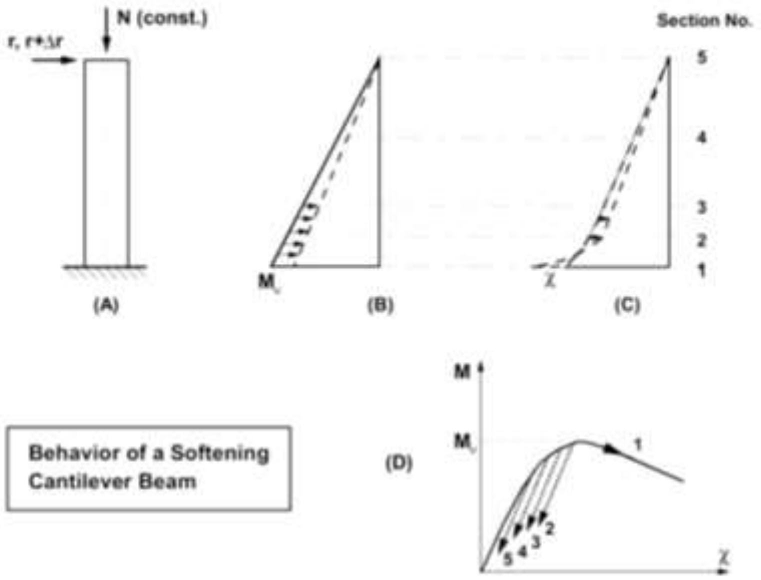

Figure 2.5. Softening cantilever model behavior, a) loading of the member, b) moment distribution, c) curvature distribution, d) relation of moment-curvature [15].

2.4. Displacement based formulation

The displacement based (DB) formulation is the first elements with distributed nonlinearity. This elements were formulated with the classical stiffness method based on linear interpolation functions for the axial displacements and cubic interpolation functions for transverse displacements of the element [67]. The three-dimensional element with axial and flexural degree of freedom was presented in **Figure 2.6** in the local coordinate system, the element degree of freedoms were also given in **Figure 2.7**. The torsional behavior was assumed to be elastic in these formulations. $\bar{\mathbf{q}}$ and $\mathbf{q}$ are the nodal displacement vectors of the element with rigid body modes and without rigid body modes, respectively and these are given as follow,

$$\bar{\mathbf{q}} = \{\bar{q}_1 \quad \bar{q}_2 \quad \bar{q}_5 \quad \bar{q}_6 \quad \bar{q}_7 \quad \bar{q}_{10}\}^T \tag{2.1}$$

$$\mathbf{q} = \{q_1 \quad q_2 \quad q_5\}^T \tag{2.2}$$

$\mathbf{a}_d(x)$ is a matrix that contains the linear interpolation functions for the axial displacements and cubic interpolation functions for the transverse displacements and it is given in Eq. (2.3).

$$\bar{\mathbf{d}}(x) = \begin{Bmatrix} u(x) \\ v(x) \end{Bmatrix} = \mathbf{a}_\mathrm{d}(x).\bar{\mathbf{q}} \tag{2.3}$$

where $u(x)$ is the axial displacement, $v(x)$ is the transverse displacement and $\bar{\mathbf{d}}(x)$ is a matrix that contains both axial and transverse displacements. $\mathbf{a}_d(x)$ in the Eq. (2.3) can be written as,

$$\mathbf{a}_d(x) = \begin{bmatrix} \psi_1(x) & 0 & 0 & \psi_2(x) & 0 & 0 \\ 0 & \varphi_1(x) & \varphi_2(x) & 0 & \varphi_3(x) & \varphi_4(x) \end{bmatrix} \tag{2.4}$$

$$\psi_1(x) = 1 - \frac{x}{L} \tag{2.5}$$

$$\psi_2(x) = \frac{x}{L} \tag{2.6}$$

$$\varphi_1(x) = 2\frac{x^3}{L^3} - 3\frac{x^2}{L^2} + 1 \tag{2.7}$$

$$\varphi_2(x) = \frac{x^3}{L^2} - 2\frac{x^2}{L} + x \tag{2.8}$$

$$\varphi_3(x) = -2\frac{x^2}{L^3} + 3\frac{x^2}{L^2} \tag{2.9}$$

$$\varphi_4(x) = \frac{x^3}{L^2} - \frac{x^2}{L} \tag{2.10}$$

It was the assumed that deformations are small and the plane section remains plane after loading. The section deformations $\mathbf{d}(x)$ are related to the nodal displacements by

$$\mathbf{d}(x) = \begin{Bmatrix} \varepsilon(x) \\ \chi_z(x) \end{Bmatrix} = \begin{Bmatrix} u'(x) \\ v''(x) \end{Bmatrix} = \bar{\mathbf{a}}(x).\bar{\mathbf{q}} \tag{2.11}$$

where, $\varepsilon(x)$ and $\chi_z(x)$ are the axial strain and the curvature about the z-axis, respectively. $\bar{\mathbf{a}}(x)$ is derived from the displacement interpolation functions and it can be written as,

$$\bar{\mathbf{a}}(x) = \begin{bmatrix} \psi'_1(x) & 0 & 0 & \psi'_2(x) & 0 & 0 \\ 0 & \varphi''_1(x) & \varphi''_2(x) & 0 & \varphi''_3(x) & \varphi''_4(x) \end{bmatrix} \tag{2.12}$$

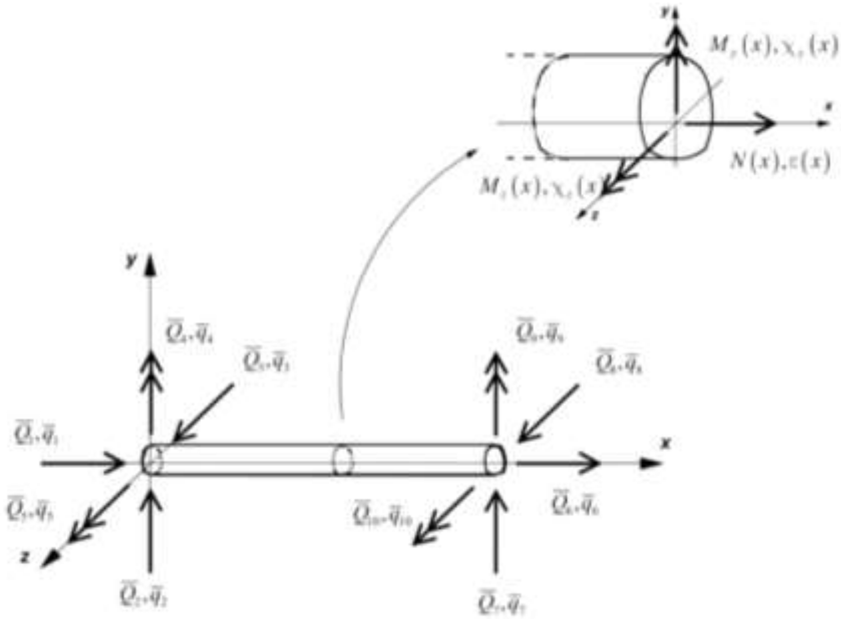

Figure 2.6. Beam element with rigid body modes in local coordinate system [15].

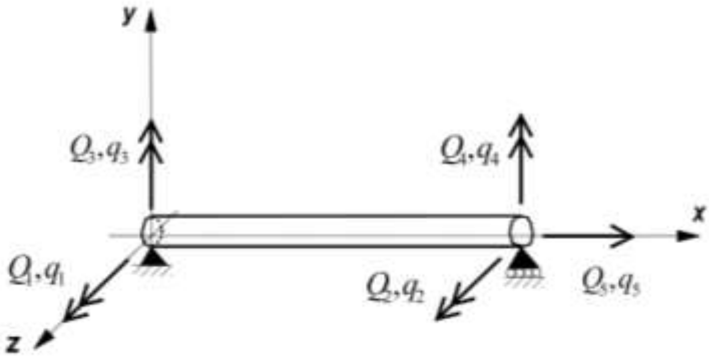

Figure 2.7. Beam element without rigid body modes in local coordinate system [15].

The stiffness matrix of beam-column elements, $\bar{\mathbf{K}}$ can be derived by the principle of minimum potential and the principle of virtual work. This matrix obtained by using each section stiffness matrix, $\mathbf{k}(x)$. Thus, the element stiffness matrix, $\bar{\mathbf{K}}$ can be derived by

$$\bar{\mathbf{K}} = \int_{0}^{L} \bar{\mathbf{a}}^{\mathrm{T}}(x).\mathbf{k}(x).\bar{\mathbf{a}}(x).dx \tag{2.13}$$

The relation between section stiffness $\mathbf{k}(x)$, section forces $\mathbf{D}(x)$ and section deformations $\mathbf{d}(x)$ are:

$$\mathbf{D}(x) = \mathbf{k}(x).\mathbf{d}(x) \tag{2.14}$$

$$\mathbf{D}(x) = \begin{Bmatrix} N(x) \\ M_z(x) \end{Bmatrix} \tag{2.15}$$

where, $N(x)$ and $M_z(x)$ are axial force and bending moment for section at the x coordinate, respectively. Due to the virtual displacement principle, the element resisting forces $\overline{\mathbf{Q}}_R$ are determined by the integration of the section resisting forces, $\mathbf{D}_R(x)$

$$\overline{\mathbf{Q}}_R = \int_0^L \bar{\mathbf{a}}^{\mathrm{T}}(x).\mathbf{D}_R(x).dx \tag{2.16}$$

The classical finite element modelling based on the stiffness method has successfully used [42, 68-70]. Due to the cubic interpolation functions are poor in representing the curvature distribution at the ends of the elements, Menegotto and Pinto [69] studied on the interpolating both section deformations and section flexibilities variables. The assumption of cubic interpolation functions are the main limitation of the displacement based methods by reason of leads to linear curvature along the element. The assumption has satisfactory results for elastic and near elastic response. However, when the significant yielding occurred at the ends of the element, the curvature distribution becomes highly nonlinear in the inelastic regions. To overcome the deficiency a fine discretization or a higher order polynomial interpolation functions are required in the inelastic regions. Moreover, due to the above mentioned limitation the DB method should be used with care and more experienced user is required.

2.5.Force based formulation

Contrary to the stiffness based method, researchers have focused on flexibility-dependent shape functions that allow to a more accurate representation of the force distribution in the element. The force based (FB) formulation was proposed by Mahasuverachai [39] for the first time. In this research, the flexibility dependent shape functions were used. These functions are continuously updated during the analysis depending on the plastic strains into the member. In the proposed formulation, deformation increments are used rather than total deformation.

$$\Delta\mathbf{d}(x) = \mathbf{f}(x).\mathbf{b}(x).\mathbf{F}^{-1}.\Delta\mathbf{q} = \mathbf{a}(x).\Delta\mathbf{q} \tag{2.17}$$

where, Δ denotes the increment of the corresponding vector, $\mathbf{d}(x)$ is section deformation, $\mathbf{f}(x)$ is section flexibility matrix, $\mathbf{b}(x)$ is a matrix containing force interpolation functions, **F** is element flexibility matrix and **q** is element deformations. The vector of element forces without rigid body modes,

$$\mathbf{Q} = \{\mathrm{Q}_1 \quad \mathrm{Q}_2 \quad \mathrm{Q}_5\}^T \tag{2.18}$$

It is assumed that the axial force distribution inside the member is constant and the bending moment distribution is linear. The interpolation functions of the force can be written as,

$$\mathbf{D}(x) = \mathbf{b}(x).\mathbf{Q} \tag{2.19}$$

where $\mathbf{D}(x)$ is the section force matrix.

$$\mathbf{b}(x) = \begin{bmatrix} 0 & 0 & 1 \\ \left(\frac{x}{L} - 1\right) & \left(\frac{x}{L}\right) & 0 \end{bmatrix} \tag{2.20}$$

where, *L* is element length. The element flexibility matrix is obtained by the application of the virtual work principle,

$$\mathbf{F} = \int_0^{\mathrm{L}} \mathbf{b}^{\mathrm{T}}(x).\mathbf{f}(x).\mathbf{b}(x).dx \tag{2.21}$$

$\mathbf{d}(x)$ is section deformation vector can be calculated as,

$$\mathbf{d}(x) = \mathbf{f}(x).\mathbf{D}(x) \tag{2.22}$$

As long as no element loads applied, the element equilibrium is satisfied by the force interpolation functions in Eqs. (2.18) and (2.19). In other words, the assumed internal force distributions are exact, whatever the material nonlinearities take place and even as the element starts softening when deformed beyond its ultimate resistance.

2.6. Constitutive law of concrete

To reproduce the real behavior of RC structures are likely to undergo inelastic response an accurate stress-strain material model is needed.

Sinha et al. [71] published the first attempt to characterize the cyclic behavior of plain concrete. 48 concrete cylinders were tested and an analytical expression in the study was developed by using the yielded data. They assumed that the stress strain relationship of concrete is uniqueness (uniqueness means that unloading and reloading curves of stress-strain relationship is independent to its previous cycle), the hypothesis of uniqueness was refuted later by subsequent experimental evidence.

Another formula was proposed for the stress-strain relation of concrete by Karsan and Jirsa [72], the results are obtained through testing 46 short columns under cyclically varying axial loads Figure 2.8. The authors reported that the stress-strain paths do not exceed the envelope curves; furthermore, the unloading and reloading curves starting from a point within the stress strain domain were not unique. To estimate the next response cycle the value of stress and strain at the peak of the previous cycle had to be known.

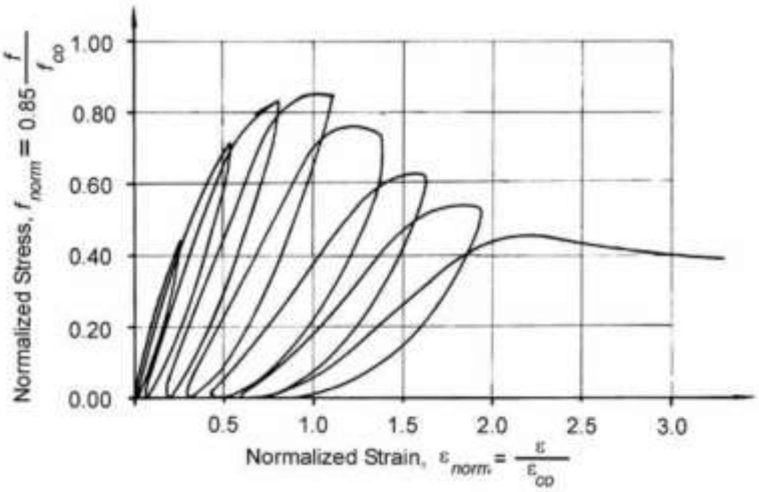

Figure 2.8. A cyclic compression typical result [72]

A stress strain representation was proposed by Yankelevesky and Reinhardt [73] geometrical properties of the loading was used to derivation of the model in the uniaxial stress strain plane. The loading/unloading cycles are modeled by a multi linear curve defined by six focal points in the stress strain plane.

Mander, Priestley and Park [63] proposed a stress-strain model for concrete subjected to uniaxial reversed compressive and tension loading for members confined by transverse reinforcement. The authors used a modified equation of Popovics [74] for monotonic compressive loading. The unloading curves were derived by the parameter adjustment based on selected experimental unloading curves for confined and unconfined concrete. For the reloading curve, a linear stress-strain relation constructed between the point of zero stress and the unloading strain, a parabolic transition curve is used between the unloading strain and the return to the monotonic stress strain. Martinez-Rueda and Elnashaai [75] modified the model for taking account the effect of degradation in stiffness and strength due to cyclic loading.

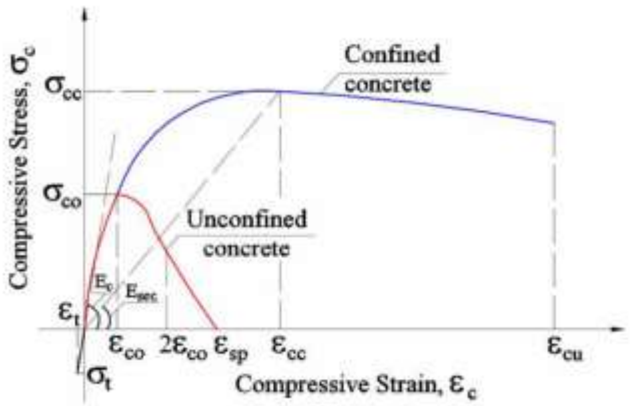

Figure 2.9. Concrete model for Mander et al. [63]

Chang and Mander [76] defined a stress-strain model for confined and unconfined concrete Figure 2.9, the model includes both cyclic tension and compression for ordinary and high strength concrete. The proposed model also calculates the effect of degradation.

Bahn and Hsu [77] introduced a model for concrete under cyclic compression loading. The model was developed based on theoretical and experimental results for unconfined concrete. A power type equation was developed for unloading curve and a linear relationship for reloading.

Palermo and Vecchio [78] proposed a constitutive model for concrete for both cyclic compression and tension. The model considers stiffness degrading.

An unloading and reloading model presented by Sakai and kawashima [28, 79-81] for confined concrete with transverse reinforcement. The model derived based on tests results on reinforced concrete column specimens. In this model the effect of the degree of confinement, concrete strength, unloading/reloading, repeated unloading/reloading, and partial loading included.

2.7. Constitutive law of steel

Modelling of reinforced steel strain-stress behavior has a significant influence on the response of reinforced concrete members under cyclic and dynamic loading. Steel exhibits a loss of linearity prior to the attainment of the yield strength in the opposite direction under cyclic loading, this phenomenon is known as Bauschinger effect. Several models have been proposed for steel material, the models are taking into account the Bauschinger effect and other characteristics of steel behavior, among others (Park et al. [82], Aktan et al. [83], Ma et al. [84], Stanton and McNiven [85], Filippou et al. [86], Monti and Nuti [61], Chang and Mander [76], Hoehler and Stanton [87]).

Menegotto and Pinto [60] proposed a model for steel material under cyclic loading Figure 2.10. The steel model that used in this study, was developed by Yassin [88] based on the model proposed by Menegotto and Pinto [60], and coupled to the isotropic hardening rules proposed by Filippou et al. [86].

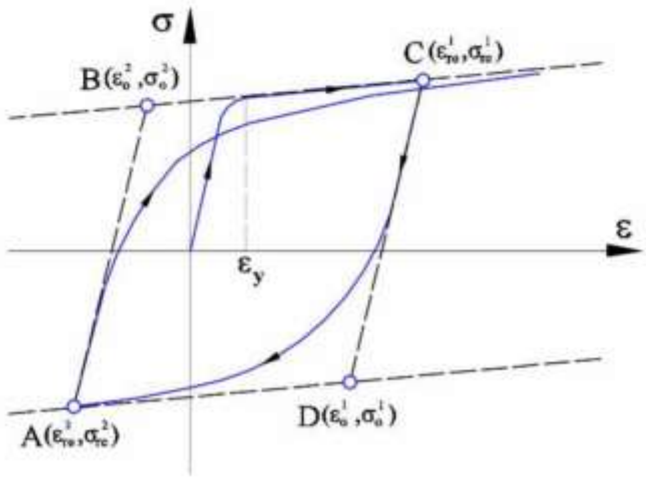

Figure 2.10. Menegotto and Pinto [60].

3.APPLICATIONS FOR THE REVERSE ENGINNERING METHOD

Numerical analyses were obtained by using Seismo-Struct software. The software can solve static and dynamic analysis of reinforced concrete and steel structure, distributed plasticity and lumped plasticity methods are included. In this thesis, distributed plasticity method was selected for analysis of the reinforced concrete buildings. For verification of numerical results, experimental test results were used as (a) a bare frame with full scale, four story building and (b) a 7.32m tall bridge pier. In the proposed numerical solution scheme, different material properties are predicted. The data for the numerical models was changed gradually for different cases according to the reverse engineering method by using ACI-318 and Turkish standard (TS 500) equations. The Mander et al. model is employed for defining the concrete material and The Menegotto-Pinto steel model is employed for defining the steel material. HHT-α method was used for dynamic integration method.

3.1. Dynamic Solution Algorithm of the Structure

Equation of motion for the building can be written as,

$$[M]\{a\}+[C]\{v\}+[K]\{u\}=\{F_g\} \tag{3.1}$$

where $\{a\}$, $\{v\}$ and $\{u\}$ are the relative acceleration, velocity and displacement vectors for the building, respectively. $[M]$, $[C]$ and $[K]$ is mass matrix, damping matrix and stiffness matrix of the building, respectively. $\{F_g\}$ is external load vector occurs due to ground acceleration. In the nonlinear behavior, improved form of Equation (1) according to $HHT-\alpha$ integration method can be written as,

$$[M]\{a\}_{i+1}+(1+\alpha)[C]\{v\}_{i+1}-\alpha[C]\{v\}_i+(1+\alpha)\{F\}_{i+1}-\alpha\{F\}_{i+1}= (1+\alpha)\{F_g\}_{n+1}-\alpha\{F\}_n \tag{3.2}$$

where, α is a parameter controlling the numerical dissipation. To ensure second-order accuracy and unconditional stability, these parameters should be chosen such that,

$$\alpha\in\left[-\frac{1}{3},0\right]; \qquad \beta=\frac{1}{4}(1-\alpha)^2; \qquad \gamma=\frac{1}{2}-\alpha$$

In this study, α is selected as -0.10. $[C]$ matrix is obtained by

$$[C]=\alpha_c[M]+\beta_c\,[K] \tag{3.3}$$

where, α_c and β_c are the mass matrix and the stiffness matrix coefficients for Rayleigh damping, respectively. These cofficients are defined by natural frequencies of two effective modes. Damping matrix calculation can be also calculated by using only mass matrix or only stiffness matrix. In this case, these cofficients are calculated by natural frequency of first effective mode.

3.2. A Bare Frame of a Full-Scale, Four Story Building

Pinto et al. [1] had tested a bare frame of a full-scale, four story building in the ELSA laboratory (Joint Research Centre, Ispra) in the framework of the ICONS project. The building is a reinforced concrete 4-storey with 3-bays which one of 2.5 m span and two of 5 m span Figure 3.1. Thickness of the slab is 0.15 m and inner-story height is 2.7 m. Elevation and plan of the building were given in Figure 3.2. Geometric properties of the columns and the beams were also shown in Figure 3.3, Figure 3.4, Figure 3.5, Table 3.1 and Table 3.2. This test is called as ELSA-JRCI in this thesis.

Figure 3.1. Reinforced concrete frame, 4-storey with 3-bays [1].

The characteristic reinforced concrete material properties of the frame were determined by using experimental tests. Uniaxial compressive strength (f_{cc}), uniaxial tensile strength (f_{ct}) and elasticity modulus (E_c) of the concrete are determined as 16.3

MPa, 1.9 MPa and 18975 MPa, respectively. Yield strength (f_y) and elasticity modulus (E_s) of the steel were specified as 343 MPa and 200000 MPa, respectively.

In the numerical analysis, two different models were established as Model-A and Model-B. In the Model-A, columns and beams were modelled through 3D force-based inelastic frame element with 4 integration sections (points). The number of fibers used in section was selected as 200. In the Model-B, columns and beams were modelled through 3D displacement-based inelastic frame element. The number of fibers used was assigned as 200.

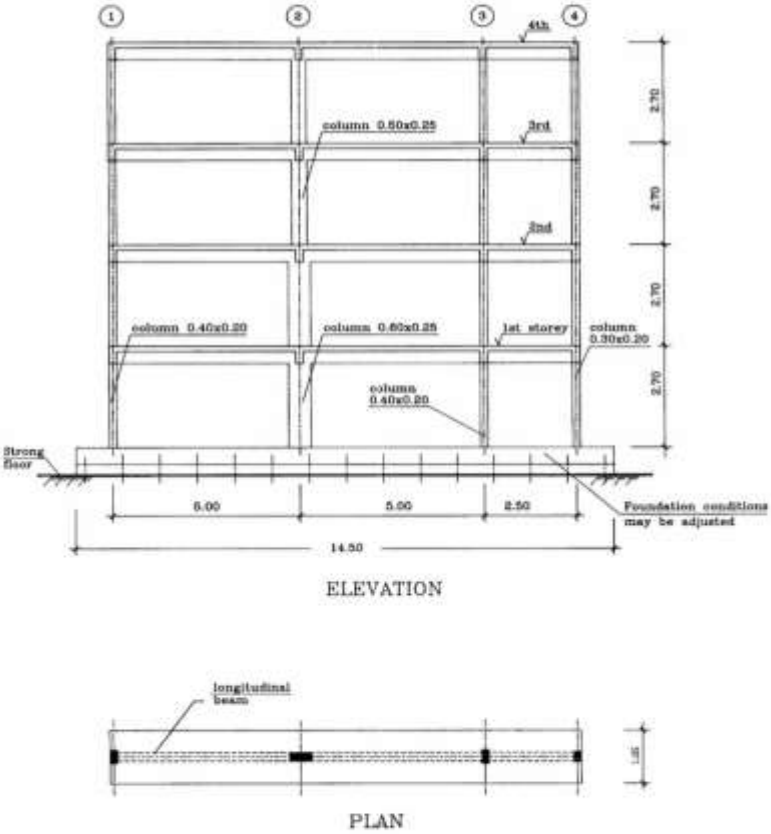

Figure 3.2. Four-story, three-bay RC frame geometry [1].

Table 3.1. The columns reinforcement and geometrical details.

Story	Col1	Col2	Col3	Col4
3to4	0.4x0.2 (6Ø12)	0.25x0.5 (4Ø16 + 2Ø12)	0.4x0.2 (6Ø12)	0.3x0.2 (6Ø12)
1to2	0.4x0.2 (6Ø12)	0.25x0.6 (8Ø16 + 2Ø12)	0.4x0.2 (8Ø12)	0.3x0.2 (6Ø12)

The masses of the stories can be assumed as distributed or lumped at floor levels. In this numerical investigation, masses were assumed as lumped and distributed masses for ELSA-JRCI frame and, were computed as Table 3.3.

Table 3.2. The beams geometrical details.

Floor	Beam
R	0.5 x 0.25 x 1.05 x 0.15 *
4	
3	
2	
Height of beam x width x effective width of slab x thickness of slab	

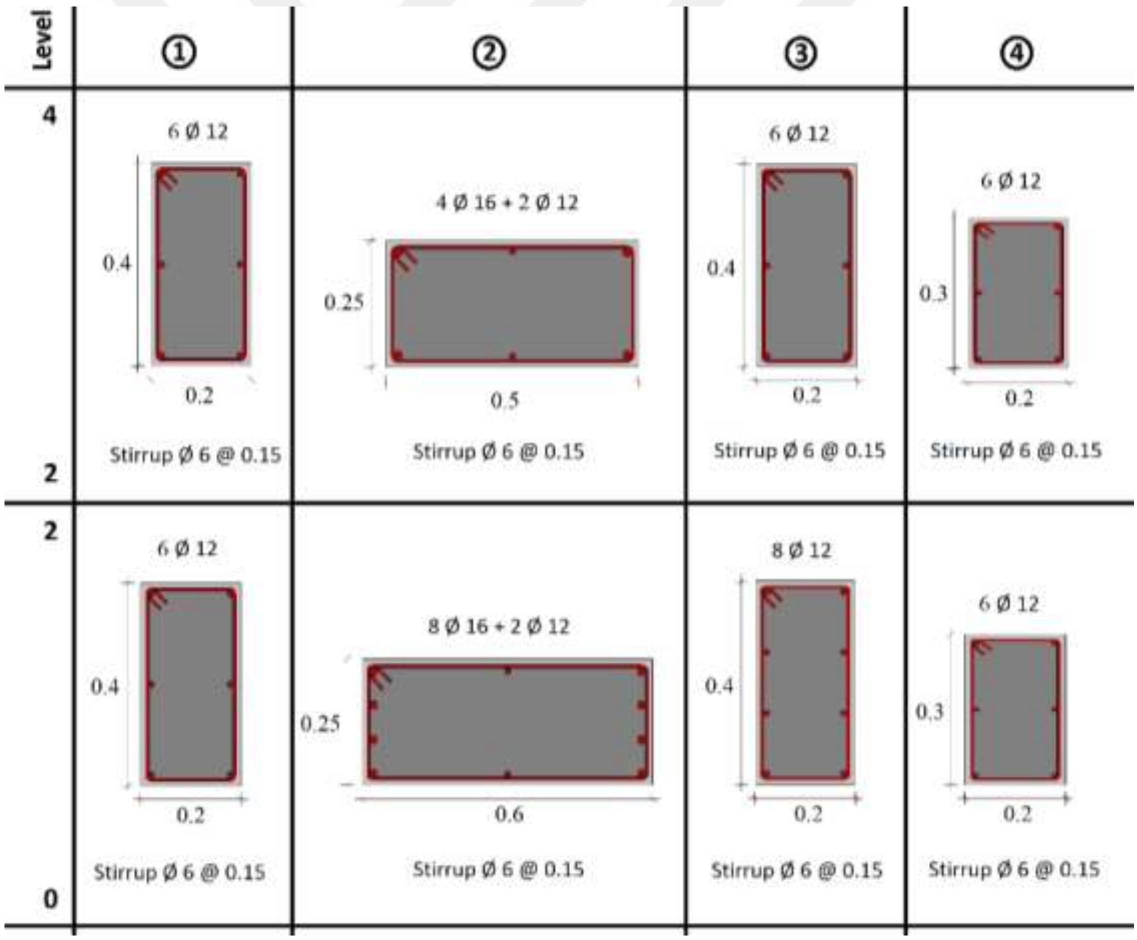

Figure 3.3. Reinforcement detail of column sections

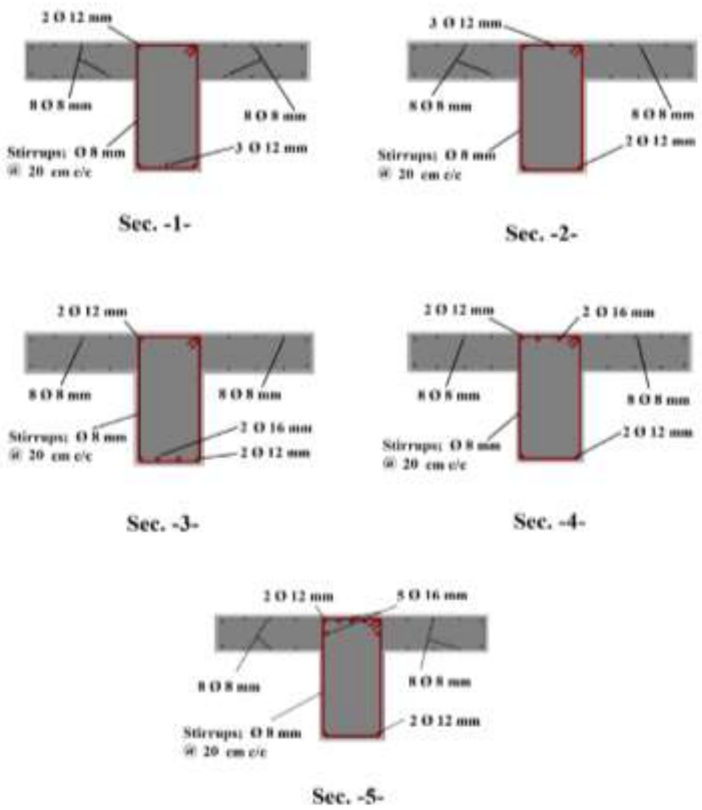

Figure 3.4. Reinforcement detail of beam sections.

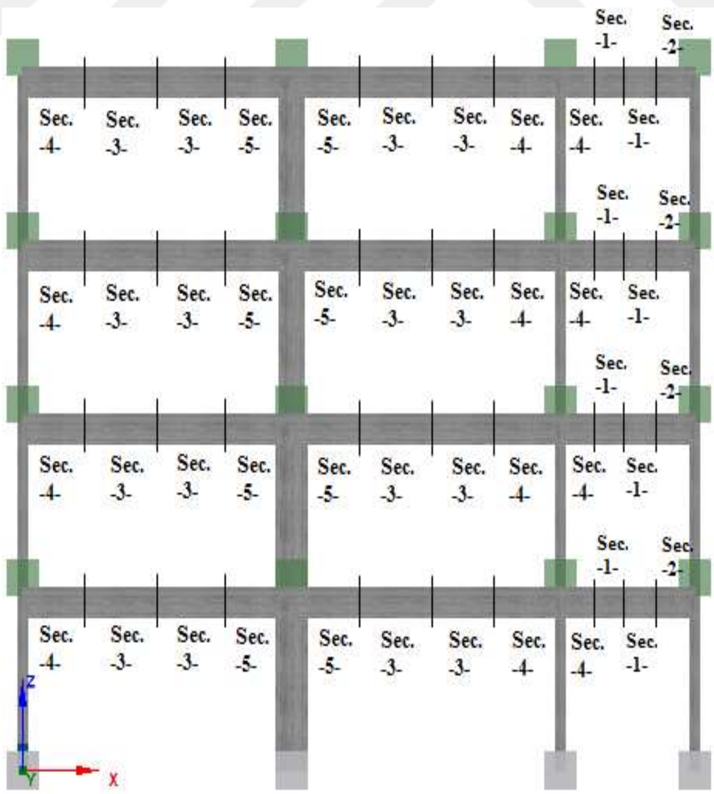

Figure 3.5. Locations of beam cross-sections.

Table 3.3. Distributed and lumped masses assigned to the frame members and joints (ton).

Floor	Column1	Column2	Column3	Column4	Distributed Mass
Roof	4.5	7.8	6.1	2.9	1.295
2, 3 and 4	5.7	9	7.4	4.1	1.539

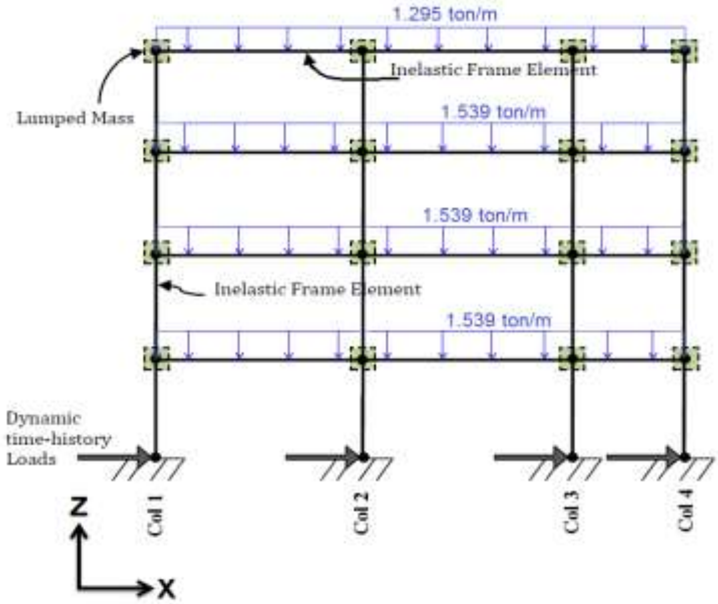

Figure 3.6. Distribution of loads to the Finite Element (FE) Model.

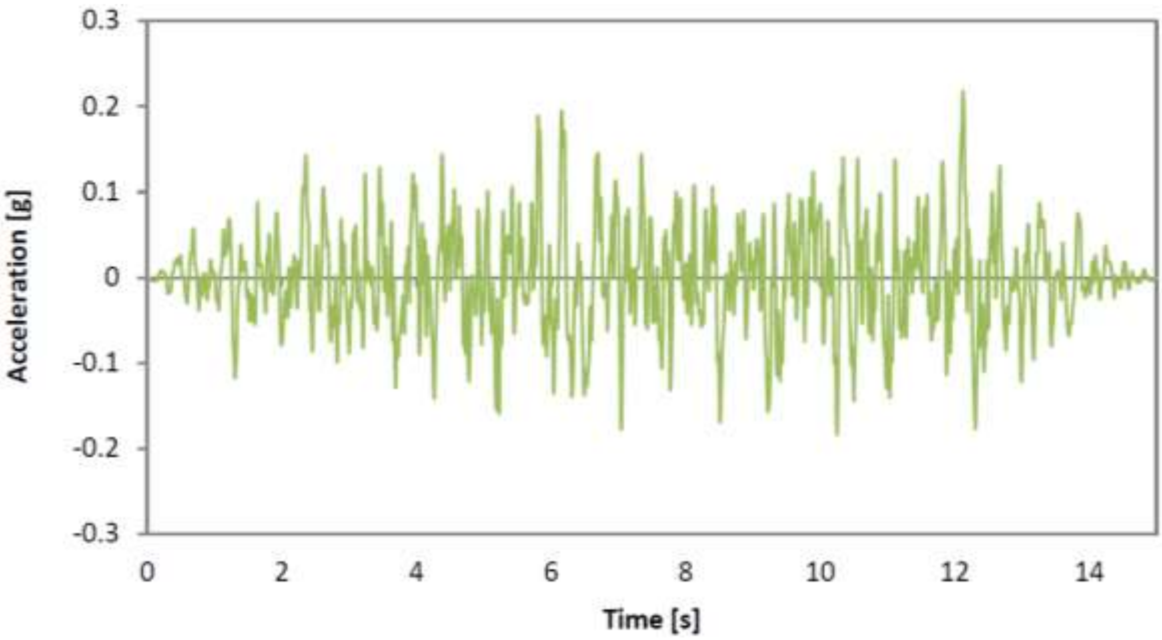

Figure 3.7. Time history acceleration loading for 475yrp (Acc-475yrp).

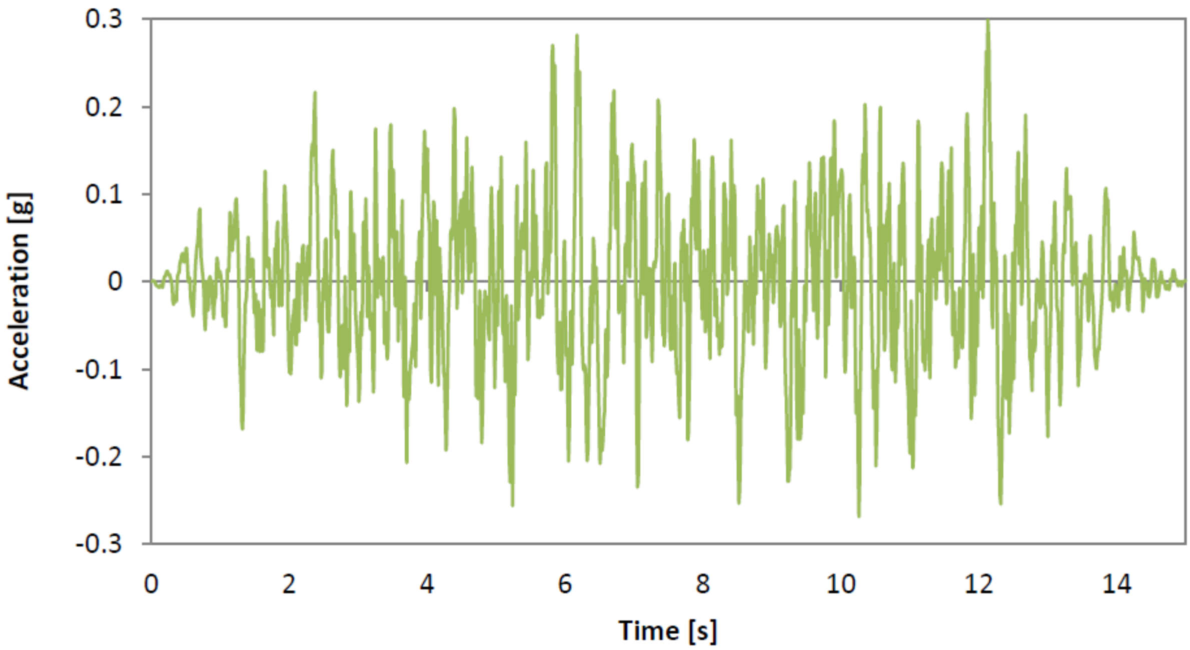

Figure 3.8. Time history acceleration loading for 975yrp (Acc-975yrp).

All base nodes were assumed as fixed support Figure 3.6. All another nodes were restrained to transition in *y* direction and rotation about *x* and *z* axes because the analysis is performed in 2D, *x-z* plane. In nonlinear time-history analysis, two time-acceleration data were used as Acc475 (475 years return period) and Acc975 (975 years return period) Figure 3.7, Figure 3.8. These integration records are artificial earthquake acceleration data and the time integration step in the dynamic analysis was selected as 0.005 sec for numerical convergence providing.

In the reverse engineering method which this thesis proposed, firstly, it is assumed that material properties of structural steel class is known. However, five different material class cases for concrete predicted. At the same time, these predictions were depended on the regional design codes, Turkish Standard Code (TS 500) and, American Standard Code (ACI-318). Elasticity modulus (E_c) and uniaxial tensile strength (f_{ct}) of concrete are depending on the uniaxial compressive strength (f_{cc}) of concrete according to TS 500 and ACI-318 codes. E_c and f_{ct} according to TS 500 code are calculated by using equations (3.4) and (3.5).

$$f_{ct} = 0.35\sqrt{f_{cc}} \qquad \text{(MPa)} \tag{3.4}$$

$$E_c = 3250\sqrt{f_{cc}} + 14000 \qquad \text{(MPa)} \tag{3.5}$$

E_c and f_{ct} values according to ACI-318 code are defined by using equations (3.6) and (3.7).

$$f_{ct} = 0.5563\sqrt{f_{cc}} \quad \text{(MPa)} \tag{3.6}$$

$$E_c = 4700\sqrt{f_{cc}} \quad \text{(MPa)} \tag{3.7}$$

Predicted five material classes according to both codes were given in Table 3.4 and Table 3.5.

Table 3.4. Concrete material properties according to TS 500 Code.

	Compressive Strength of concrete (MPa)	**Tensile strength of concrete (MPa)**	**Modulus of elasticity (MPa)**
Case-1	10.0	1.106	24277.402
Case-2	12.0	1.212	25258.330
Case-3	14.0	1.309	26160.386
Case-4	16.0	1.400	27000.000
Case-5	18.0	1.485	27788.582

Table 3.5. Concrete material properties according to ACI-318 Code.

	Compressive Strength of concrete (MPa)	**Tensile strength of concrete (MPa)**	**Modulus of elasticity (MPa)**
Case-1	10.0	1.759	14862.705
Case-2	12.0	1.927	16281.277
Case-3	14.0	2.081	17585.789
Case-4	16.0	2.225	18800.000
Case-5	18.0	2.360	19940.411

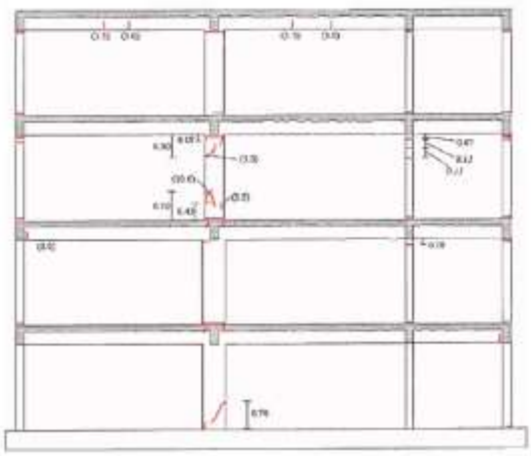

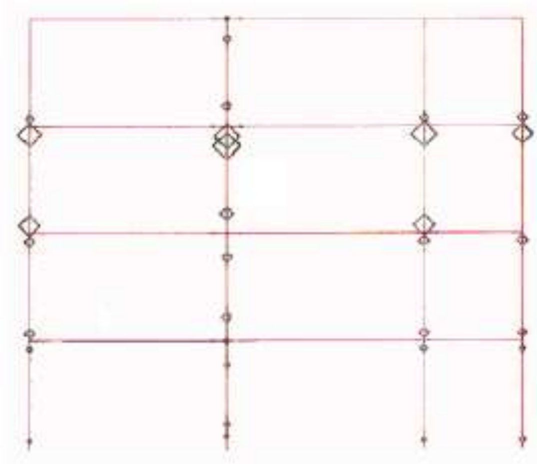

a) Cracking Zones b) Relative rotations

Figure 3.9. Cracking zones and relative rotation values of the frame [1].

Comparison for top displacements between the experimental and numerical results obtained for 475 year return period (475yrp) acceleration loading, sixteen maximum peak displacement points in the time history graphs for each case were selected. In this research, damage regions obtained from numerical analysis were not compared with experimental result because slight damage regions were seen in laboratory test under 475yrp loading type. Thus, these results were neglected. Important damages were observed under 975yrp acceleration loading and the test was terminated after around 7.5 seconds in order to prevent total collapse of the structure and because the failure of the 3rd storey was imminent in this time. Therefore, the comparison for damage regions for the experimental and numerical model results was studied for the first 7.5 seconds under the 975yrp loading.

Damage regions were determined by using cracking cases and relative rotations which obtained from inclinometer devices Figure 3.9. Damage regions of lower and upper sides of Column-2 at third story and lower side of Column-2 at first story were defined as heavy, severe and severe damage in the report of ELSA test, respectively. Additionally, it was determined that relative rotations of lower and upper sides of Column-1 and Column-2 at third story were in heavy damage region. Damages occurred at upper side of Column-4 at third story were assumed as moderate. Other frame elements were in the no damage, light damage and minor damage regions. Categorized damage regions of the frame were given in Figure 3.10.

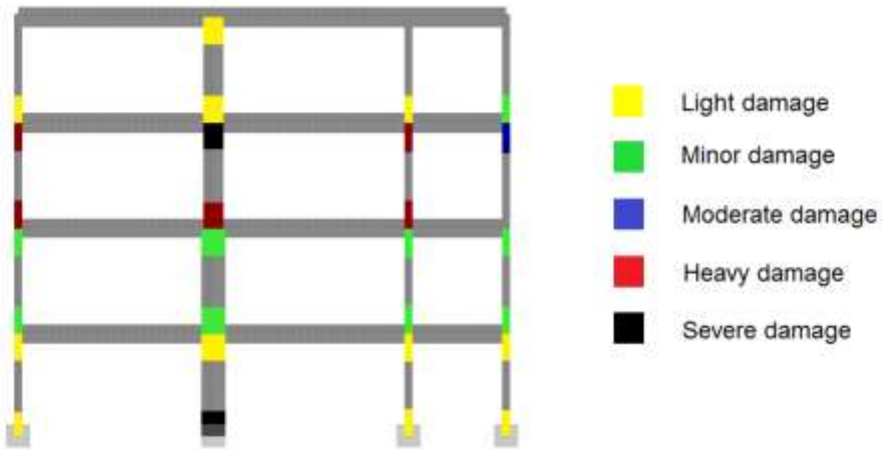

Figure 3.10. Damage regions defined from experimental results.

3.2.1.Comparison of Model-A according to ACI-318

Top story displacement time history graphs of numerical and experimental results for Case-1, Case-2, Case-3, Case-4 and Case-5 according to ACI-318 were shown in Figure 3.11-Figure 3.15. Differences between displacements obtained from experimental and numerical results were determined and mean of the differences were given in Table 3.6. Mean differences between experimental and the Case-1, Case-2, Case-3, Case-4, Case-5 numerical solutions were calculated as 97.1%, 58.5%, 20.3%, 15.6% and 19.1%, respectively. Minimum difference was obtained for Case-4 solution.

Damage regions obtained from Model-A according to ACI-318 under earthquake loading with 975 years return period were given in Figure 3.16. Differences between damage ratios obtained from experimental and numerical results were determined and mean of the differences were given in Table 3.7. Mean differences between experimental and the Case-1, Case-2, Case-3, Case-4, Case-5 numerical solutions were calculated as 19.4%, 16.3%, 16.9%, 13.1% and 14.4%, respectively. Minimum difference was obtained for Case-4 solution.

Comparison of material properties obtained from Model-A according to ACI-318 by using reverse engineering and, from experiment test were given in Table 3.8. Differences for compressive strength and elasticity modulus of concrete are determined as 1.84% and 0.92%, respectively. However, difference for tensile strength of concrete was founded as 17.1%. The result of Case 4 has the best agreement with the ELSA test results.

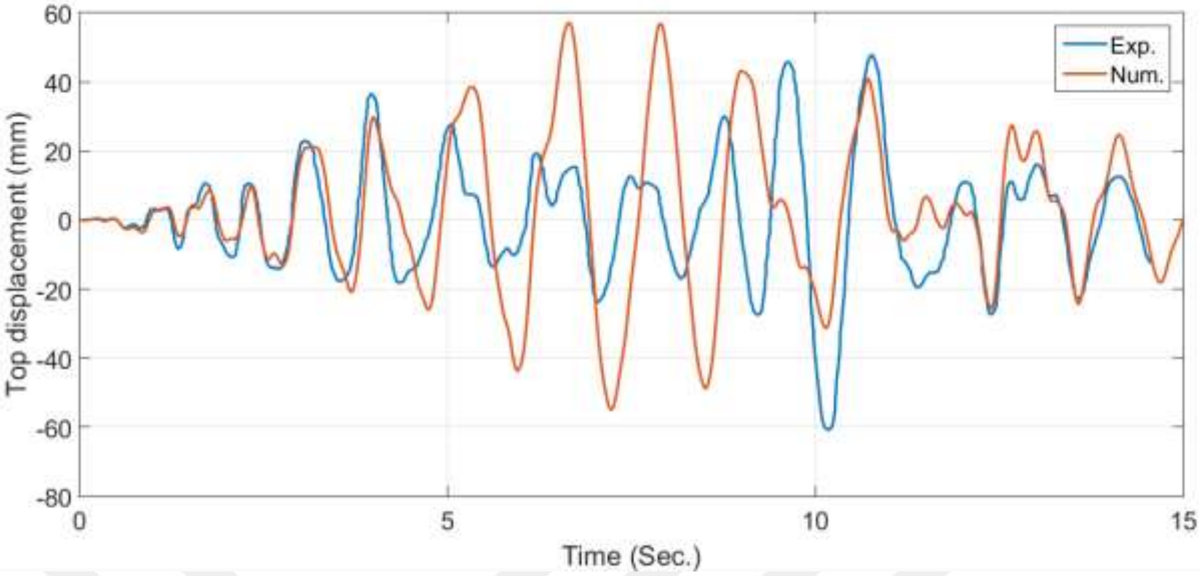

Figure 3.11. Top story displacement of numerical and experimental results for Case-1 according to ACI-318.

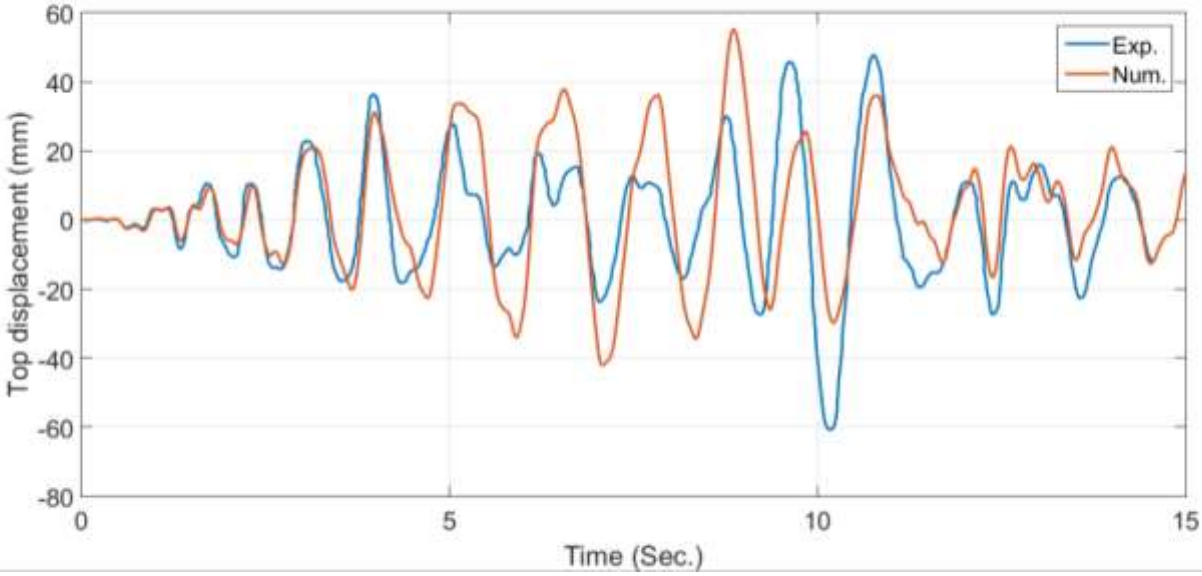

Figure 3.12. Top story displacement of numerical and experimental results for Case-2 according to ACI-318.

Table 3.6. Comparison maximum peak displacements obtained from Model-A according to ACI-318 and from experiment tests.

	Differences (%)																**Mean Differences (%)**
Time (sec)	3.05	3.56	3.96	4.51	5.05	5.78	6.41	7.07	7.66	8.19	8.73	9.23	9.66	10.16	10.69	11.35	-----
Case 1	7.76	17.90	18.64	43.04	39.37	224.3	183.6	136.6	345.7	186.9	43.63	86.58	87.23	48.26	14.52	69.48	97.1
Case 2	8.32	13.88	14.78	21.88	22.24	152.8	88.08	81.16	184.8	102.2	83.79	5.54	44.15	50.86	24.60	36.85	58.5
Case 3	7.67	9.69	7.51	2.32	31.84	63.84	51.22	10.43	37.28	17.13	29.42	0.73	9.39	10.02	0.02	36.75	20.3
Case 4	3.49	9.35	1.40	1.93	34.34	55.51	49.93	10.47	20.25	6.89	11.55	2.41	3.08	0.38	6.53	32.42	15.6
Case 5	0.22	14.33	4.44	4.75	31.94	65.48	63.54	13.32	32.65	23.66	4.33	5.94	0.46	0.56	7.89	31.29	19.1

Table 3.7. Differences of damaged ratio obtained from Model-A according to ACI-318 and from experiment tests.

	Differences (%)																																**Mean Differences (%)**
Column No.	C11-L	C11-U	C12-L	C12-U	C13-L	C13-U	C14-L	C14-U	C21-L	C21-U	C22-L	C22-U	C23-L	C23-U	C24-L	C24-U	C31-L	C31-U	C32-L	C32-U	C33-L	C33-U	C34-L	C34-U	C41-L	C41-U	C42-L	C42-U	C43-L	C43-U	C44-L	C44-U	
Case 1	0	0	20	20	40	60	0	20	20	20	40	40	20	20	20	0	0	0	20	20	40	40	0	20	0	0	20	20	40	20	40	0	19.4
Case 2	0	0	20	0	40	40	0	20	40	20	40	40	0	0	20	0	0	0	20	20	20	20	0	20	0	0	20	20	40	20	40	0	16.3
Case 3	0	0	20	20	40	40	0	20	20	20	40	40	20	0	20	0	0	0	20	20	20	20	0	20	0	0	20	20	60	0	40	0	16.9
Case 4	0	0	20	0	40	40	0	20	20	20	40	40	20	0	0	0	0	0	0	0	0	0	0	20	0	0	20	20	60	0	40	0	13.1
Case 5	0	0	20	0	40	40	0	20	20	20	40	40	20	0	0	0	0	0	0	0	20	20	0	20	0	0	20	20	60	0	40	0	14.4

Table 3.8. Comparison of material properties obtained from Model-A according to ACI-318 by using reverse engineering and from experiment test.

	Compressive Strength (MPa)	**Tensile Strength (MPa)**	**Elasticity Modulus (MPa)**
Reverse Engineering	16.0	2.225	18800
Laboratory Test Results	16.3	1.90	18975
Difference	1.84%	17.1%	0.92%

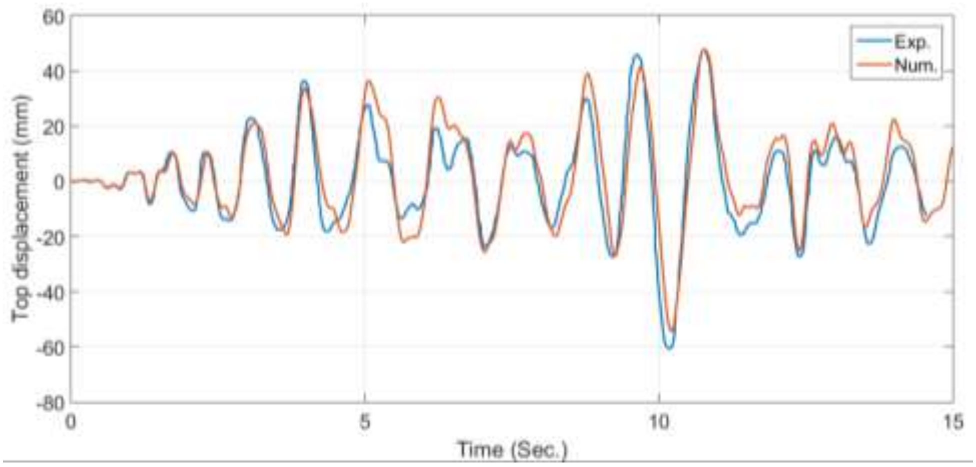

Figure 3.13. Top story displacement of numerical and experimental results for Case-3 according to ACI-318.

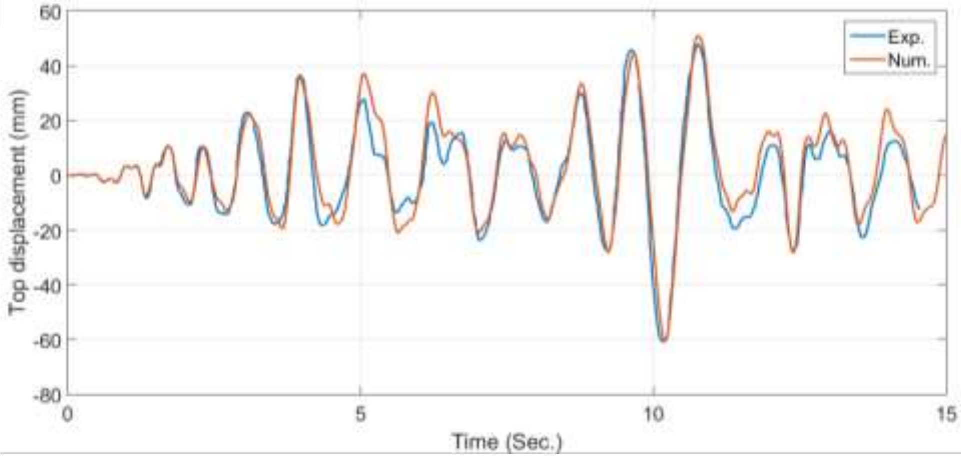

Figure 3.14. Top story displacement of numerical and experimental results for Case-4 according to ACI-318.

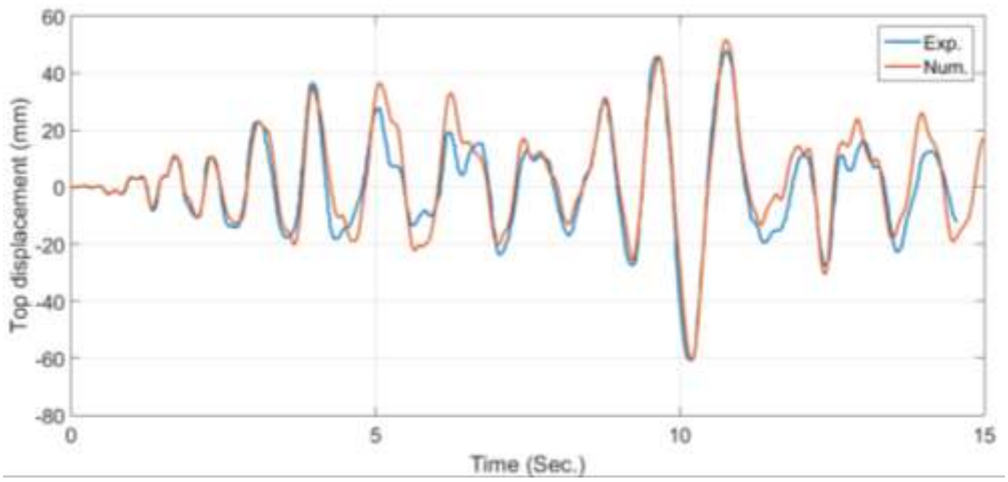

Figure 3.15. Top story displacement of numerical and experimental results for Case-5 according to ACI-318.

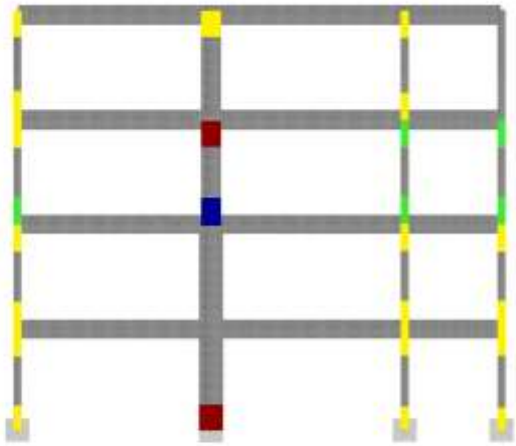

a) Case-1

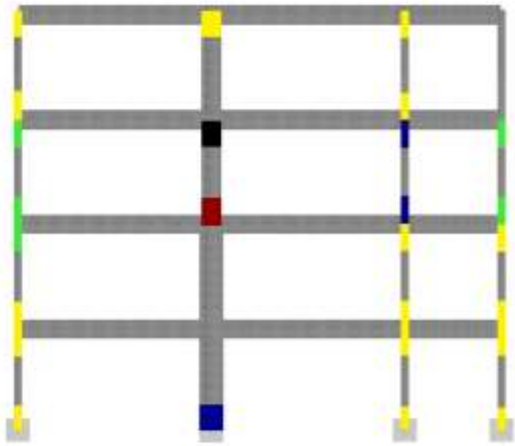

b) Case-2

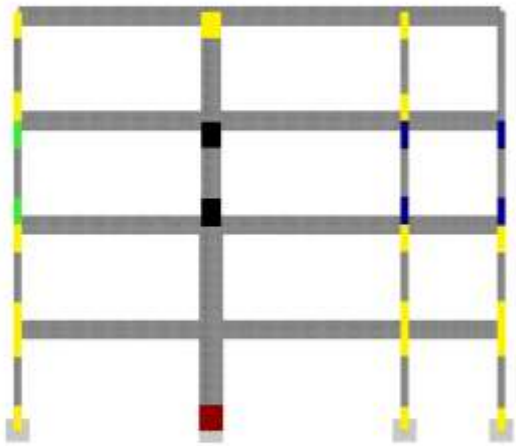

c) Case-3

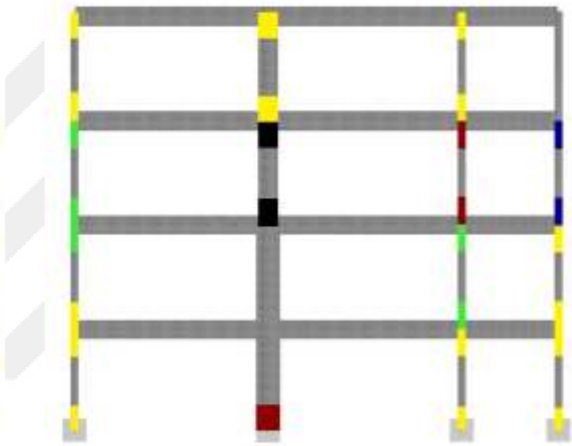

d) Case-4

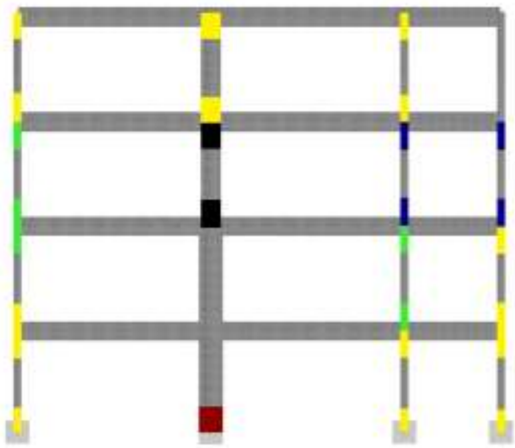

e) Case-5

Figure 3.16. Damage regions obtained from Model-A according to ACI-318 for all cases.

3.2.2.Comparison of Model-A according to TS 500

Top story displacement time history graphs of numerical and experimental results for Case-1, Case-2, Case-3, Case-4 and Case-5 according to TS 500 were shown in Figure 3.17-Figure 3.21. Differences between displacements obtained from experimental and numerical results were determined and mean of the differences were given in Table 3.9. Mean differences between experimental and the Case-1, Case-2, Case-3, Case-4, Case-5 numerical solutions were calculated as 97.1%, 63.5%, 45.5%, 28.6% and 30.5%, respectively. Minimum difference was obtained for Case-4 solution.

Damage regions obtained from Model-A according to TS 500 under earthquake loading with 975 years return period were given in Figure 3.22. Differences between damage ratios obtained from experimental and numerical results were determined and mean of the differences were given in Table 3.10. Mean differences between experimental and the Case-1, Case-2, Case-3, Case-4, Case-5 numerical solutions were calculated as 18.8%, 16.3%, 15.6%, 11.88% and 13.12%, respectively. Minimum difference was obtained for Case-4 solution.

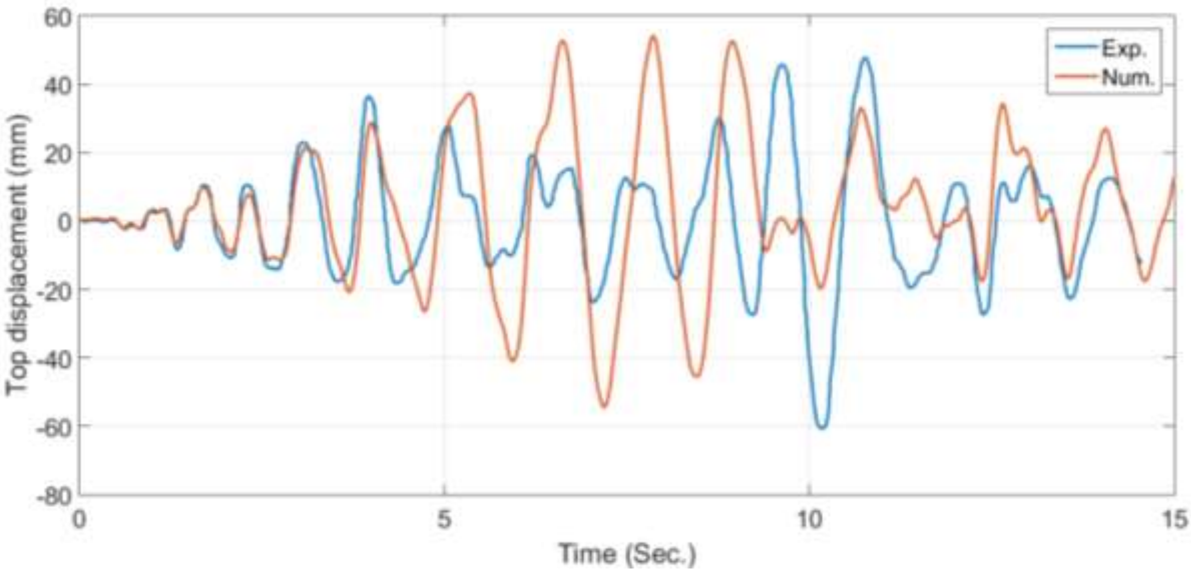

Figure 3.17. Top story displacement of numerical and experimental results for Case-1 according to TS 500.

Comparison of material properties obtained from Model-A according to TS 500 by using reverse engineering and from experiment test were given in Table 3.11. Difference was defined as 1.84% for compressive strength. However, differences for tensile strength and elasticity modulus were found as 26.3% and 42.3%, respectively. The results of Case 4 showed best agreement with the ELSA test results.

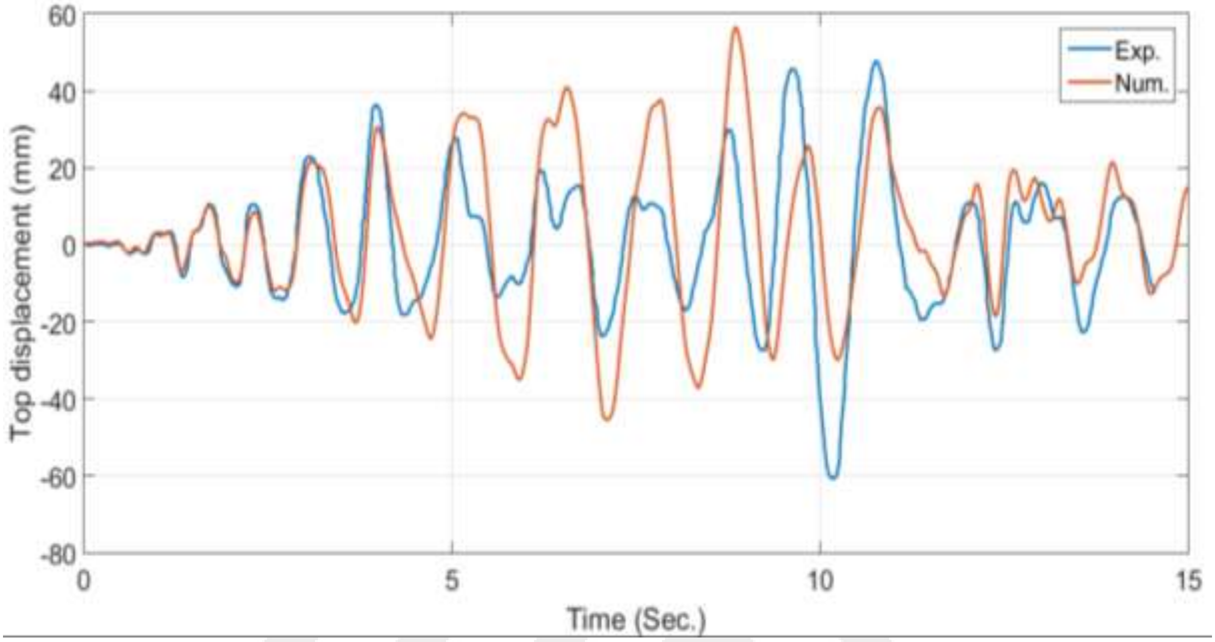

Figure 3.18. Top story displacement of numerical and experimental results for Case-2 according to TS 500.

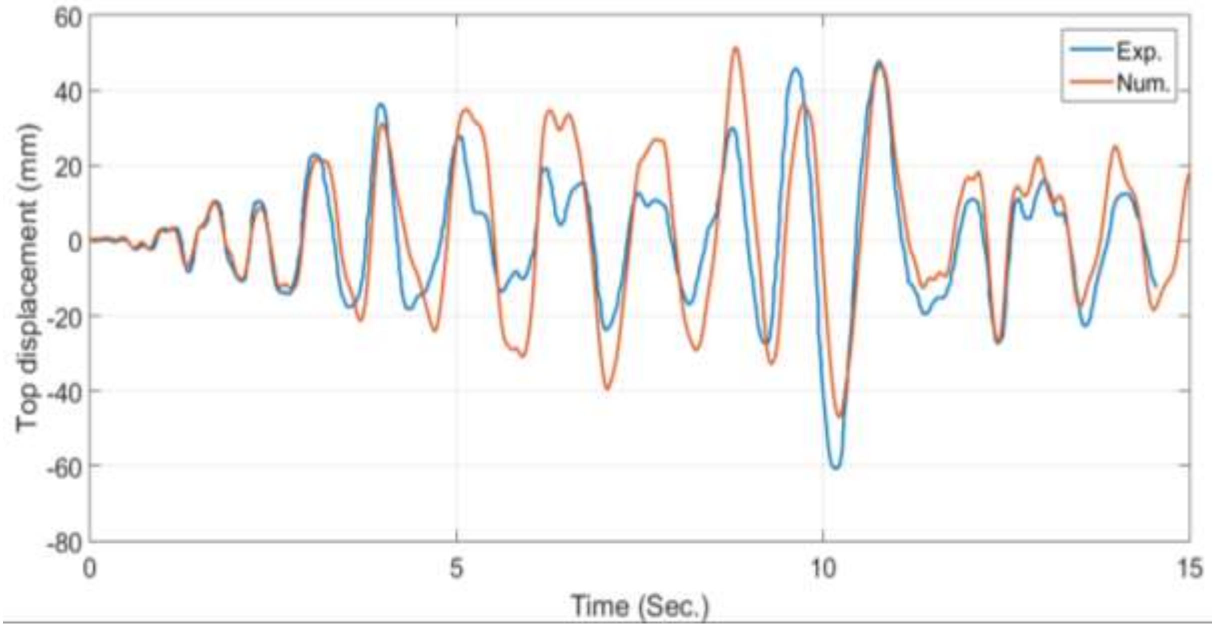

Figure 3.19. Top story displacement of numerical and experimental results for Case-3 according to TS 500.

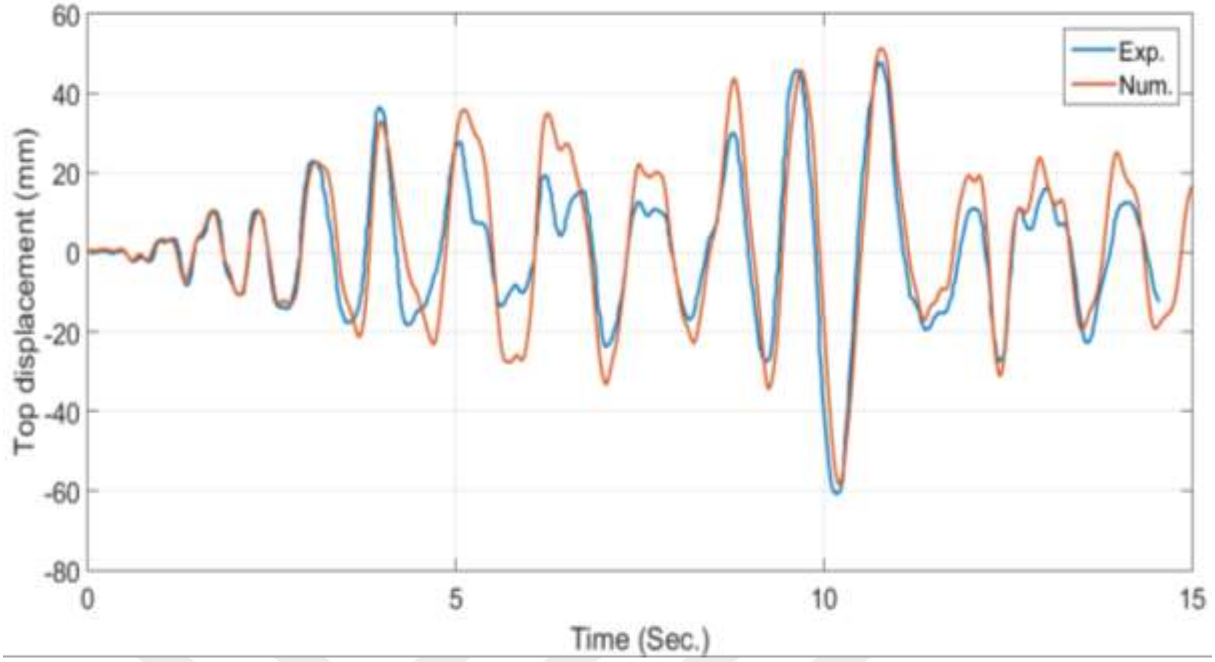

Figure 3.20. Top story displacement of numerical and experimental results for Case-4 according to TS 500.

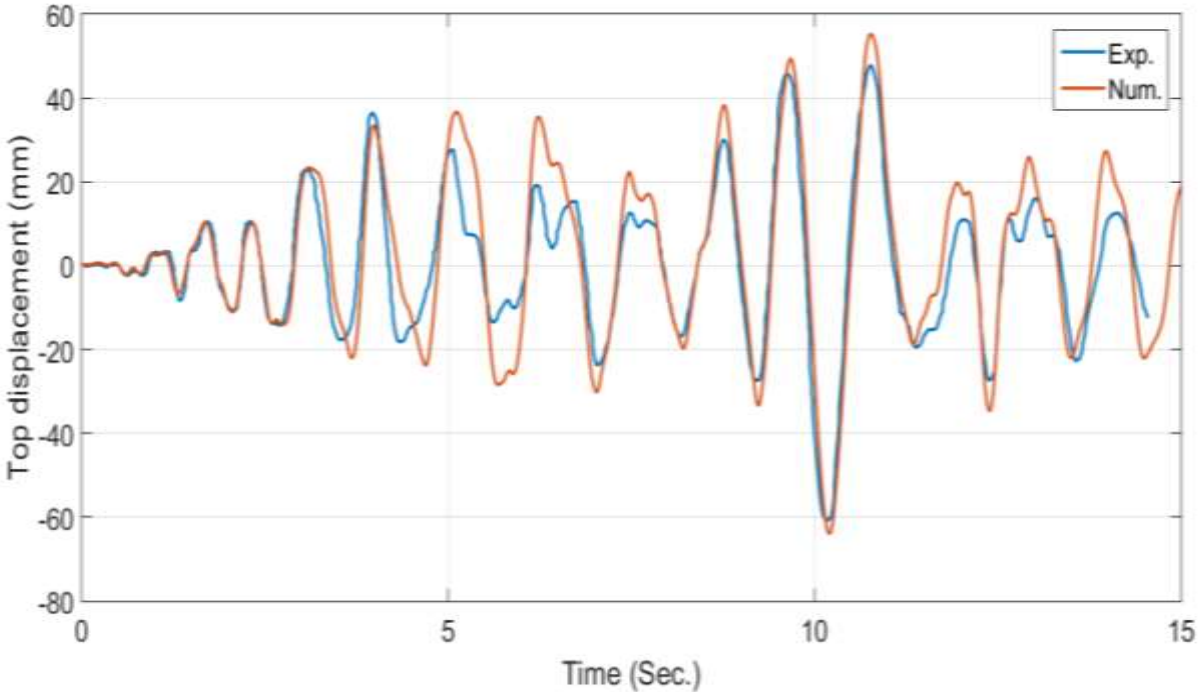

Figure 3.21. Top story displacement of numerical and experimental results for Case-5 according to TS 500.

Table 3.9. Comparison maximum peak displacements obtained from Model-A according to TS 500 and from experiment tests.

	Differences (%)																**Mean Differences (%)**
Time (sec)	3.05	3.56	3.96	4.51	5.05	5.78	6.41	7.07	7.66	8.19	8.73	9.23	9.66	10.16	10.69	11.35	-----
Case 1	7.67	17.39	26.75	45.86	35.28	205.0	161.6	134.5	324.8	167.2	74.88	73.19	97.99	67.54	31.05	83.43	97.13
Case 2	5.80	14.22	16.01	34.48	23.76	160.0	103.5	94.91	195.8	118.4	88.15	8.53	43.97	50.71	25.25	32.06	63.47
Case 3	5.62	20.34	14.56	32.87	26.73	129.5	72.53	70.26	111.6	71.22	71.28	19.37	21.07	22.42	3.05	35.92	45.52
Case 4	1.05	20.06	9.98	27.68	29.84	104.9	35.07	43.02	57.69	33.61	45.36	24.91	0.07	3.72	7.78	12.35	28.57
Case 5	1.83	24.59	8.39	31.05	32.71	111.2	76.30	29.83	75.43	15.95	27.15	21.48	7.71	5.65	15.54	3.50	30.52

Table 3.10. Differences of damaged ratio obtained from Model-A according to TS 500 and from experiment tests.

	Differences (%)																																**Mean Differences (%)**
Column No.	C11-L	C11-U	C12-L	C12-U	C13-L	C13-U	C14-L	C14-U	C21-L	C21-U	C22-L	C22-U	C23-L	C23-U	C24-L	C24-U	C31-L	C31-U	C32-L	C32-U	C33-L	C33-U	C34-L	C34-U	C41-L	C41-U	C42-L	C42-U	C43-L	C43-U	C44-L	C44-U	
Case 1	0	0	20	20	60	40	0	20	40	20	40	40	0	0	20	0	0	0	20	20	40	40	0	20	0	0	20	20	40	20	40	0	18.8
Case 2	0	0	20	0	40	40	0	20	40	20	20	40	20	0	20	0	0	0	20	20	20	20	0	20	0	0	20	20	60	0	40	0	16.3
Case 3	0	0	20	0	40	40	0	20	20	20	20	40	20	0	20	0	0	0	20	20	20	20	0	20	0	0	20	20	60	0	40	0	15.6
Case 4	0	0	20	20	40	40	0	20	20	0	40	40	20	0	0	0	0	0	0	0	0	0	0	20	0	0	0	0	60	0	20	20	11.88
Case 5	0	0	20	0	40	20	0	20	0	20	40	40	20	0	0	20	0	0	0	0	0	0	0	20	0	0	0	0	80	20	40	20	13.12

Table 3.11. Comparison of material properties obtained from Model-A according to TS 500 by using reverse engineering and from experiment test.

	Compressive Strength (MPa)	**Tensile Strength (MPa)**	**Elasticity Modulus (MPa)**
Reverse Engineering	16.0	1.4	27000
Laboratory Test Results	16.3	1.90	18975
Difference	1.84%	26.3%	42.3%

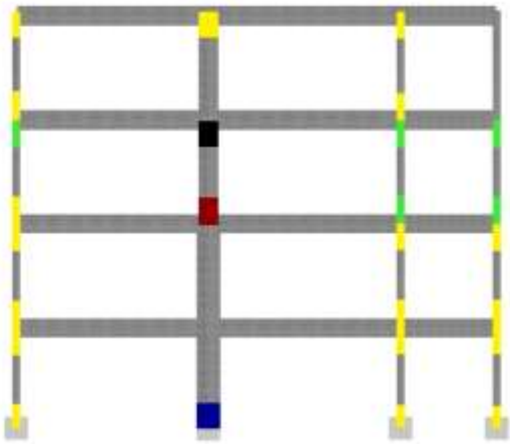

a) Case-1

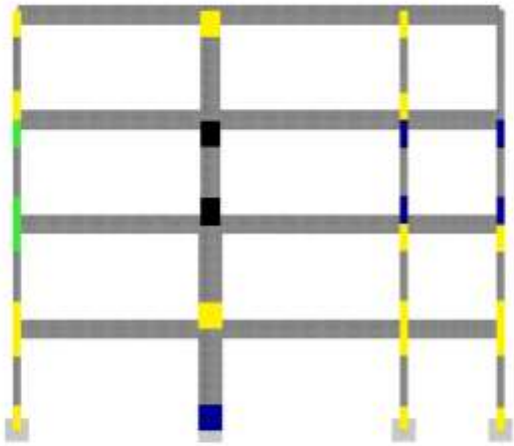

b) Case-2

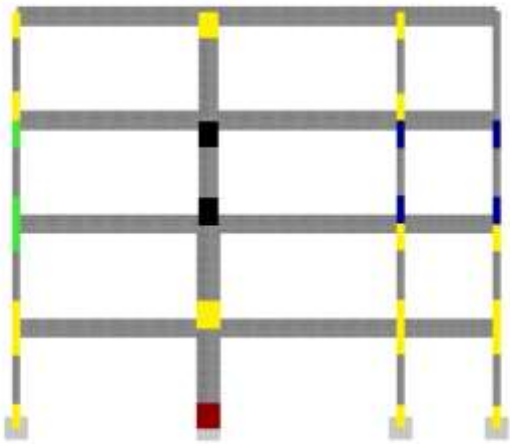

c) Case-3

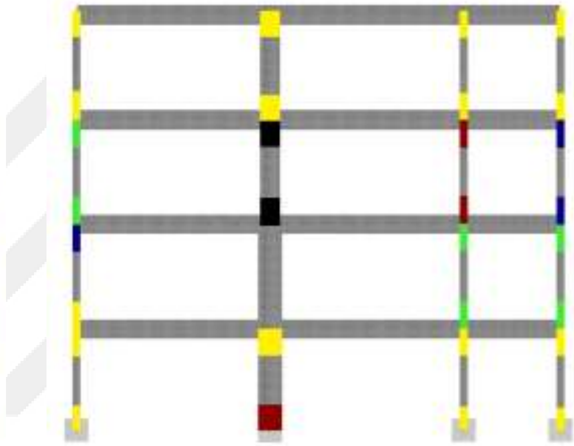

d) Case-4

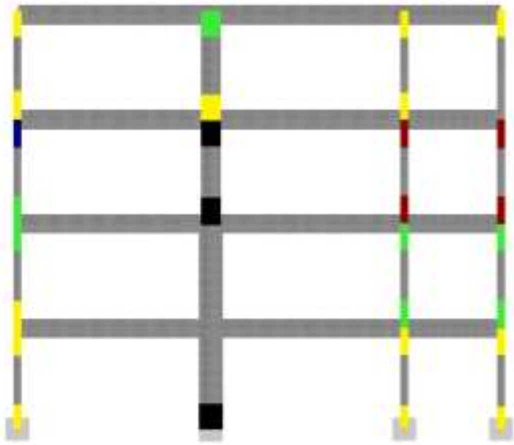

e) Case-5

Figure 3.22. Damage regions obtained from Model-A according to TS 500 for all cases.

3.2.3.Comparison of Model-B according to ACI-318

Top story displacement time history graphs of numerical and experimental results for Case-1, Case-2, Case-3, Case-4 and Case-5 according to ACI-318 were shown in Figure 3.23-Figure 3.27. Differences between displacements obtained from experimental and numerical results were determined and mean of the differences were given in Table 3.12. Mean differences between experimental and the Case-1, Case-2, Case-3, Case-4, Case-5 numerical solutions were calculated as 35.24%, 15.74%, 11.94%, 13.95% and 15.71%, respectively. Minimum difference was obtained for Case-3 solution.

Damage regions obtained from Model-B according to ACI-318 under earthquake loading with 975 years return period were given in

Figure **3.28**. differences between damage ratios obtained from experimental and numerical results were determined and mean of the differences were given in Table 3.13. Mean differences between experimental and the Case-1, Case-2, Case-3, Case-4, Case-5 numerical solutions were calculated as 21.3%, 20.6%, 20%, 23.1% and 22.5%, respectively. Minimum difference was obtained for Case-3 solution.

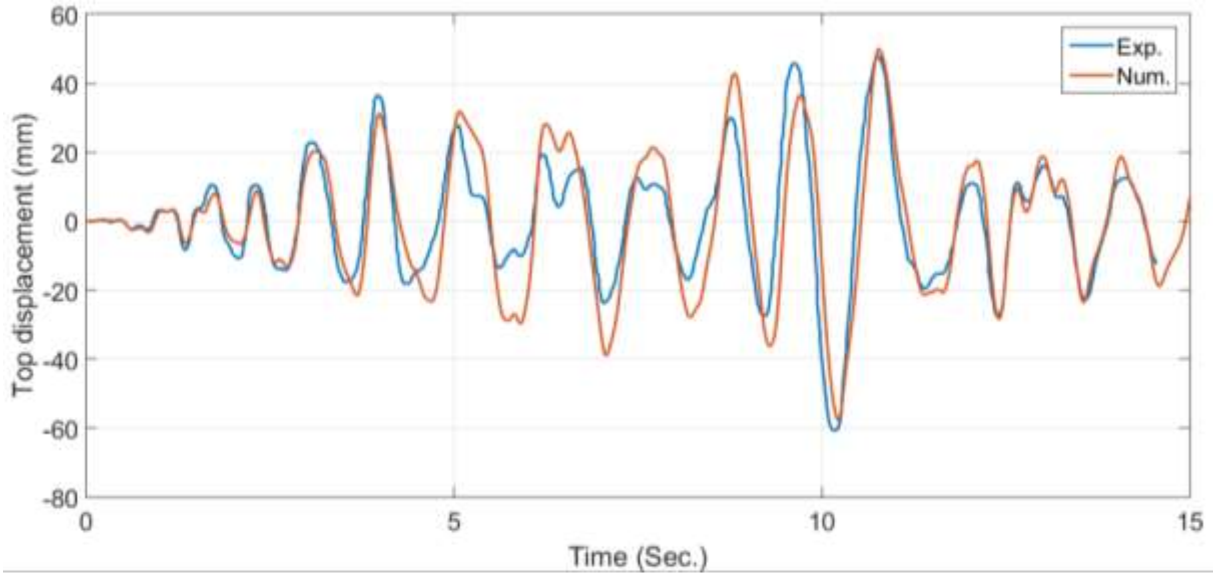

Figure 3.23. Top story displacement of numerical and experimental results for Case-1 according to ACI-31

Table 3.12. Comparison maximum peak displacements obtained from Model-B according to ACI-318 and from experiment tests.

	Differences (%)																Mean Differences (%)
Time (sec)	3.05	3.56	3.96	4.51	5.05	5.78	6.41	7.07	7.66	8.19	8.73	9.23	9.66	10.16	10.69	11.35	-----
Case 1	11.55	21.76	14.75	28.29	15.10	120.6	39.64	67.46	68.21	63.04	42.33	31.80	20.41	4.73	4.33	9.78	35.24
Case 2	10.81	12.12	9.48	6.74	13.94	69.79	16.15	7.46	24.57	4.59	5.36	7.04	9.56	5.13	15.21	33.81	15.74
Case 3	7.84	6.97	6.06	4.86	7.97	32.89	5.46	8.41	3.77	12.18	0.60	16.74	3.01	9.31	22.15	42.87	11.94
Case 4	1.53	9.46	1.81	16.57	7.03	17.04	17.29	1.08	14.52	23.78	6.32	23.09	1.24	10.68	24.87	46.94	13.95
Case 5	4.18	22.61	2.30	21.44	11.88	36.31	17.39	2.28	10.52	14.77	10.35	3.98	2.25	9.18	26.07	55.79	15.71

Table 3.13. Differences of damaged ratio obtained from Model-B according to ACI-318 and from experiment tests.

	Differences (%)																																Mean Differences (%)
Column No.	C11-L	C11-U	C12-L	C12-U	C13-L	C13-U	C14-L	C14-U	C21-L	C21-U	C22-L	C22-U	C23-L	C23-U	C24-L	C24-U	C31-L	C31-U	C32-L	C32-U	C33-L	C33-U	C34-L	C34-U	C41-L	C41-U	C42-L	C42-U	C43-L	C43-U	C44-L	C44-U	
Case 1	0	0	20	20	60	60	20	0	40	20	40	40	40	20	20	0	0	0	20	20	40	40	20	0	0	0	20	20	20	40	40	0	21.25
Case 2	0	0	20	20	60	60	0	0	40	20	40	40	40	0	20	0	0	0	20	20	60	40	20	0	0	0	20	20	40	20	40	0	20.625
Case 3	0	0	20	20	60	60	20	0	20	20	40	40	40	0	20	0	0	0	20	20	40	40	20	0	0	0	20	20	20	40	40	0	20
Case 4	0	0	20	20	60	60	20	0	20	20	40	40	40	40	20	0	0	0	20	20	60	60	0	20	0	20	20	20	20	40	40	0	23.125
Case 5	0	0	20	20	60	60	0	20	0	20	40	40	40	40	20	0	0	0	20	20	60	60	0	20	0	20	20	20	20	40	20	20	22.5

Table 3.14. Comparison of material properties obtained from Model-B according to ACI-318 by using reverse engineering and from experiment test.

	Compressive Strength (MPa)	Tensile Strength (MPa)	Elasticity Modulus (MPa)
Reverse Engineering	14	2.08	17585.79
Laboratory Test Results	16.3	1.90	18975
Difference	14.11%	9.53%	7.32%

Comparison of material properties obtained from Model-B according to ACI-318 by using reverse engineering and from experiment tests were given in Table 3.14. Difference was defined as 14.11% for compressive strength. However, differences for tensile strength and elasticity modulus were computed as 9.53% and 7.32%, respectively.

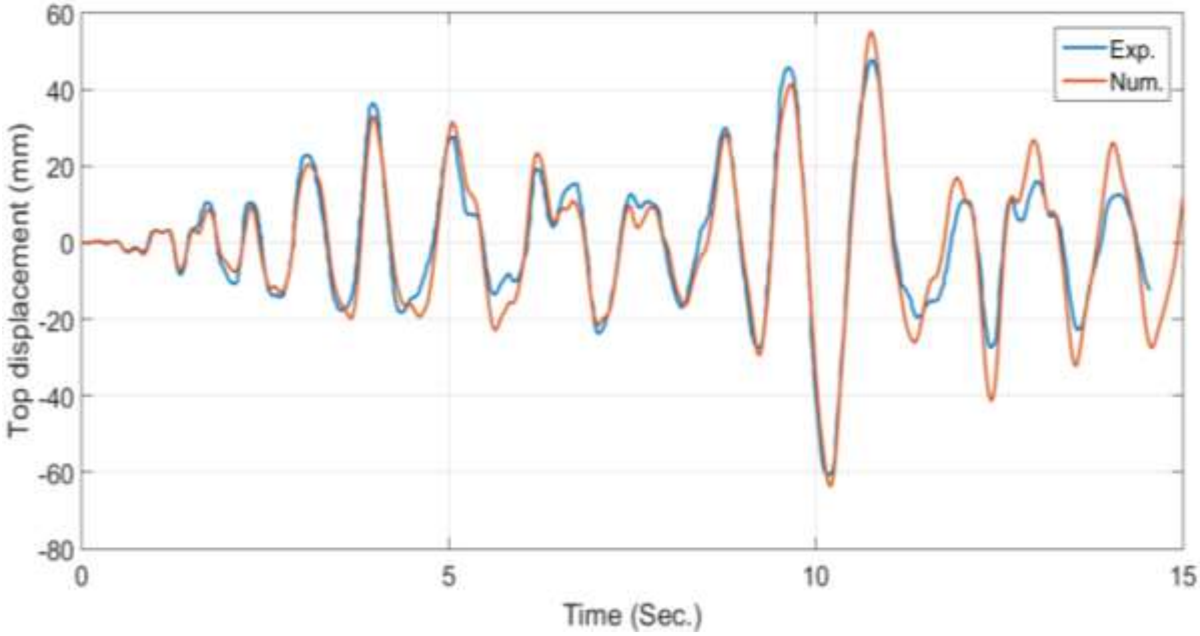

Figure 3.24. Top story displacement of numerical and experimental results for Case-2 according to ACI-318.

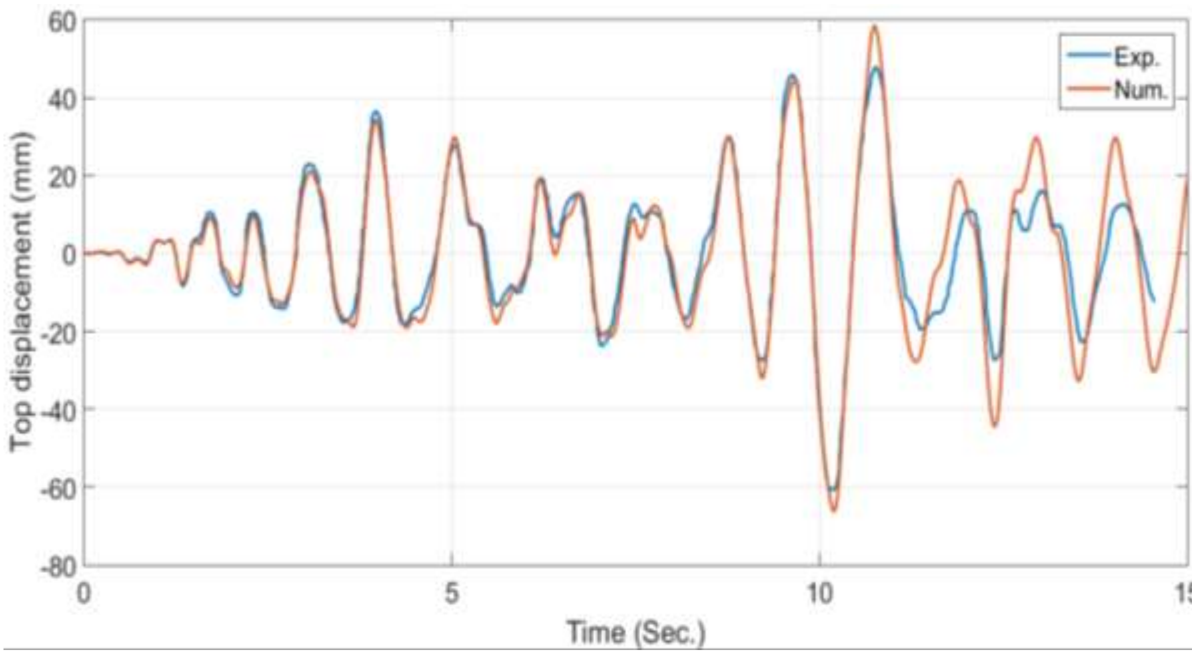

Figure 3.25. Top story displacement of numerical and experimental results for Case-3 according to ACI-318.

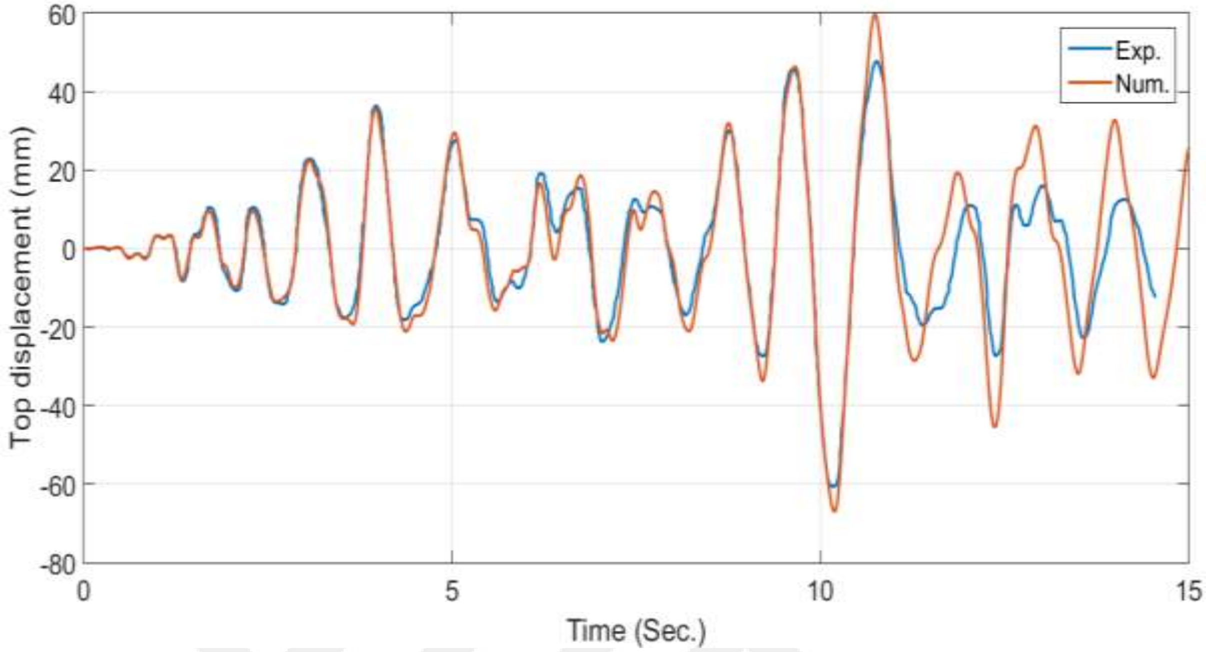

Figure 3.26. Top story displacement of numerical and experimental results for Case-4 according to ACI-318-318.

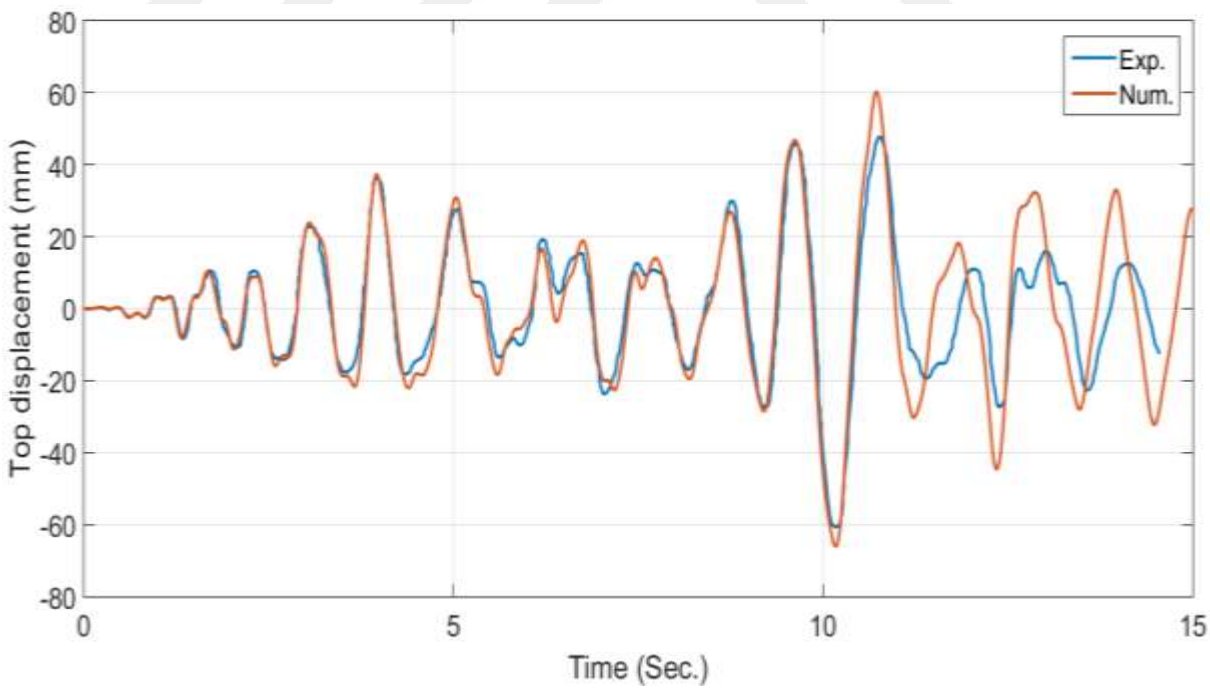

Figure 3.27. Top story displacement of numerical and experimental results for Case-5 according to ACI-318.

a) Case-1

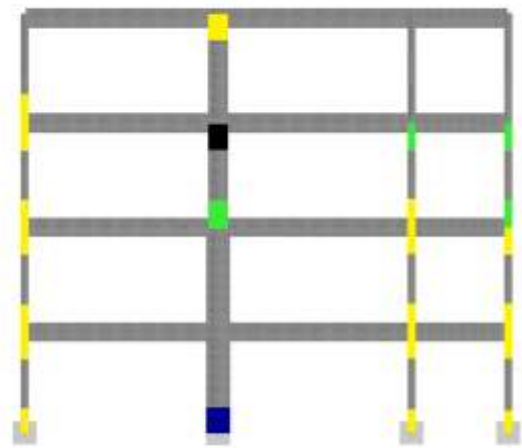

b) Case-2

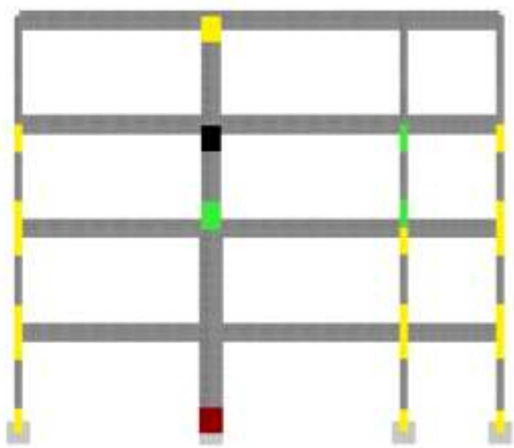

c) Case-3

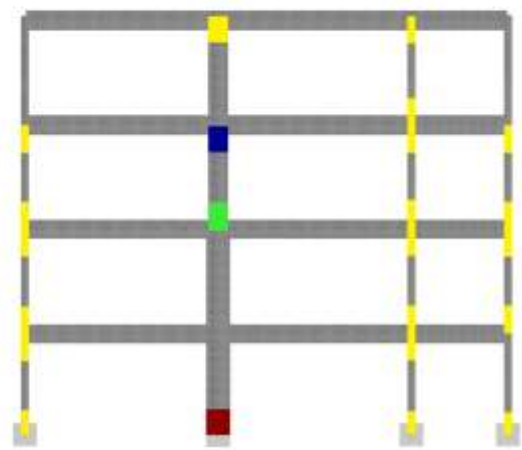

d) Case-4

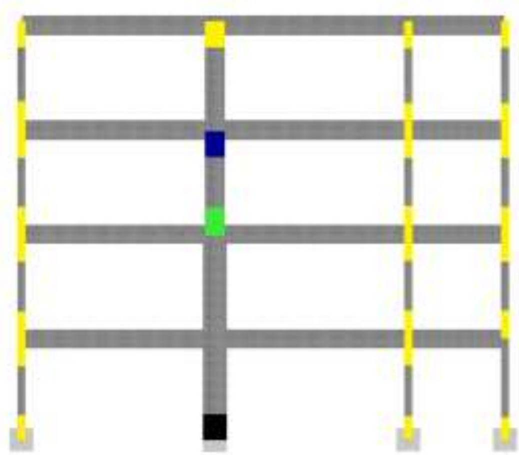

e) Case-5

Figure 3.28. Damage regions obtained from Model-B according to ACI-318 for all cases.

3.2.4.Comparison of Model-B according to TS 500

Top story displacement time history graphs of numerical and experimental results for Case-1, Case-2, Case-3, Case-4 and Case-5 according to TS 500 were shown in Figure 3.29-Figure 3.33. Differences between displacements obtained from experimental and numerical results were determined and mean of the differences were given in Table 3.15. Mean differences between experimental and the Case-1, Case-2, Case-3, Case-4, Case-5 numerical solutions were computed as 39.33%, 16.71%, 17.39%, 15.85% and 18.01%, respectively. Minimum difference was obtained for Case-4 solution.

Damage regions obtained from Model-A according to ACI-318 under earthquake loading with 975 years return period were given in Figure 3.34. Differences between damage ratios obtained from experimental and numerical results were determined and mean of the differences were given in Table 3.16. Mean differences between experimental and the Case-1, Case-2, Case-3, Case-4, Case-5 numerical solutions were calculated as 19.4%, 19.4%, 20%, 20% and 19.4%, respectively. Minimum difference was obtained for Case-1, Case-2 and Case-5 solutions. In the solutions obtained from Model-B according to TS 500, no agreements were observed for the differences between numerical and experimental results with regard to top displacement and damage ratio.

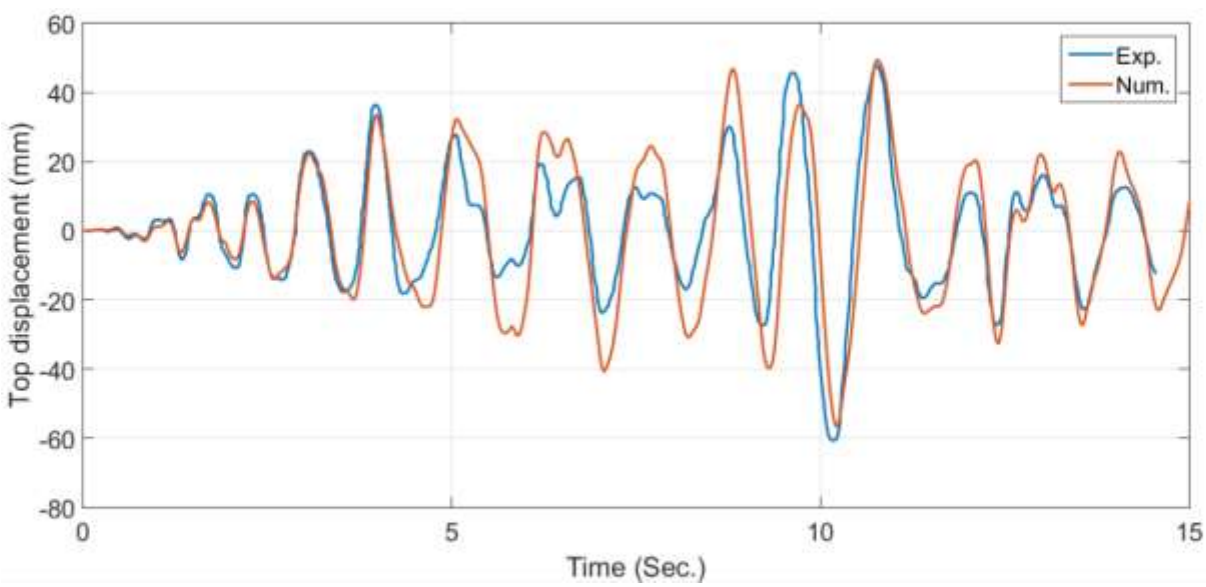

Figure 3.29. Top story displacement of numerical and experimental results for Case-1 according to TS 500.

Table 3.15. Comparison maximum peak displacements obtained from Model-B according to TS 500 and from experiment tests.

	Differences (%)																Mean Differences (%)
Time (sec)	3.05	3.56	3.96	4.51	5.05	5.78	6.41	7.07	7.66	8.19	8.73	9.23	9.66	10.16	10.69	11.35	-----
Case 1	2.27	12.41	8.44	21.27	16.88	125.7	41.23	74.74	92.15	80.99	55.51	45.11	20.44	6.53	3.18	22.44	39.33
Case 2	1.83	6.80	4.44	9.56	14.74	91.59	31.99	5.34	0.55	5.24	8.75	7.55	7.03	9.79	18.60	43.59	16.71
Case 3	7.02	7.25	1.01	8.07	11.81	76.12	18.68	22.84	28.89	9.18	12.21	1.86	6.72	8.71	19.92	37.93	17.39
Case 4	9.02	12.92	2.17	17.68	12.79	69.57	5.91	13.75	9.89	0.59	8.79	4.85	3.38	9.71	22.95	49.72	15.85
Case 5	13.12	16.66	5.43	26.96	10.87	48.66	3.73	0.43	18.21	21.48	5.92	11.09	1.40	12.67	28.05	63.46	18.01

Table 3.16. Differences of damaged ratio obtained from Model-B according to TS 500 and from experiment tests.

	Differences (%)																																Mean Differences (%)
Column No.	C11-L	C11-U	C12-L	C12-U	C13-L	C13-U	C14-L	C14-U	C21-L	C21-U	C22-L	C22-U	C23-L	C23-U	C24-L	C24-U	C31-L	C31-U	C32-L	C32-U	C33-L	C33-U	C34-L	C34-U	C41-L	C41-U	C42-L	C42-U	C43-L	C43-U	C44-L	C44-U	
Case 1	0	0	20	20	60	60	0	20	40	0	40	40	20	20	20	0	0	0	20	20	40	40	0	20	0	0	20	20	20	20	40	0	19.375
Case 2	0	0	20	20	60	60	0	20	20	20	40	40	20	0	20	0	0	0	20	20	40	40	20	0	0	0	20	20	40	20	40	0	19.375
Case 3	0	0	20	20	60	60	0	20	20	20	40	40	20	20	20	0	0	0	20	20	40	40	0	20	0	0	20	20	40	20	40	0	20
Case 4	0	0	20	20	60	60	0	20	20	20	40	40	20	20	20	0	0	0	20	20	40	40	0	20	0	0	20	20	40	20	40	0	20
Case 5	0	0	20	20	60	60	0	20	0	20	40	40	20	20	20	0	0	0	20	20	40	40	0	20	0	0	20	20	20	40	20	20	19.375

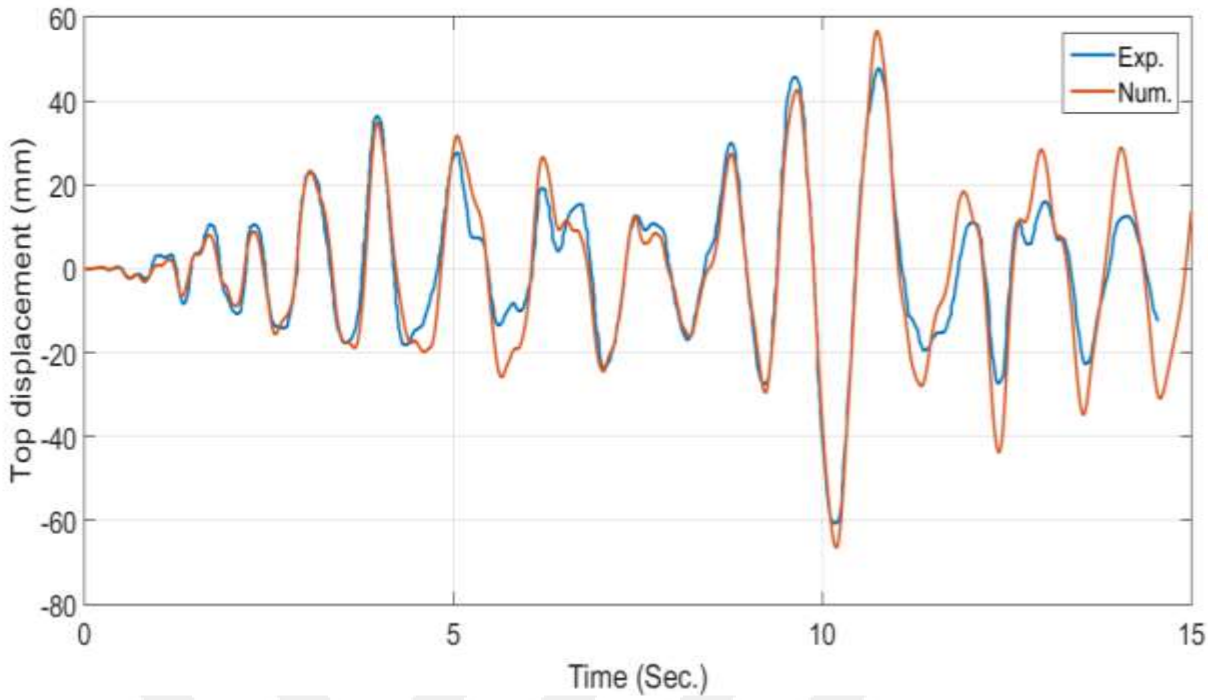

Figure 3.30. Top story displacement of numerical and experimental results for Case-2 according to TS 500.

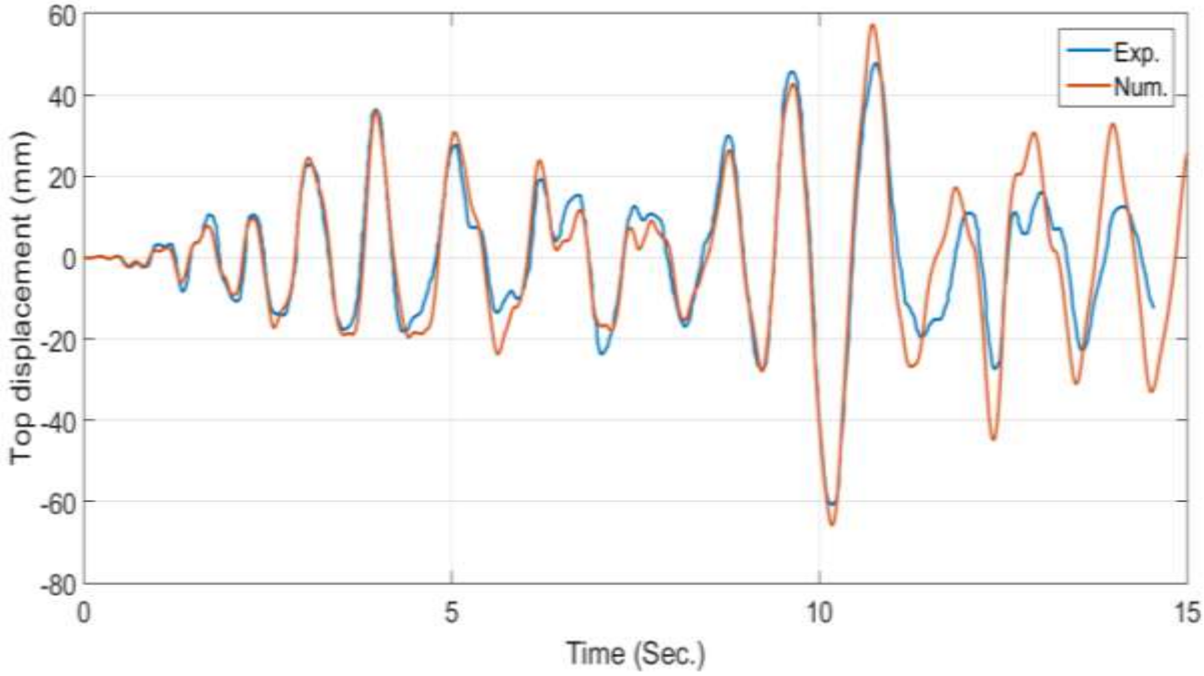

Figure 3.31. Top story displacement of numerical and experimental results for Case-3 according to TS 500.

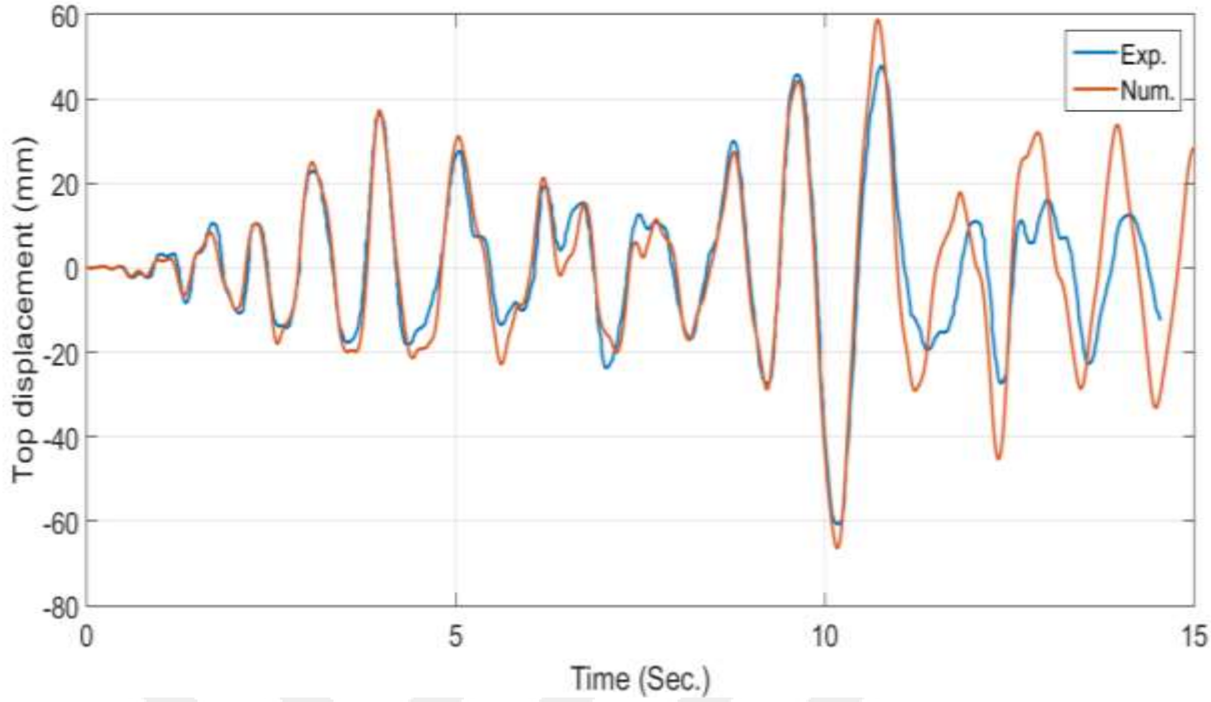

Figure 3.32. Top story displacement of numerical and experimental results for Case-4 according to TS 500.

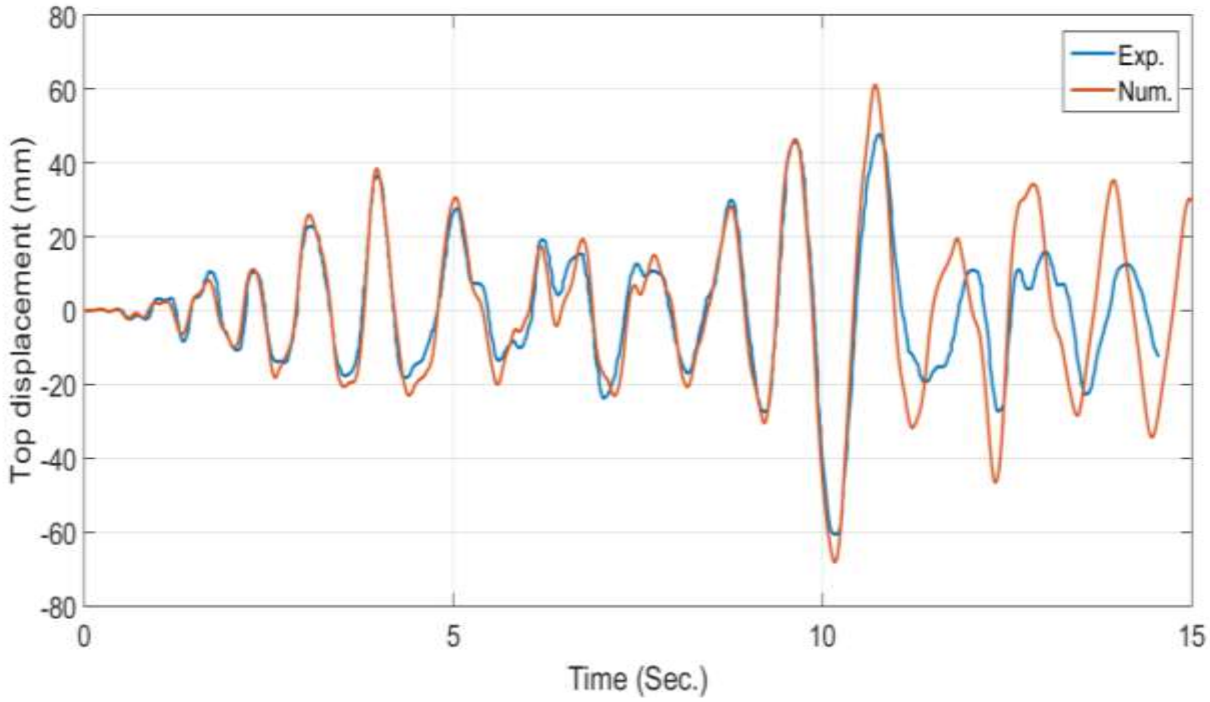

Figure 3.33. Top story displacement of numerical and experimental results for Case-5 according to TS 500.

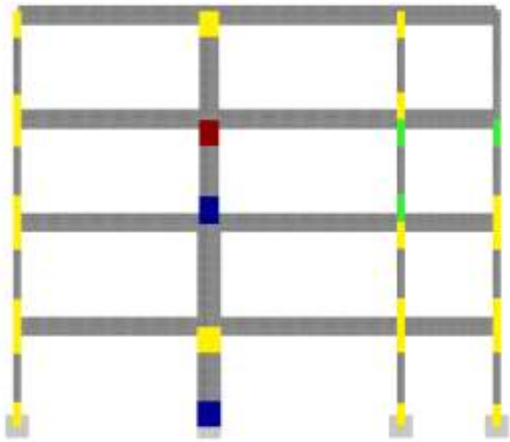

a) Case-1

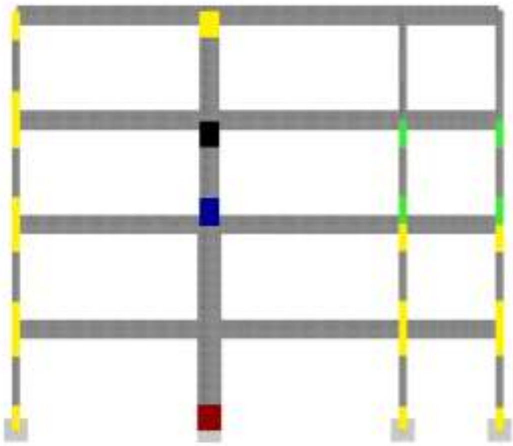

b) Case-2

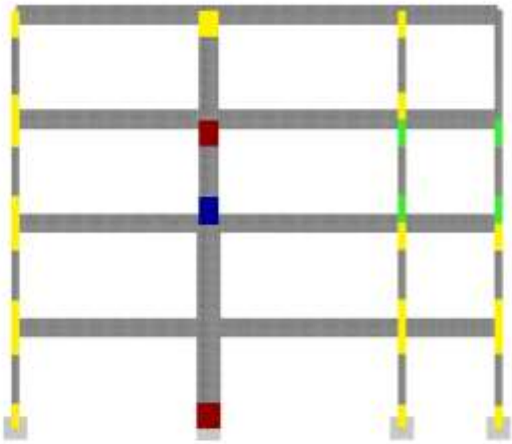

c) Case-3

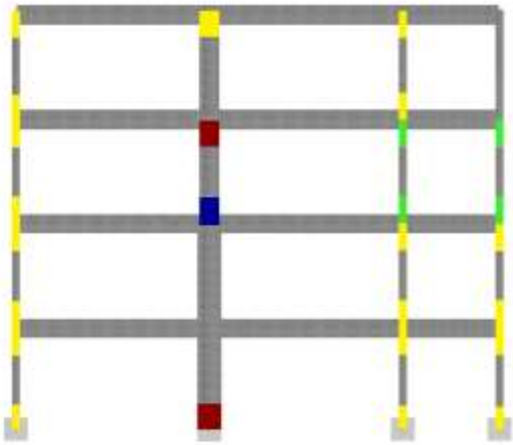

d) Case-4

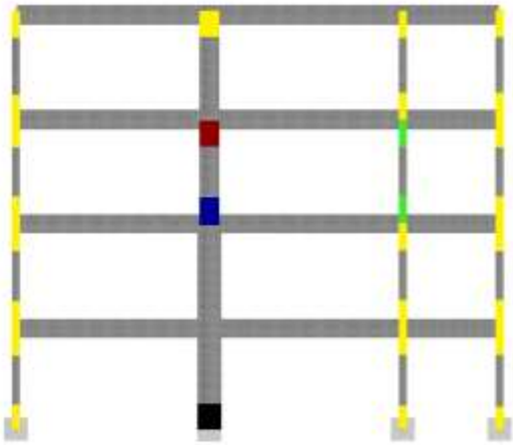

e) Case-5

Figure 3.34. Damage regions obtained from Model-B according to TS 500 for all cases.

3.2.5.Fiber Element Number Effect on the Numerical Solution

In this subsection, the effect on numerical solution of fiber element number was investigated. In the numerical analyses, Case-3 for Model-A and Model-B according to ACI-318 were used. 16 peak points of top displcement time history graph were selected for comparison of numerical and experimental results Figure 3.35, Figure 3.36. This comparison were given in Table 3.17 and Table 3.18. Each cross section was divided as 100, 200, 300, 400, 500, 600, 700 and 800 fiber element number for the Model A. In this model, mean differences were determined as 21.56%, 20.33%, 18.98%, 17.87%, 17.59%, 17.25%, 17.38% and 17.40% for fiber element number 100, 200, 300, 400, 500, 600, 700 and 800, respectively. Optimum fiber element number was obtained for 600.

Additional solutions were obtained for the Model B and each cross section was divided to 100, 200, 300, 400 and 500 fiber element number. In numerical results of the model, mean differences were determined as 12.07%, 11.94%, 11.26%, 11.74% and 11.84% for fiber element number 100, 200, 300, 400 and 500, respectively. Optimum difference was obtained as 11.26% for solution with 300 fiber element number.

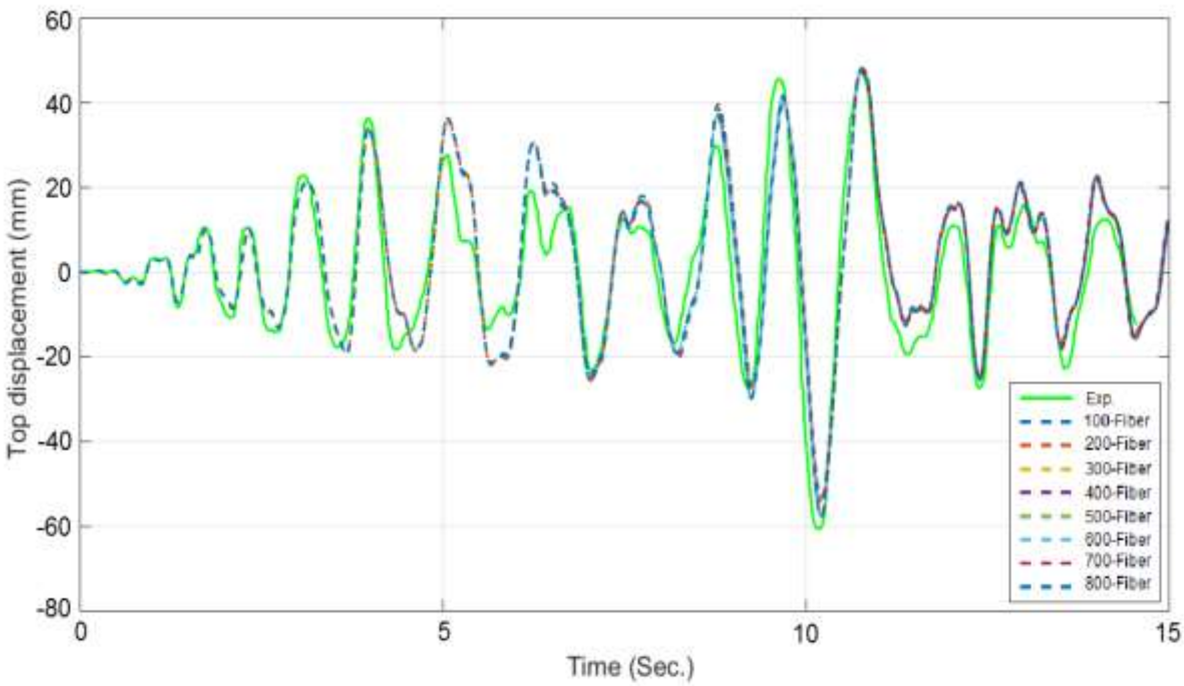

Figure 3.35. Numerical Model-A according to ACI-318, Case-3

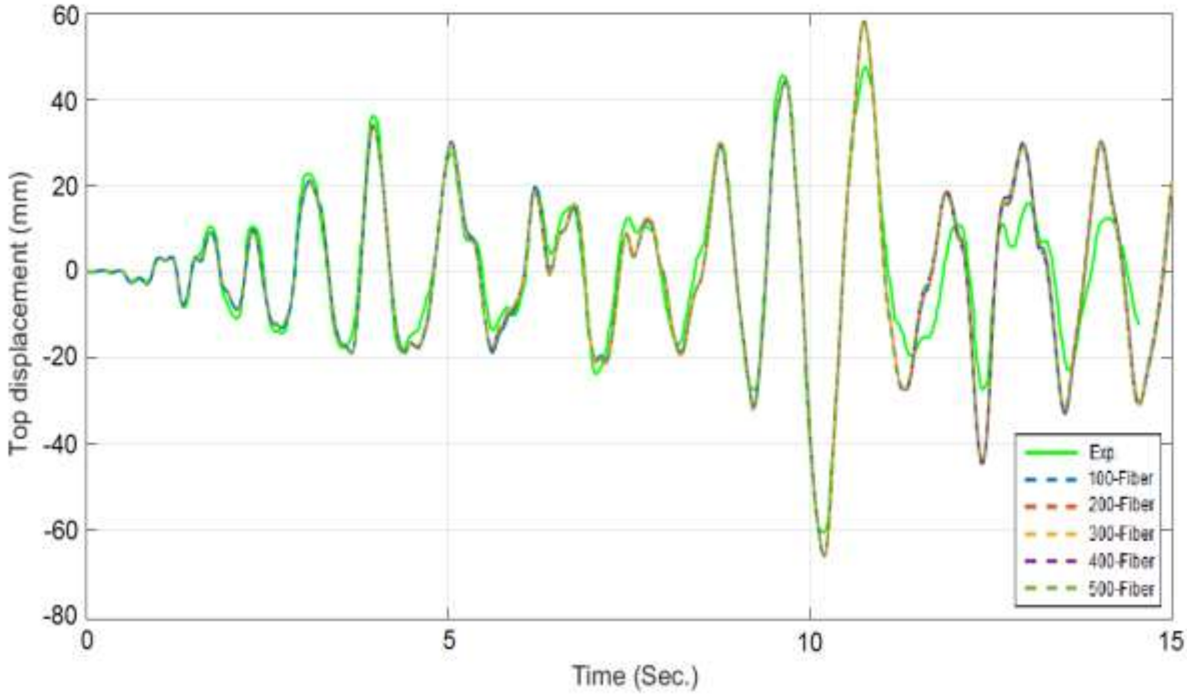

Figure 3.36. Numerical Model-B according to ACI-318, Case-3

Table 3.17. Comparison between experimental data and Model-A, Case-3

Fiber No.	**Differences (%)**																**Mean Differences (%)**
Time (sec)	3.05	3.56	3.96	4.51	5.05	5.78	6.41	7.07	7.66	8.19	8.73	9.23	9.66	10.16	10.69	11.35	
100- fiber	6.71	8.95	6.41	1.60	32.96	62.80	52.11	12.63	41.44	20.07	32.21	1.50	11.88	11.76	1.44	40.50	21.56
200- fiber	7.67	9.69	7.51	2.32	31.84	63.84	51.22	10.43	37.28	17.13	29.42	0.73	9.39	10.02	0.02	36.75	20.33
300- fiber	7.10	10.14	6.36	1.33	31.91	62.35	50.02	6.51	32.18	13.83	25.22	8.24	8.76	4.51	0.21	35.05	18.98
400- fiber	6.88	10.25	6.30	1.44	31.80	61.61	51.71	6.12	11.38	12.65	24.49	8.86	8.78	4.91	1.00	37.73	17.87
500- fiber	6.84	10.20	6.17	1.27	31.76	61.16	51.52	5.60	11.22	12.18	24.13	8.86	8.82	4.56	0.98	36.18	17.59
600- fiber	6.80	10.08	6.14	0.88	31.87	60.79	51.22	4.83	10.52	11.30	23.33	8.86	8.41	4.05	1.21	35.72	17.25
700- fiber	6.58	9.80	5.98	0.72	31.98	60.19	50.82	6.21	10.75	13.18	24.43	8.24	9.04	4.65	0.21	35.31	17.38
800- fiber	6.62	9.80	5.95	0.77	31.98	60.04	50.72	5.99	11.77	12.95	24.53	8.42	8.67	4.38	0.77	35.05	17.40

Table 3.18. Comparison between experimental data and Model-B, Case-3

Fiber No.	**Differences (%)**																**Mean Differences (%)**
100- fiber	7.49	7.37	5.98	2.65	9.89	39.36	1.54	11.29	6.44	9.71	2.03	14.26	3.23	9.36	21.76	40.71	12.07
200- fiber	7.84	6.97	6.06	4.86	7.97	32.89	5.46	8.41	3.77	12.18	0.60	16.74	3.01	9.31	22.15	42.87	11.94
300- fiber	6.62	6.40	6.11	5.47	7.10	28.87	6.81	7.54	0.71	14.13	1.03	17.51	3.32	8.76	20.77	39.06	11.26
400- fiber	6.32	6.86	5.59	5.80	7.93	31.70	5.91	9.61	1.41	13.13	0.27	16.89	2.82	9.14	21.99	42.56	11.74
500- fiber	6.45	7.08	5.59	9.94	7.93	30.13	6.56	9.66	1.02	13.83	0.10	16.96	3.08	9.04	22.07	39.99	11.84

3.3. Investigation of a Bridge Pier with Reverse Engineering Method

A full scale 7.32m tall bridge pier was selected as second case study for verification of the numerical models validity in this thesis. Diameter of the circular pier was 1.22m Figure 3.37. The bridge pier was tested in Pacific Earthquake Engineering Research Center (PEER) under ten consequent artificial accelerations respectively by using shaking table dynamic testing. The response of the pier bridge was recorded in terms of top displacement, base shear, etc. Damaged regions with the level of damage also recorded after each acceleration loading. For verification of the numerical models, the results of the 3rd earthquake test was used because in that test significant damage occurred [2].

In the proposed numerical solution scheme, different material properties are predicted. The data for the numerical models was changed gradually for different numerical cases according to the reverse engineering method for ACI-318 and TS-500.

Figure 3.37. General layout of the tested bridge pier [2].

Two numerical models verified by using SeismoStruct-2016 software package, Model-A force based and Model-B displacement based. Mander et al. model is used for uniaxial reversal response of the concrete material. The Menegotto-Pinto steel model is selected for nonlinear behavior of the steel material.

3.3.1.Reverse Engineering Approach for The Bridge Pier.

In the reverse engineering method proposed in this thesis, firstly, it is assumed that material properties of structural steel is known, However, four different material class cases for concrete predicted to Model–A and six different material class cases predicted for Model-B. At the same time, these predictions were obtained according to the American Concrete Institute (ACI-318) and the Turkish Reinforced Concrete Design Code (TS 500). Elasticity modulus (E_c) and uniaxial tensile strength (f_{ct}) of concrete are depending on the uniaxial compressive strength (f_{cc}) of concrete for both codes. E_c and f_{ct} values according to TS 500 and ACI-318 codes are defined by using equations (3.4)-(3.5) and equations (3.6)-(3.7), respectively. Predicted material properties of concrete for both codes were given in Table 3.19, Table 3.20, Table 3.21 and Table 3.22 according to Force Based Approach (Model A) and Displacement Based Approach (Model B), respectively.

Table 3.19. Concrete material properties according to ACI-318 for Model-A.

	Compressive Strength of concrete (MPa)	Tensile strength of concrete (MPa)	Modulus of elasticity (MPa)
Case-1	26	2.84	23965
Case-2	28	2.94	24870
Case-3	30	3.05	25743
Case-4	32	3.15	26587

Table 3.20. Concrete material properties according to TS 500 for Model-A.

	Compressive Strength of concrete (MPa)	Tensile strength of concrete (MPa)	Modulus of elasticity (MPa)
Case-1	26	1.78	30572
Case-2	28	1.85	31197
Case-3	30	1.92	31800
Case-4	32	1.98	32384

Table 3.21. Concrete material properties according to ACI-318 for Model-B

	Compressive Strength of concrete (MPa)	Tensile strength of concrete (MPa)	Modulus of elasticity (MPa)
Case-1	25	2.78	23500
Case-2	26	2.84	23965
Case-3	27	2.89	24421
Case-4	28	2.94	24870
Case-5	29	2.99	25310
Case-6	30	3.05	25743

Table 3.22. Concrete material properties according to TS 500 for Model-B

	Compressive Strength of concrete (MPa)	Tensile strength of concrete (MPa)	Modulus of elasticity (MPa)
Case-1	25	1.75	30250
Case-2	26	1.78	30572
Case-3	27	1.82	30887
Case-4	28	1.85	31197
Case-5	29	1.88	31502
Case-6	30	1.92	31800

Comparison for top displacements between the experimental and numerical results obtained for the bridge pier, four maximum peak displacement points in the time history graphs for each case were selected. In the example, damage regions obtained from numerical analysis were not compared with experimental results because same damage level (severe damage) was observed for all numerical models.

3.3.2. Comparison of Model-A according to ACI-318

Top story displacement time history graphs of numerical and experimental results for Case-1 to Case-4 according to ACI-318 are shown in Figure 3.38-Figure 3.41. Differences between displacements obtained from experimental and numerical results are determined and mean values of the differences are given in Table 3.23. Mean differences between experimental with numerical solutions of the Case-1, Case-2, Case-3 and Case-4 were obtained as 4.2%, 3.2%, 2.4% and 3.0%, respectively. Minimum difference is determined for Case-3 solution. Differences between experimental and numerical result of C30 concrete class for compressive strength and elasticity modulus of concrete are 0.0% and 7.2%, respectively Table 3.24.

Table 3.23. Comparison maximum top displacement obtained from Model-A according to ACI-318 and from experiment tests.

f_c (MPa)	Difference %				Mean Difference %
	Point-1	Point-2	Point-3	Point-4	
26	0.2	1.5	9.3	5.9	4.2
28	0.5	0.0	5.6	6.8	3.2
30	0.5	1.5	0.8	6.9	2.4
32	2.0	2.8	4.5	2.8	3.0

Table 3.24. Comparison of material properties obtained from Model-A according to ACI-318 by using reverse engineering and from experiment test.

	Compressive Strength (MPa)	Elasticity Modulus (MPa)
Reverse Engineering	30.0	25742.0
Laboratory Test Results	30.0	24000.0
Difference	0.0%	7.2 %

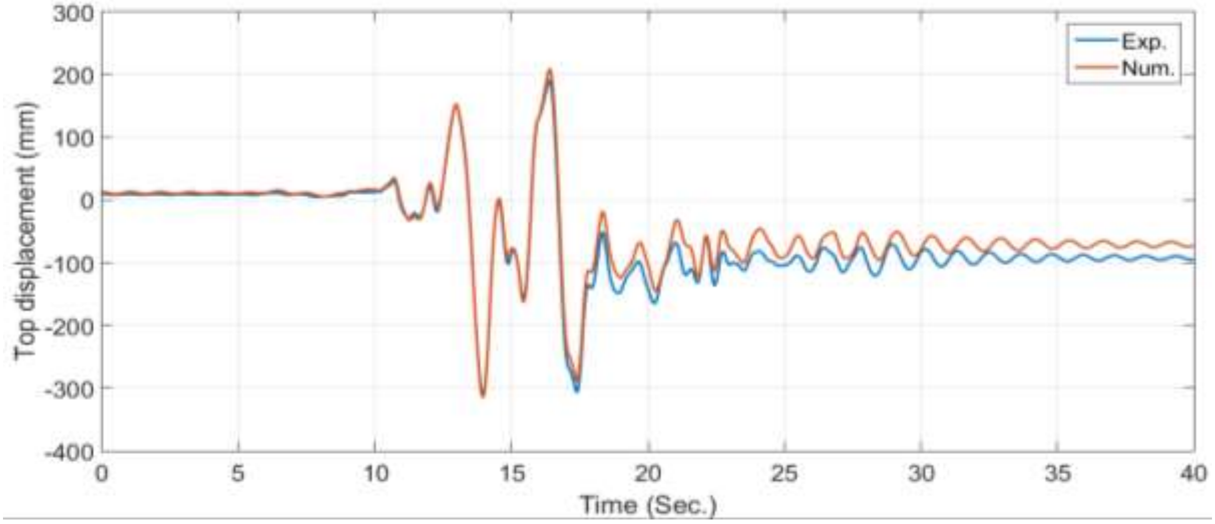

Figure 3.38. Top story displacement of numerical and experimental results for 26 MPa according to ACI-318.

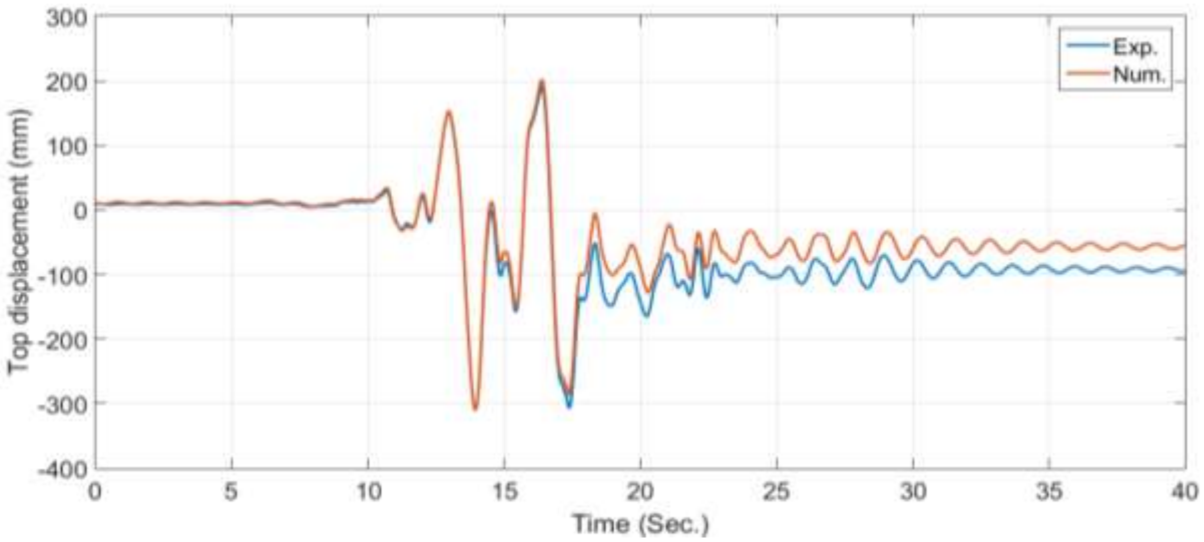

Figure 3.39. Top story displacement of numerical and experimental results for 28 MPa according to ACI-318.

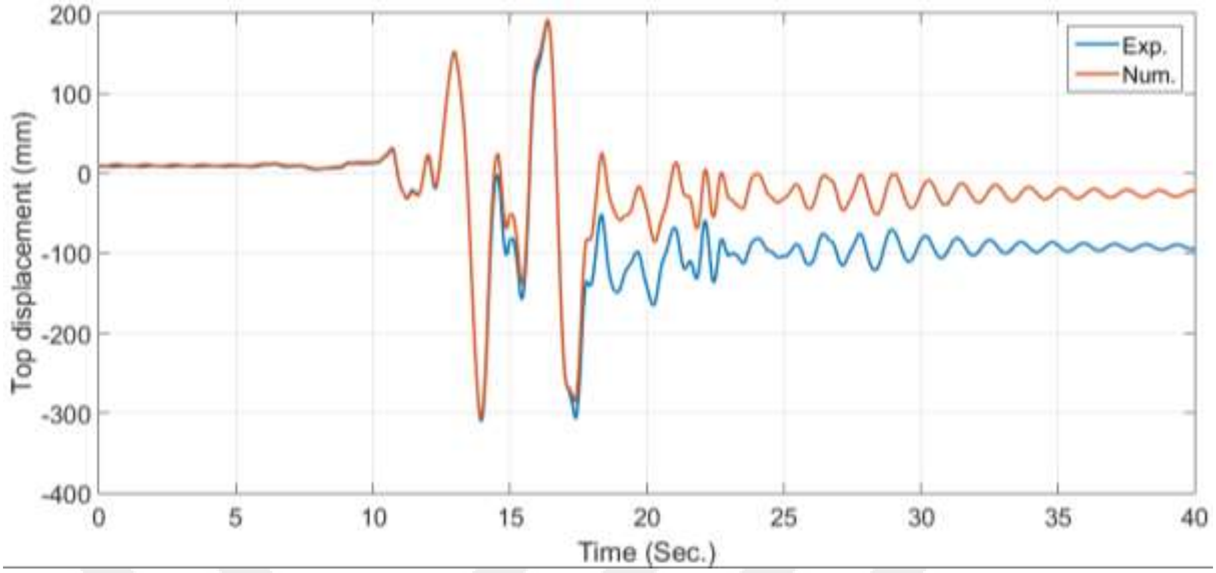

Figure 3.40. Top story displacement of numerical and experimental results for 30 MPa according to ACI-318.

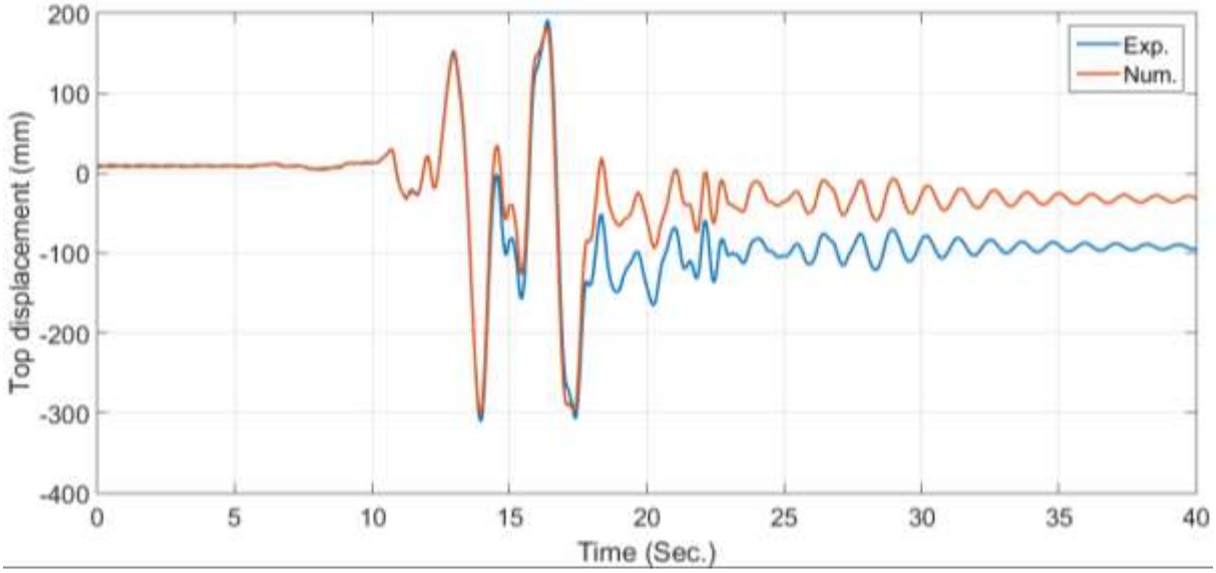

Figure 3.41. Top story displacement of numerical and experimental results for 32 MPa according to ACI-318.

3.3.3. Comparison of Model-B according to ACI-318

Top story displacement time history graphs of numerical and experimental results for Case-1, Case-2, Case-3, Case-4, Case-5 and Case-6 according to ACI-318 are shown in Figure 3.42-Figure 3.47. Differences between displacements obtained from experimental and numerical results were determined and mean of the differences were given in Table

3.25. Mean differences between experimental and the Case-1, Case-2, Case-3, Case-4, Case-5, Case-6 numerical solutions are 4.53%, 3.65%, 3.19%,3.66%, 3.76%, 3.88% and 3.98%, respectively. Minimum displacement difference is obtained for Case-3 solution.

Table 3.25. Comparison maximum top displacement obtained from Model-B according to ACI-318 and from experimental results.

f_c (MPa)	Difference %				Mean Difference %
	Point-1	Point-2	Point-3	Point-4	
25	2.2	1.1	4.5	10.4	4.53
26	2.4	0.3	1.9	10.0	3.65
27	2.4	0.5	0.4	9.5	3.19
28	2.2	1.2	2.4	8.8	3.66
29	2.5	2.2	2.6	7.7	3.76
30	3.6	3.4	1.6	7.0	3.88

Table 3.26. Comparison of material properties obtained from Model-B according to ACI-318 by using reverse engineering and from experiment test.

	Compressive Strength (MPa)	Elasticity Modulus (MPa)
Reverse Engineering	27.0	24422.0
Laboratory Test Results	30.0	24000.0
Difference	10 %	1.76 %

Differences between experimental and numerical result of C27 concrete class for compressive strength and elasticity modulus of concrete are 10.0% and 1.76%, respectively Table 3.26. The Force Based Fiber Element Method with regard to compressive strength of concrete is better than Displacement Based Fiber Element Method. The Displacement Based Fiber Element Method with regard to elasticity modulus of concrete is also given excellent result.

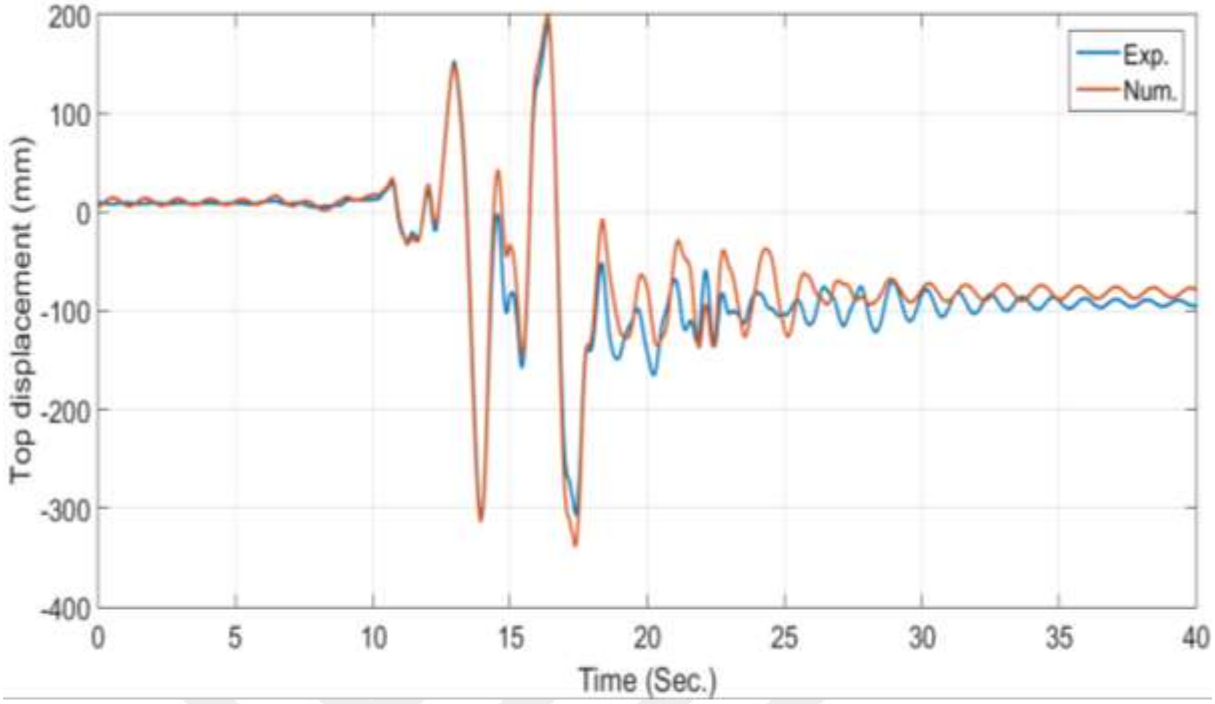

Figure 3.42. Top story displacement of numerical and experimental results for 25 MPa according to ACI-318.

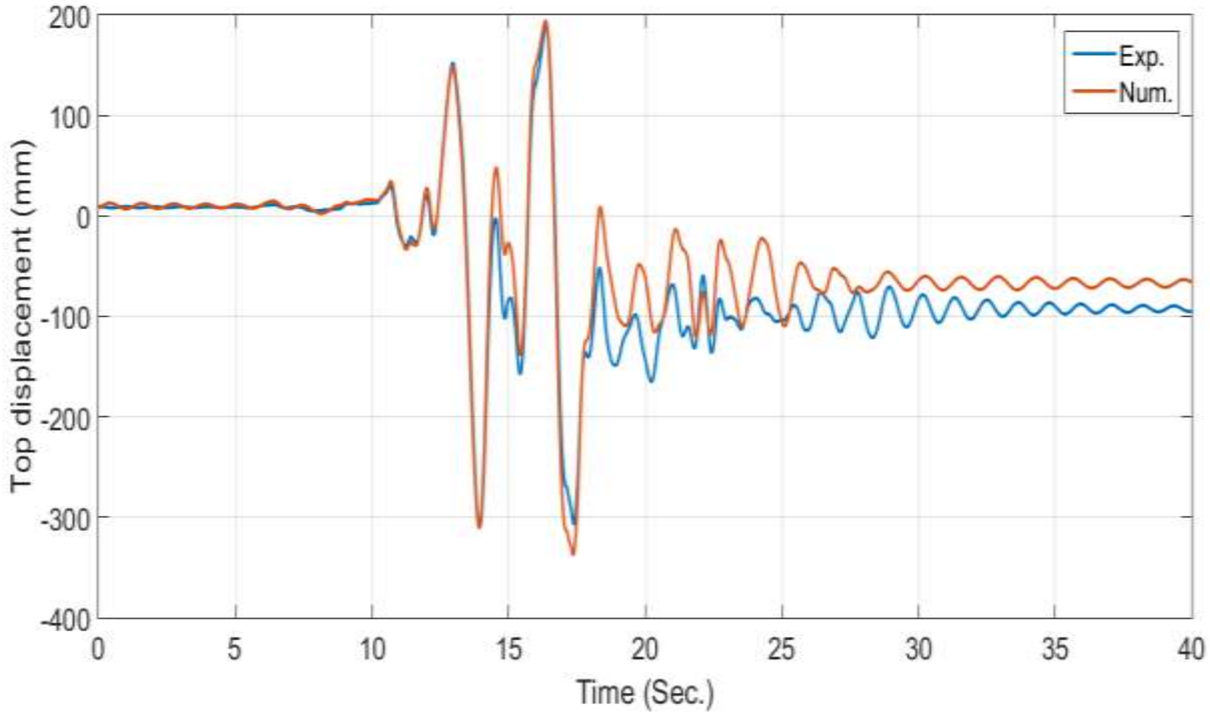

Figure 3.43. Top story displacement of numerical and experimental results for 26 MPa according to ACI-318.

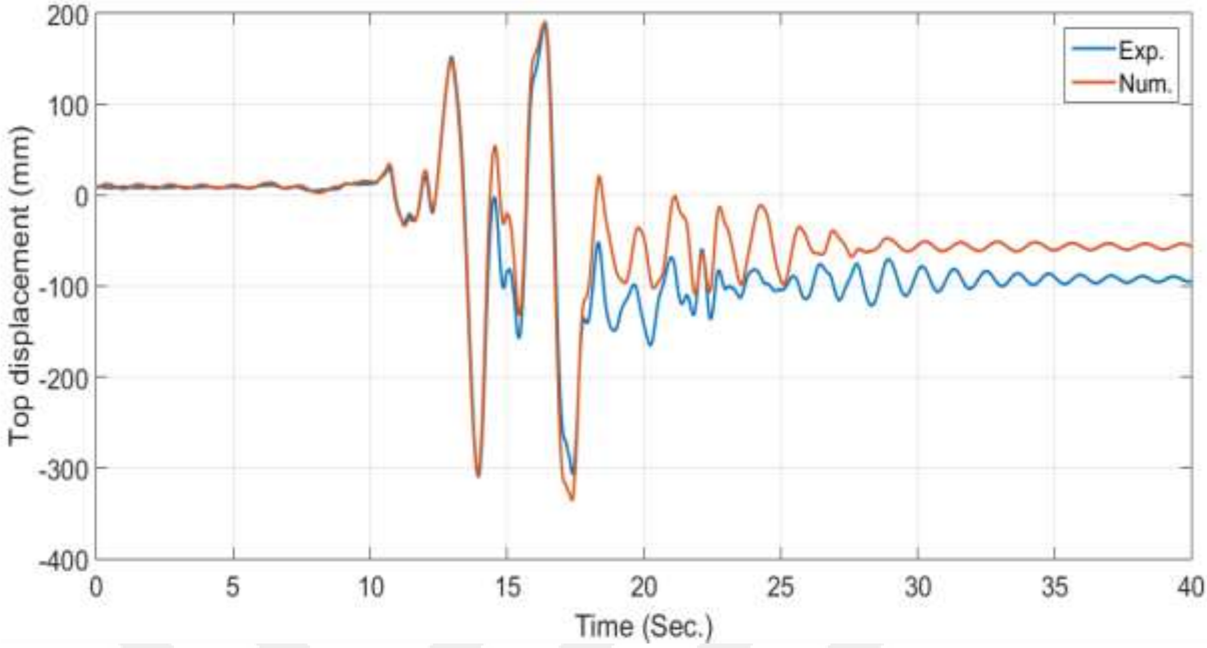

Figure 3.44. Top story displacement of numerical and experimental results for 27 MPa according to ACI-318.

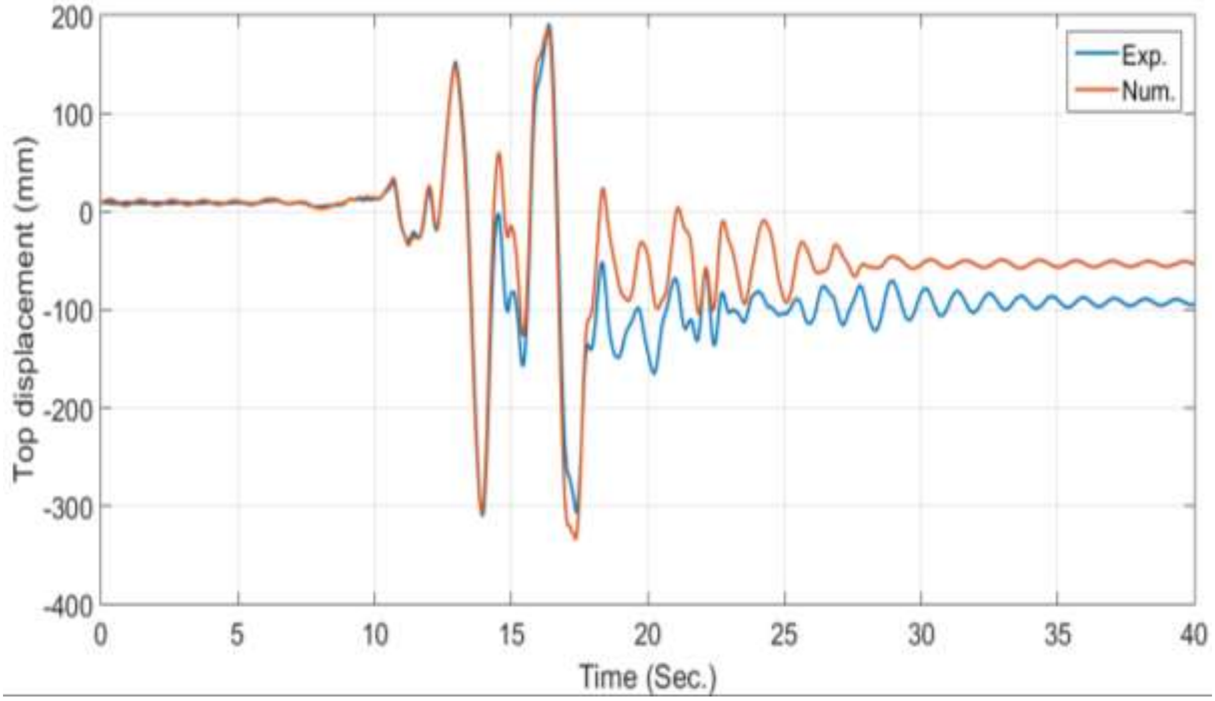

Figure 3.45. Top story displacement of numerical and experimental results for 28 MPa according to ACI-318.

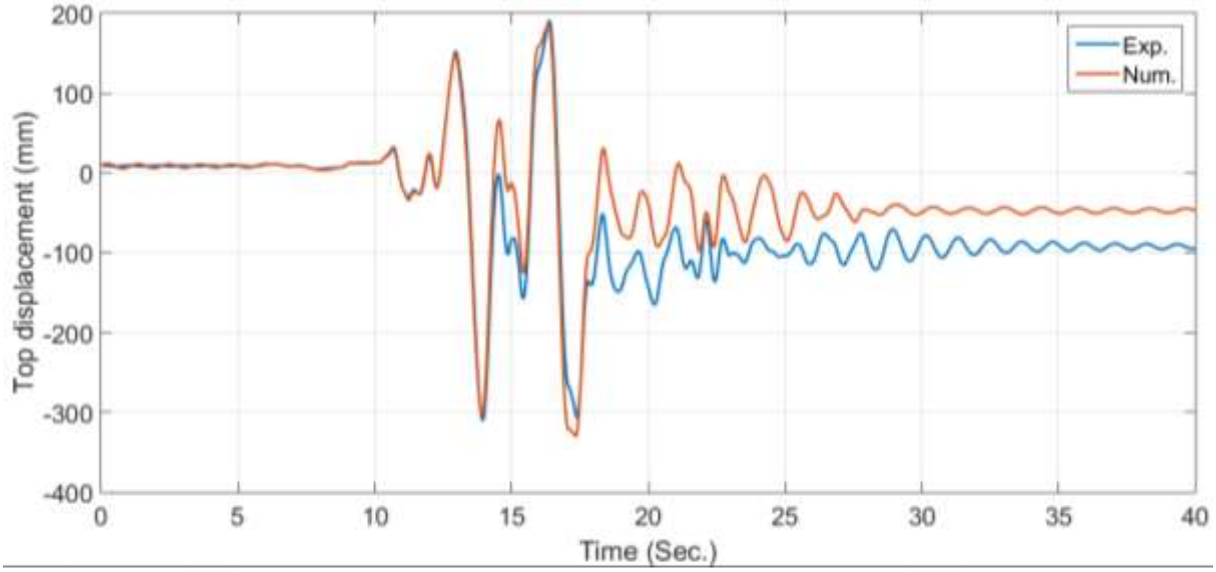

Figure 3.46. Top story displacement of numerical and experimental results for 29 MPa according to ACI-318.

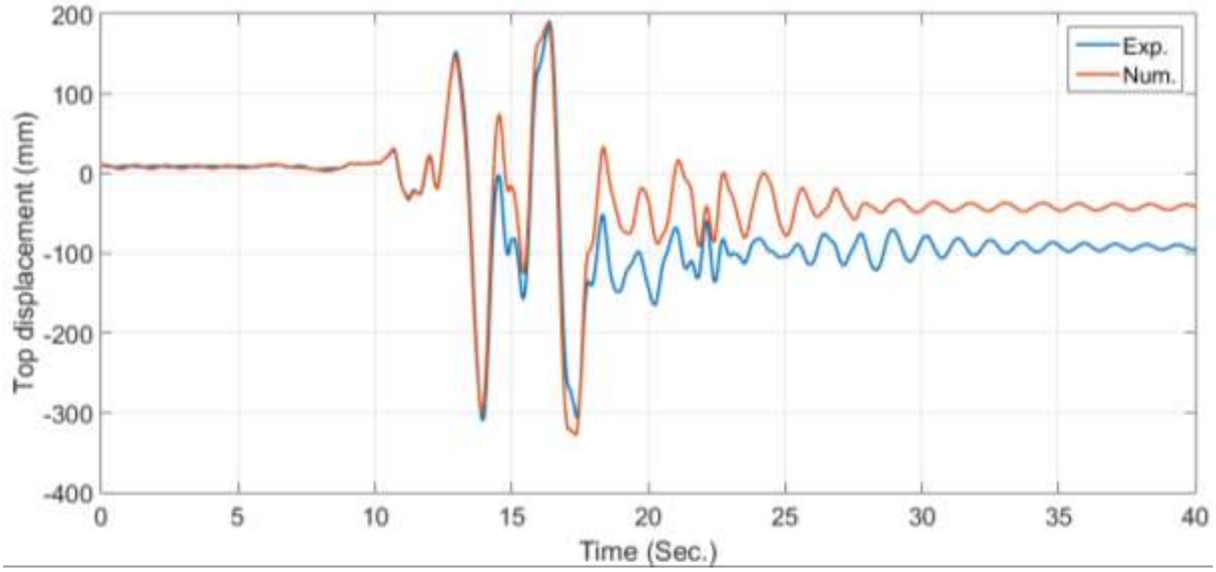

Figure 3.47. Top story displacement of numerical and experimental results for 30 MPa according to ACI-318.

3.3.4.Comparison of Model-A according to TS 500

Top story displacement time history graphs of numerical and experimental results for Case-1, Case-2, Case-3, and Case-4 according to TS 500 are shown in Figure 3.48-Figure 3.51. Differences between displacements obtained from experimental and numerical results were determined and mean of the differences were given in Table 3.27. Mean differences between experimental and the Case-1, Case-2, Case-3, Case-4 numerical solutions are 3.9%, 3.3%, 4.6% and 5.5%, respectively. Minimum difference was obtained for Case-2 solution.

Table 3.27. Comparison maximum top displacement obtained from Model-A according to TS 500 and from experimental results.

f_c (MPa)	Difference %				Mean Difference %
	Point-1	Point-2	Point-3	Point-4	
26	2.0	2.0	3.6	8.1	3.9
28	3.0	3.3	2.3	4.4	3.3
30	3.4	4.3	6.5	4.4	4.6
32	4.8	5.6	7.9	3.9	5.5

Table 3.28. Comparison of material properties obtained from Model-A according to TS 500 by using reverse engineering and from experiment test.

	Compressive Strength (MPa)	Elasticity Modulus (MPa)
Reverse Engineering	28	31197
Laboratory Test Results	30	24000
Difference	6.7 %	29.9 %

Differences between experimental and numerical result of C28 concrete class for compressive strength and elasticity modulus of concrete are 6.7% and 29.9%, respectively Table 3.28.

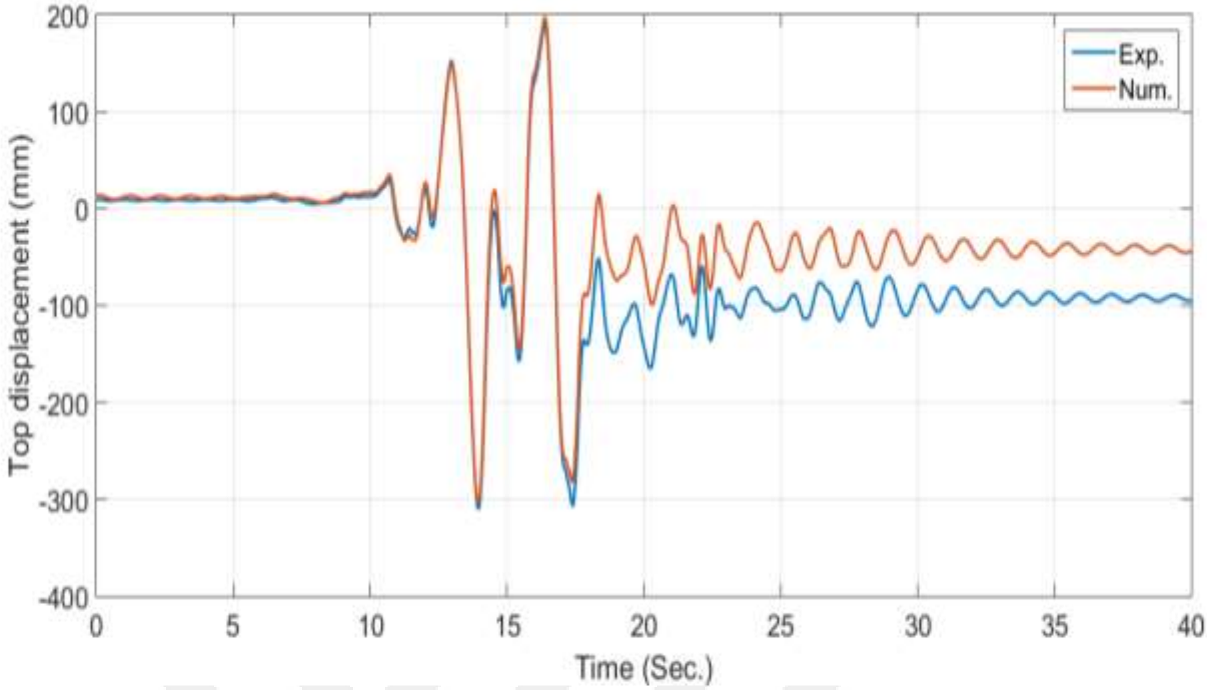

Figure 3.48. Top story displacement of numerical and experimental results for 26 MPa according to TS 500.

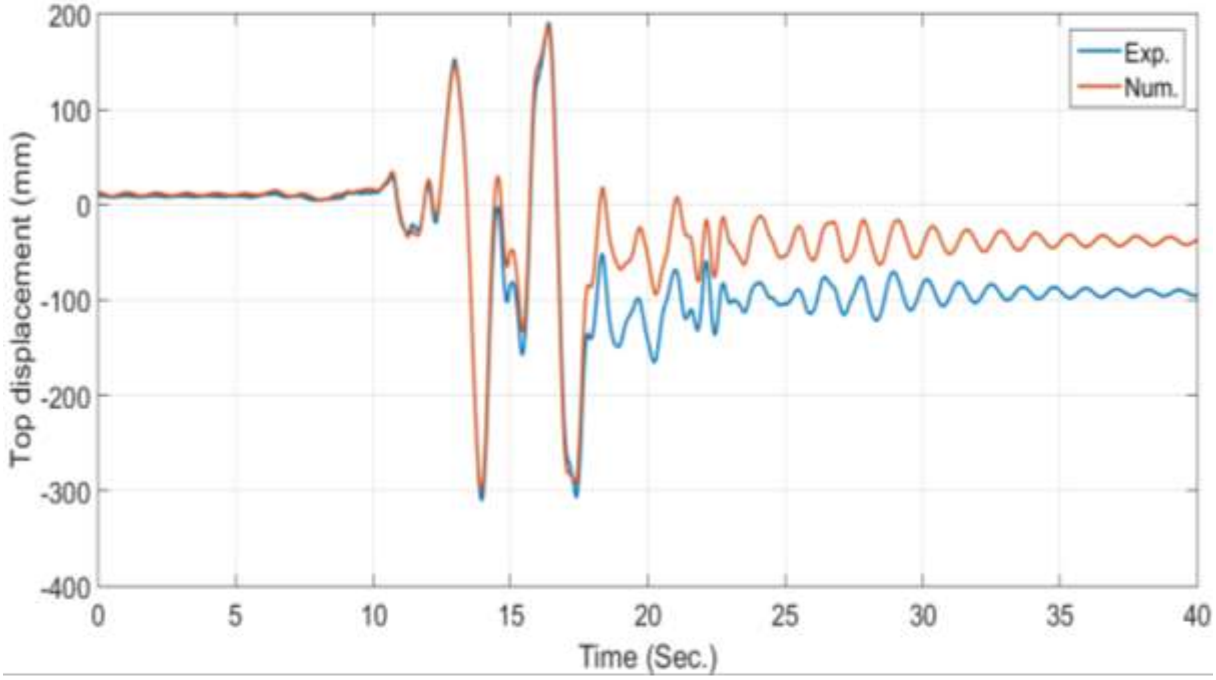

Figure 3.49. Top story displacement of numerical and experimental results for 28 MPa according to TS 500.

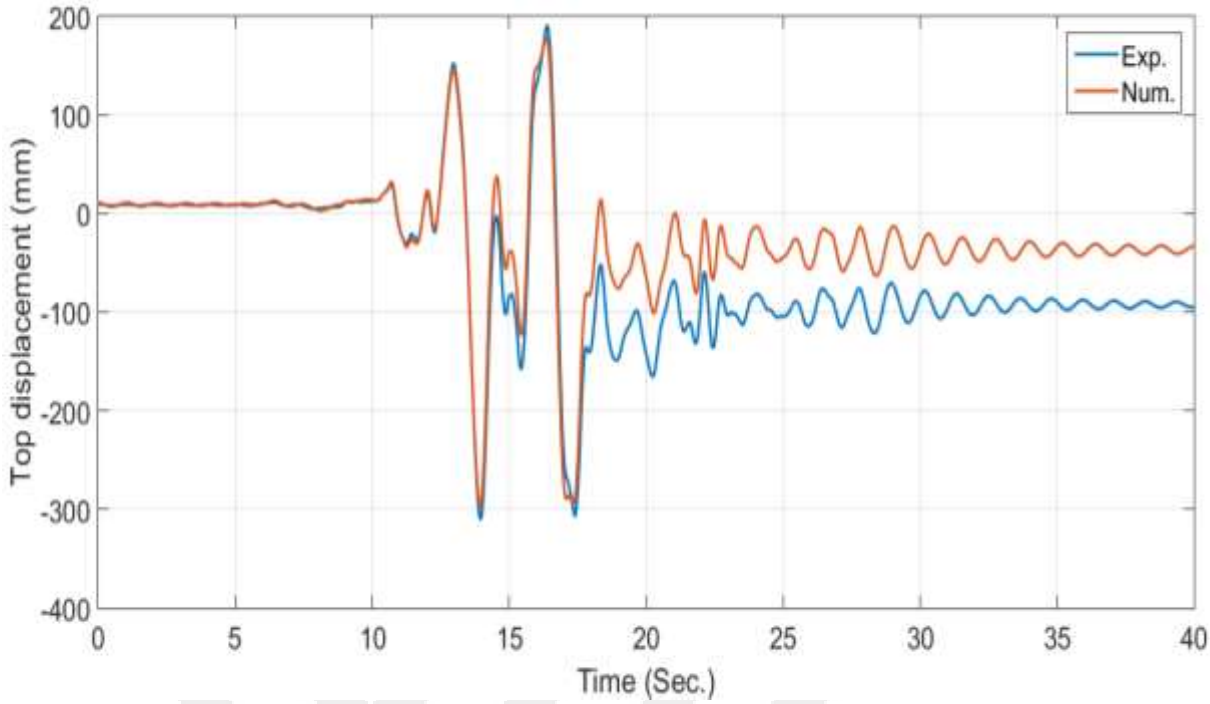

Figure 3.50. Top story displacement of numerical and experimental results for 30 MPa according to TS 500.

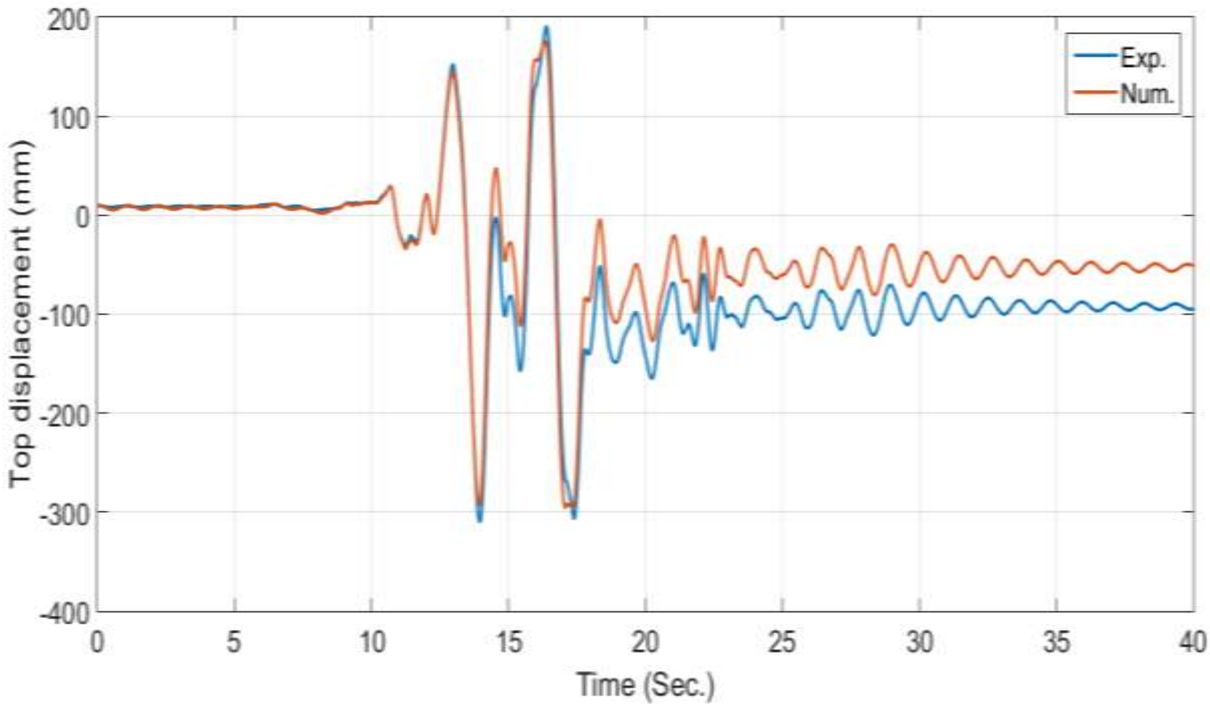

Figure 3.51. Top story displacement of numerical and experimental results for 32 MPa according to TS 500.

3.3.5.Comparison of Model-B according to TS 500

Top story displacement time history graphs of numerical and experimental results for Case-1, Case-2, Case-3, Case-4, Case-5 and Case-6 according to TS 500 are shown in Figure 3.52-Figure 3.57. Differences between displacements obtained from experimental and numerical results were determined and mean of the differences were given in Table 3.29. Mean differences between experimental and the Case-1, Case-2, Case-3, Case-4, Case-5, Case-6 numerical solutions are 2.82%, 3.42%, 4.57%, 4.59%, 5.20% and 4.39%, respectively. Minimum displacement difference is obtained for Case-1 solution.

Table 3.29. Comparison maximum top displacement obtained from Model-B according to TS 500 and from experiment tests.

f_c (MPa)	Difference %				Mean Difference %
	Point-1	Point-2	Point-3	Point-4	
25	1.8	0.5	3.7	5.3	2.82
26	3.0	2.0	1.2	7.5	3.42
27	5.1	3.4	3.1	6.8	4.57
28	5.3	3.7	3.5	5.9	4.59
29	5.3	4.3	3.0	5.2	5.20
30	5.6	5.0	2.3	4.7	4.39

Table 3.30. Comparison of material properties obtained from Model-A according to TS 500 by using reverse engineering and from experiment test.

	Compressive Strength (MPa)	Elasticity Modulus (MPa)
Reverse Engineering	28	30250
Laboratory Test Results	30	24000
Difference	16.7 %	26.0%

Differences between experimental and numerical result of C28 concrete class for compressive strength and elasticity modulus of concrete are 16.7% and 26.0%, respectively Table 3.30. The Force Based Fiber Element Method with regard to compressive strength of concrete is better than Displacement Based Fiber Element Method. The Displacement Based Fiber Element Method with regard to elasticity modulus of concrete is also given good result.

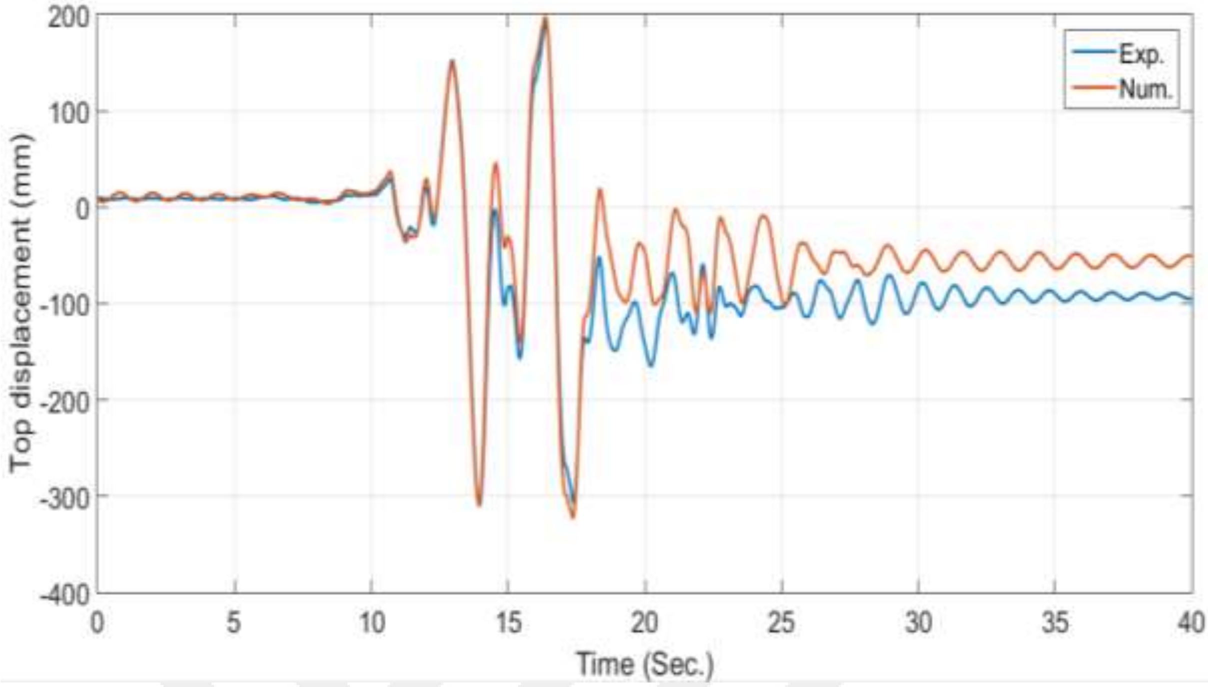

Figure 3.52. Top story displacement of numerical and experimental results for 25 MPa according to TS 500.

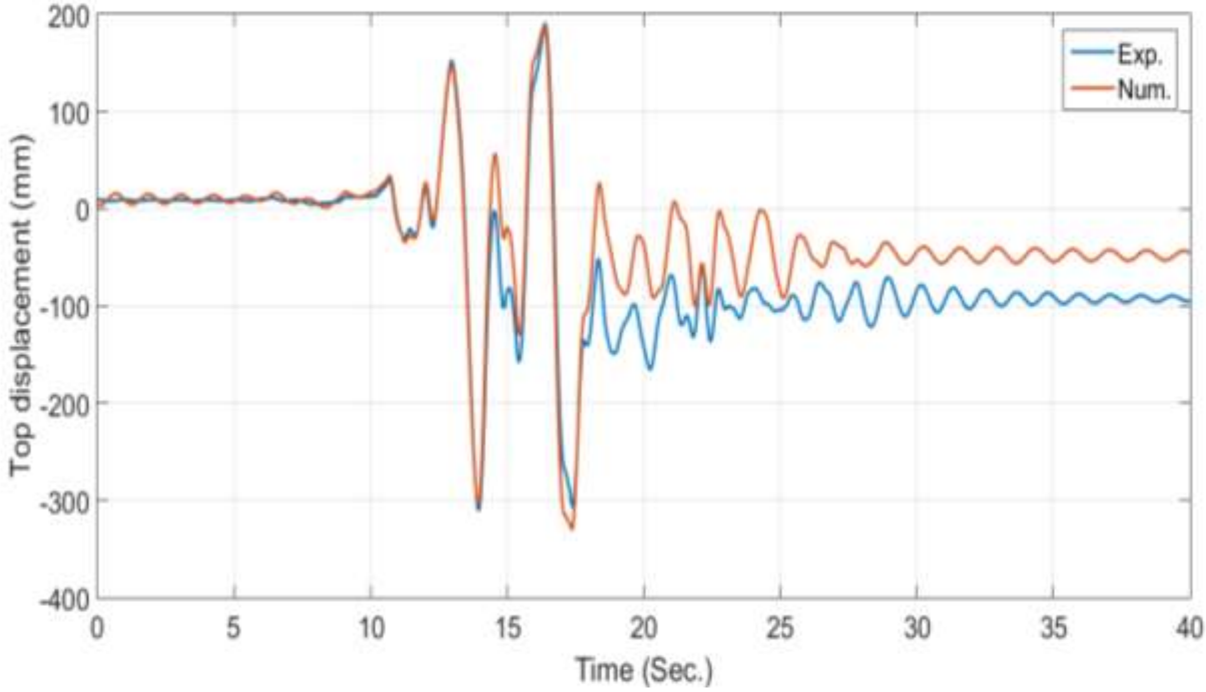

Figure 3.53. Top story displacement of numerical and experimental results for 26 MPa according to TS 500.

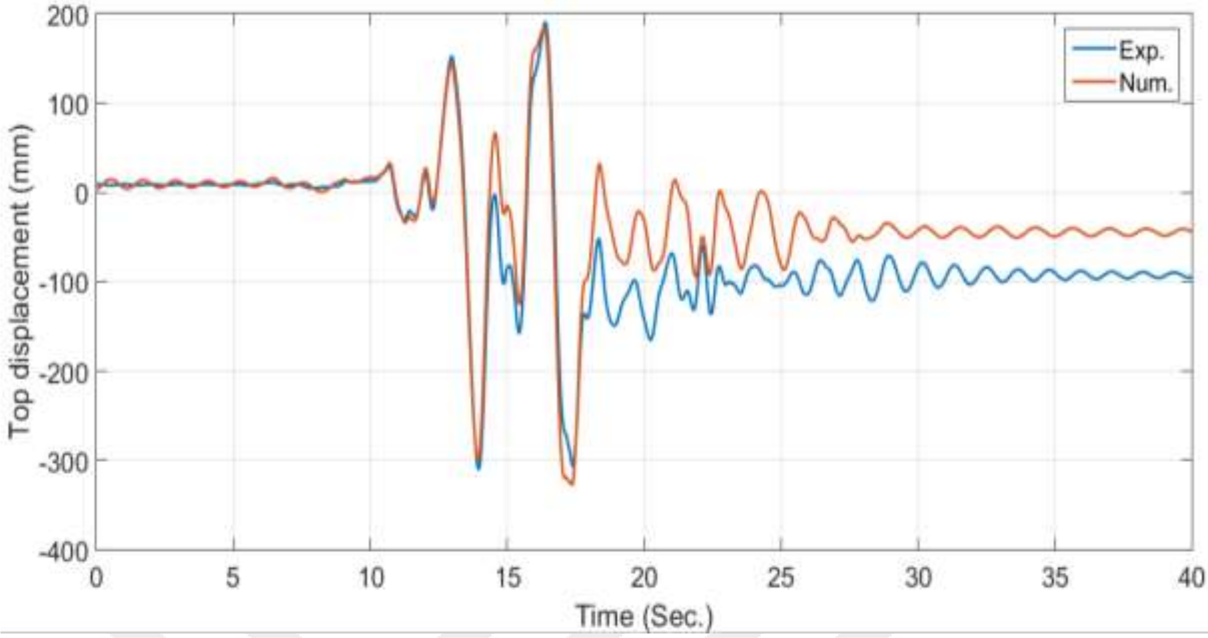

Figure 3.54. Top story displacement of numerical and experimental results for 27 MPa according to T.S-500.

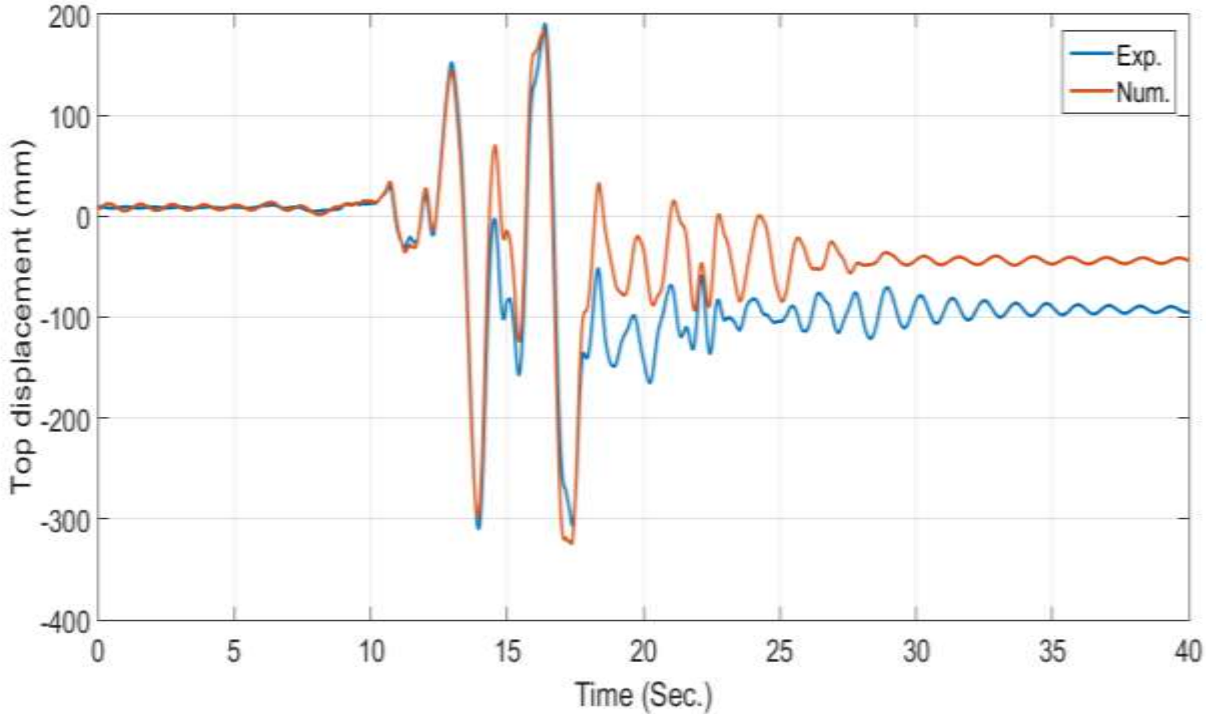

Figure 3.55. Top story displacement of numerical and experimental results for 28 MPa according to TS 500.

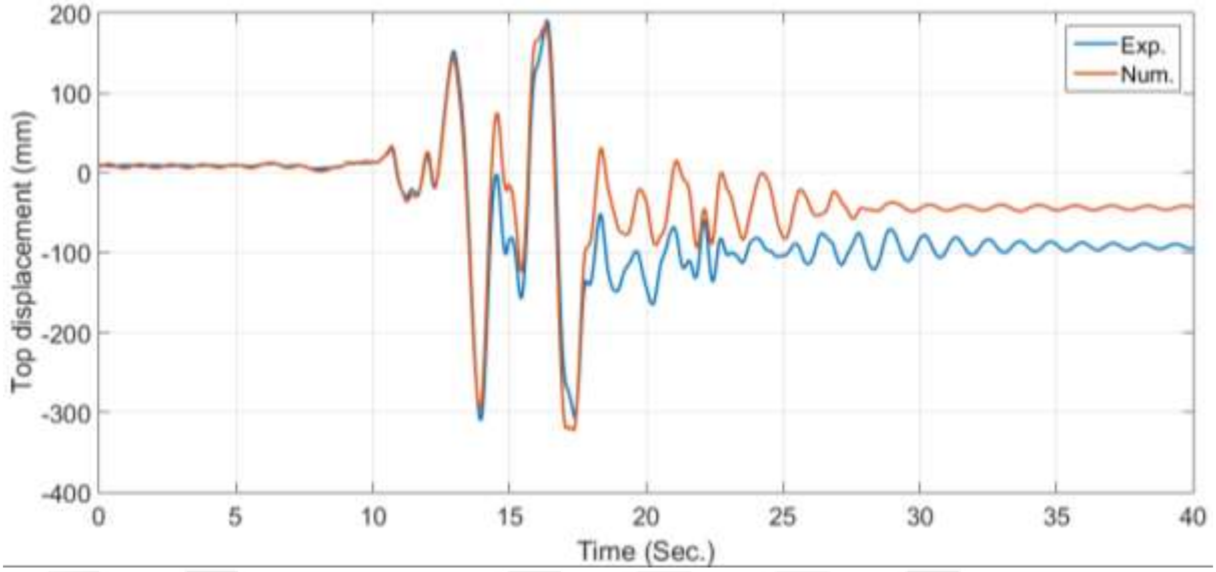

Figure 3.56. Top story displacement of numerical and experimental results for 29MPa according to TS 500.

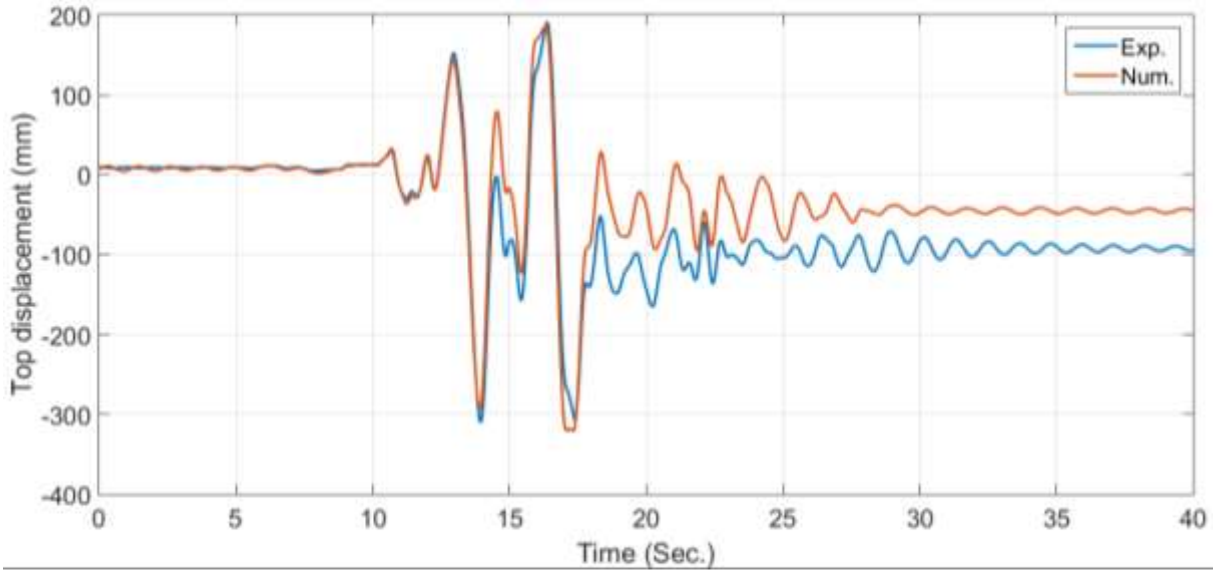

Figure 3.57. Top story displacement of numerical and experimental results for 30 MPa according to TS 500.

3.3.6.Comparison of Damage Regions

Schoettler et al. [2] indicated that after the 3rd earthquake acceleration loading, significant cracking developed at the base of the bridge pier and spalling at pier concrete occurred Figure 3.58. Severe damage regions at the base of the bridge pier were obtained from the analysis results of all numerical modelling approaches. No significant difference between damaged regions determined from experimental and numerical results were observed.

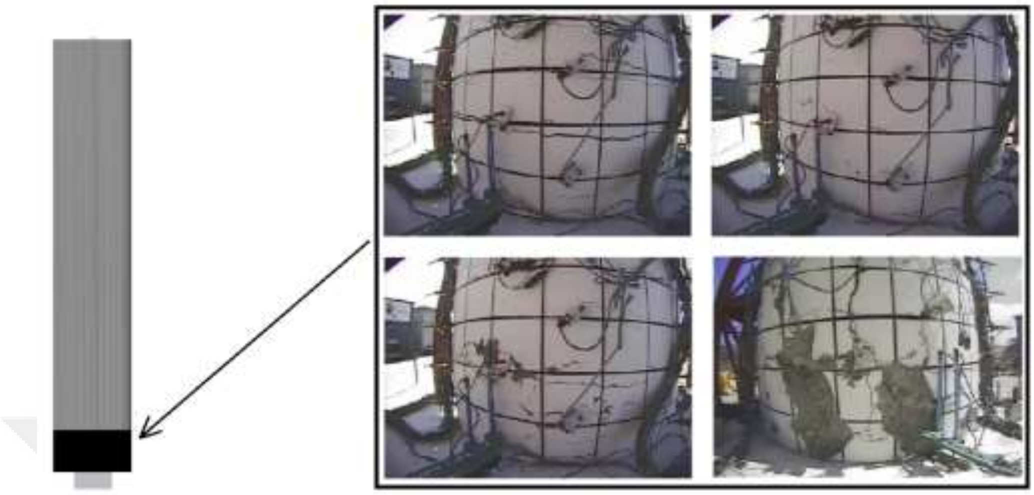

Figure 3.58. The damage regions at the base of the pier in different sides.

3.3.7.Fiber Element Number Effect on the Numerical Solution

In this subsection, the effect on numerical solution of fiber element number was investigated. In the numerical analyses, Case-3 for Model-A and Model-B according to ACI-318 were used. Four peak points of top displcement time history graph were selected for comparison of numerical and experimental results Figure 3.59, Figure 3.60. This comparison were given in Table 3.31 and Table 3.32. Each cross section was divided as 50, 75, 100, 150, 200, 250 and 350 fiber element number for the Model A. In this model, mean differences were determined as 8.01%, 3.39%, 1.66%, 1.59%, 2.37%, 2.45% and 2.65% for fiber element number 50, 75, 100, 150, 200, 250 and 350, respectively. Optimum fiber element number was obtained for 150.

Additional solutions were obtained for the Model B and each cross section was divided to 50, 100, 200, 250, 350, 400 and 500 fiber element number. In numerical results of the model, mean differences were determined as 6.21%, 3.27%, 3.19%, 2.91%, 3.0%, 3.16% and 3.19% for fiber element number 50, 100, 200, 250, 350, 400 and 500, respectively. Optimum difference was obtained as 2.91% for solution with 250 fiber element number.

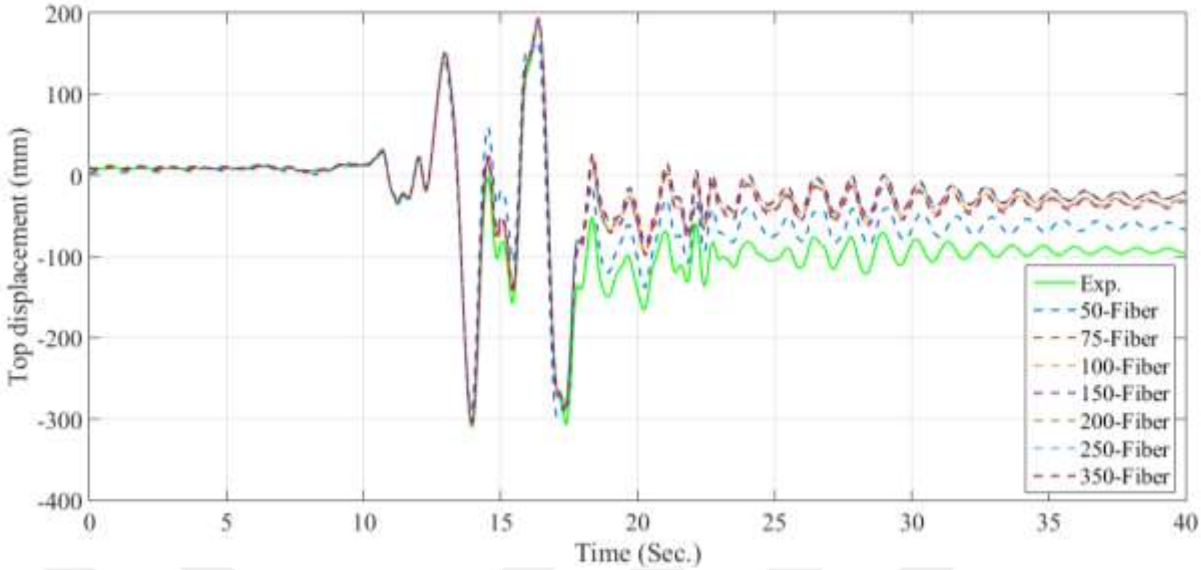

Figure 3.59. Numerical Model-A according to ACI-318, Case-3

Table 3.31. Comparison between experimental data and Model-A, Case-3

f_c (MPa)	Difference %				Mean Difference %
	Point-1	Point-2	Point-3	Point-4	
50-Fiber	5.8	7.7	15.4	3.1	8.01
75-Fiber	0.7	2.4	1.9	8.6	3.39
100-Fiber	0.1	0.6	0.8	5.2	1.66
150-Fiber	0.0	1.1	0.5	4.8	1.59
200-Fiber	0.4	1.6	0.7	6.8	2.37
250-Fiber	0.7	1.6	0.5	7.1	2.45
350-Fiber	0.4	1.5	1.0	7.7	2.65

Table 3.32. Comparison between experimental data and Model-B, Case-3

f_c (MPa)	Difference %				Mean Difference %
	Point-1	Point-2	Point-3	Point-4	
50-Fiber	6.9	7.3	4.5	6.2	6.21
100-Fiber	1.6	0.5	0.4	10.5	3.27
200-Fiber	2.2	0.5	0.4	9.7	3.19
250-Fiber	2.4	0.4	0.3	8.6	2.91
350-Fiber	2.4	0.5	0.4	8.7	3.0
400-Fiber	2.4	0.5	0.3	9.5	3.16
500-Fiber	2.4	0.5	0.4	9.5	3.19

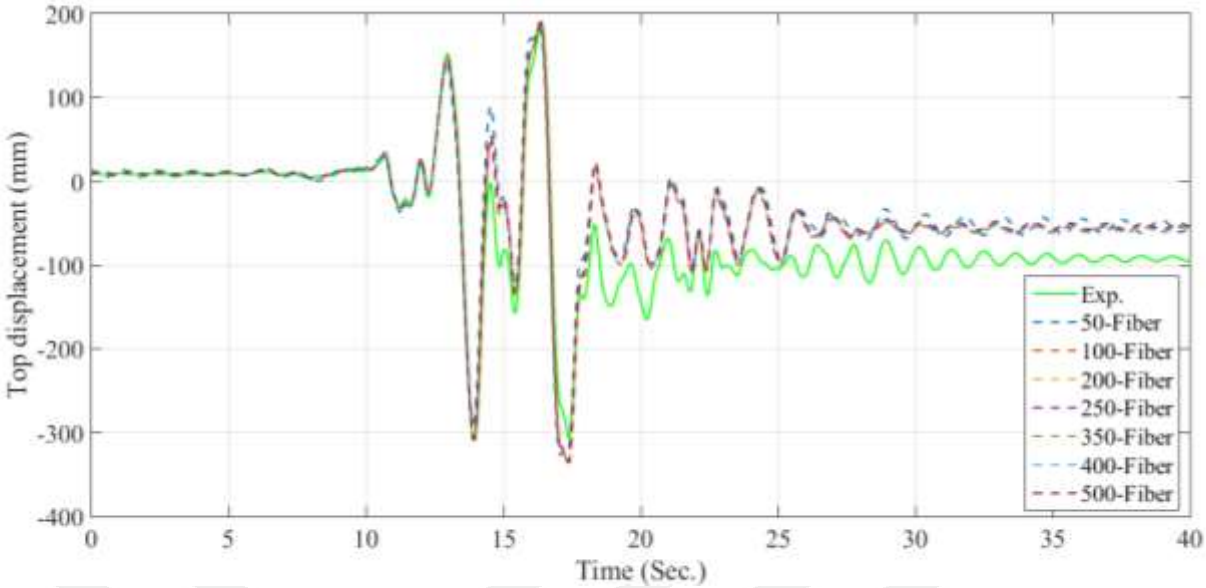

Figure 3.60. Numerical Model-B according to ACI-318, Case-3

4.CONCLUSION

In this thesis, in order to predict the actual characteristics of materials of collapsed or damaged reinforced concrete buildings induced by serious earthquakes, a novel reverse engineering technique is investigated. Two full-scale laboratory structures are used to verify the technique for this purpose. First structure is a two dimensional three bay and four story reinforced concrete bare frame that tested in European Laboratory for Structural Assessment (ELSA). Other structure is also reinforced concrete tall bridge pier that tested in Pacific Earthquake Engineering Research Center (PEER). The numerical solutions are obtained by using Fiber Element Approaches based on displacement and force. The material properties for the reinforced concrete elements are defined according to American Concrete Institute 318 code (ACI-318) and Turkish Standard 500 (TS 500) code. The comparisons are assessed from the experimental and numerical outcomes in terms of story displacement and damage zones. The material classes of the structures are determined by numerical solution the best compatible with experimental response. Finally, following conclusion can be drawn:

- It is observed that in comparison of material properties obtained from force based Fiber element approach according to ACI-318 with the ELSA test results by using reverse engineering, differences for compressive strength, tensile strength and elasticity modulus of concrete are determined as 1.84%, 17.1% and 0.92%, respectively. In the comparison of material properties obtained from displacement based Fiber element approach according to ACI-318 with the ELSA test results by using reverse engineering, differences for compressive strength, tensile strength and elasticity modulus of concrete are determined as 14.11%, 9.53% and 7.32%, respectively.
- It is determined that in comparison of material properties obtained from force based Fiber element approach according to TS 500 with the ELSA test results by using reverse engineering, differences for compressive strength, tensile strenght and elasticity modulus of concrete are determined as 1.84%, 26.3% and 42.3%, respectively. In the comparison of material properties obtained from displacement based Fiber element approach according to TS 500 with the ELSA test results by using reverse engineering, no agreements were observed for the differences between numerical and experimental results.

- Minimum differences between top displacement time history graph for force based and displacement based Fiber element approaches are obtained as 17.25% for solution with 600 fiber and as 11.26% for solution with 300 fiber, respectively, for the numerical Case-3 according to ACI-318.
- It is noted that in comparison of material properties obtained from force based Fiber element approach according to ACI-318 with the PEER test results by using reverse engineering, differences for compressive strength and elasticity modulus of concrete are determined as 0.0% and 7.2%, respectively. In the comparison of material properties obtained from displacement based Fiber element approach according to ACI-318 with the PEER test results by using reverse engineering, differences for compressive strength and elasticity modulus of concrete are determined as 10.0% and 1.76%, respectively.
- It is estimated that in comparison of material properties obtained from force based Fiber element approach according to TS 500 with the PEER test results by using reverse engineering, differences for compressive strength and elasticity modulus of concrete are determined as 6.7% and 29.9%, respectively. In comparison of material properties obtained from displacement based Fiber element approach according to TS 500 with the PEER test results by using reverse engineering, differences for compressive strength and elasticity modulus of concrete are determined as 16.7% and 26.0%, respectively.
- Minimum differences between top displacement time history graph for force based and displacement based Fiber element approaches are obtained as 1.59% for solution with 150 fiber and as 2.91% for solution with 250 fiber, respectively.
- Force based Fiber element method is given the better results than displacement based Fiber element methods according to numerical results.
- ACI-318 code results are better than the numerical results obtained from TS500 code.
- For the future study, the proposed reverse engineering method can be investigated according to design codes of different countries.

REFERENCES

[1]. Pinto, A., et al., *Pseudo-dynamic tests on non-seismic resisting RC frames (bare and selective retrofit frames).* EUR Report, 2002. **20244**.

[2]. Schoettler, M.J., et al., *A full-scale, single-column bridge bent tested by shake-table excitation.* Center for Civil Engineering Earthquake Research, Department of Civil Engineering, University of Nevada, 2012.

[3]. Abou-Elfath, H., *Simplified fiber beam-column model for inelastic analysis of moment-resisting steel frames.* Alexandria engineering journal, 2018. **57**(4): p. 2865-2877.

[4]. Chikofsky, E.J. and J.H. Cross, *Reverse engineering and design recovery: A taxonomy.* IEEE software, 1990. **7**(1): p. 13-17.

[5]. Otrokov, A., G. Khazanovich, and N. Afonina, *Engineering design technique development of continuous loading modules.* Procedia Engineering, 2015. **129**: p. 81-86.

[6]. Gao, H., et al., *Reverse analysis of scan strategies for controlled 3D laser forming of sheet metal.* Procedia Engineering, 2017. **183**: p. 369-374.

[7]. Ghosal, K., et al., *Electrospinning tissue engineering and wound dressing scaffolds from polymer–titanium dioxide nanocomposites.* Chemical Engineering Journal, 2018.

[8]. Li, D., et al., *Investigation methods for analysis of transient phenomena concerning design and operation of hydraulic-machine systems—A review.* Renewable and Sustainable Energy Reviews, 2019. **101**: p. 26-46.

[9]. Yeo, T.Y., J. Ashok, and S. Kawi, *Recent developments in sulphur-resilient catalytic systems for syngas production.* Renewable and Sustainable Energy Reviews, 2019. **100**: p. 52-70.

[10]. Mancas, C., *Should reverse engineering remain a computer science Cinderella.* J Inform Tech Soft Engg S, 2013. **5**: p. 2.

[11]. Yang, I.T., et al., *Reverse Engineering of a Bobsleigh Structure using LiDAR.* International Journal of Applied Engineering Research, 2017. **12**(6): p. 976-980.

[12]. Lee, M., et al., *A study on scan data matching for reverse engineering of pipes in plant construction.* KSCE Journal of Civil Engineering, 2017. **21**(6): p. 2027-2036.

[13]. Chiara, C. and P. Rui, *Seismic response of continuous span bridges through fiber-based finite element analysis.* Earthquake Engineering and Engineering Vibration, 2006. **5**(1): p. 119-131.

[14]. Karaton, M. and H. Awla, *Numerical investigation of the effect on ultimate loading capacity of different longitudinal reinforcement ratios of a RC portal frame.* Journal of Structural Engineering, 2018. **1**(3): p. 147-154.

[15]. Taucer, F., E. Spacone, and F.C. Filippou, *A fiber beam-column element for seismic response analysis of reinforced concrete structures*. Vol. 91. 1991: Earthquake Engineering Research Center, College of Engineering, University of California, Berkeley.

[16]. Brum, S. and J. Fernando, *A model for the non linear dynamic analysis of reinforced concrete and masonry framed structures*. 2010: Universitat Politecnica de Catalunya.

[17]. Papadopoulos, V. and M. Fragiadakis, *Plastic Hinge and Plastic Zone Seismic Analysis of Frames.* Encyclopedia of Earthquake Engineering, 2015: p. 1926-1933.

[18]. Clough, R.W. *Effect of stiffness degradation on earthquake ductility requirements*. in *Proceedings of Japan earthquake engineering symposium*. 1966.

[19]. Giberson, M.F., *The response of nonlinear multi-story structures subjected to earthquake excitation.* 1967.

[20]. TAKIZAWA, H., *Notes on some basic problems in inelastic analysis of planar R/C structures (part i).* Transactions of the Architectural Institute of Japan, 1976. **240**: p. 51-62.

[21]. Takeda, T., M.A. Sozen, and N.N. Nielsen, *Reinforced concrete response to simulated earthquakes.* Journal of the Structural Division, 1970. **96**(12): p. 2557-2573.

[22]. Brancaleoni, F., V. Ciampi, and R. Di Antonio. *Rate-type models for non linear hysteretic structural behavior*. in *EUROMECH colloquium*. 1983.

[23]. Clough, R.W. and K.L. Benuska, *Nonlinear earthquake behavior of tall buildings.* Journal of the Engineering Mechanics Division, 1967. **93**(3): p. 129-146.

[24]. Banon, H., H.M. Irvine, and J.M. Biggs, *Seismic damage in reinforced concrete frames.* Journal of the Structural Division, 1981. **107**(9): p. 1713-1729.

[25]. Filip, C. and I. Ahmad, *Nonlinear analysis of reinforced concrete frames under cyclic load reversals*. 1988.

[26]. Otani, S., *Inelastic analysis of R/C frame structures.* Journal of the Structural Division, 1974. **100**(Proc. Paper 10686).

[27]. Takayanagi, T. and W.C. Schnobrich, *Non-linear analysis of coupled wall systems.* Earthquake Engineering & Structural Dynamics, 1979. **7**(1): p. 1-22.

[28]. Charney, F.A. and V.V. Bertero, *An evaluation of the design and analytical seismic response of a seven-story reinforced concrete frame-wall structure.* NASA STI/Recon Technical Report N, 1982. **83**.

[29]. Bertero, V., et al., *Earthquake simulator tests and associated experimental, analytical, and correlation studies of one-fifth scale model.* Special Publication, 1984. **84**: p. 375-424.

[30]. Fedak, L.K. *Evaluation of plastic hinge models and inelastic analysis tools for performance-based seismic design of RC bridge columns*. in *Masters Abstracts International*. 2012.

[31]. Hines, E.M., *Seismic performance of hollow rectangular reinforced concrete bridge piers with confined corner elements.* 2003.

[32]. Lai, S.-S., G.T. Will, and S. Otani, *Model for inelastic biaxial bending of concrete members.* Journal of structural engineering, 1984. **110**(11): p. 2563-2584.

[33]. Spacone, E. and S. El-Tawil, *Nonlinear analysis of steel-concrete composite structures: State of the art.* Journal of Structural Engineering, 2004. **130**(2): p. 159-168.

[34]. Soleimani, D., E.P. Popov, and V.V. Bertero. *Nonlinear beam model for R/C frame analysis*. in *Electronic computation*. 1979. ASCE.

[35]. Meyer, C., M.S. Roufaiel, and S.G. Arzoumanidis, *Analysis of damaged concrete frames for cyclic loads.* Earthquake Engineering & Structural Dynamics, 1983. **11**(2): p. 207-228.

[36]. Roufaiel, M.S. and C. Meyer, *Analytical modeling of hysteretic behavior of R/C frames.* Journal of Structural Engineering, 1987. **113**(3): p. 429-444.

[37]. Darvall, P.L. and P.A. Mendis, *Elastic-plastic-softening analysis of plane frames.* Journal of Structural Engineering, 1985. **111**(4): p. 871-888.

[38]. Kang, Y.-J. and A.C. Scordelis, *Nonlinear analysis of prestressed concrete frames.* Journal of the structural division, 1980. **106**(ASCE 15191).

[39]. Mahasuverachai, M. and G.H. Powell, *Inelastic analysis of piping and tubular structures*. 1982: Earthquake Engineering Research Center, University of California.
[40]. Chan, E.C., *NONLINEAR GEOMETRIC, MATERIAL AND TIME DEPENDENT ANALYSIS OF REINFORCED CONCRETE SHELLS WITH EDGE BEAMS.* 1984.
[41]. Kaba, S.A. and S.A. Mahin, *Refined modelling of reinforced concrete columns for seismic analysis*. 1984: University of California, Earthquake Engineering Research Center.
[42]. Mari, A.R., *Nonlinear geometric, material and time dependent analysis of three dimensional reinforced and prestressed concrete frames*. 1984: Department of Civil Engineering, University of California.
[43]. Zeris, C.A. and S.A. Mahin, *Analysis of reinforced concrete beam-columns under uniaxial excitation.* Journal of structural engineering, 1988. **114**(4): p. 804-820.
[44]. Ulm, F.-J., J.-L. Clément, and J. Guggenberger. *Recent advances in 3D non-linear FE-analysis of R/C and P/C Beam Structures*. in *Structures Congress XII*. 1994. ASCE.
[45]. Spacone, E., F.C. Filippou, and F.F. Taucer, *Fibre beam–column model for non-linear analysis of R/C frames: Part I. Formulation.* Earthquake Engineering & Structural Dynamics, 1996. **25**(7): p. 711-725.
[46]. Petrangeli, M. and V. Ciampi, *Equilibrium based iterative solutions for the non-linear beam problem.* International Journal for Numerical Methods in Engineering, 1997. **40**(3): p. 423-437.
[47]. Karaton, M., *Nonlinear earthquake analysis of reinforced concrete frames with fiber and bernoulli-euler beam-column element.* The Scientific World Journal, 2014. **2014**.
[48]. Karaton, M., *Comparisons of Elasto-Fiber and Fiber & Bernoulli-Euler reinforced concrete beam-column elements.* Structural Engineering and Mechanics, 2014. **51**(1): p. 89-110.
[49]. Guedes, J. and A. Pinto. *A numerical model for shear dominated bridge piers*. in *Proc. of the second Italian-Japan Workshop on seismic design and retrofit of bridges*. 1997.
[50]. RANZO, G. and M. PETRANGELI, *A fibre finite beam element with section shear modelling for seismic analysis of RC structures.* Journal of earthquake engineering, 1998. **2**(03): p. 443-473.
[51]. Petrangeli, M., *Fiber element for cyclic bending and shear of RC structures. II: Verification.* Journal of engineering mechanics, 1999. **125**(9): p. 1002-1009.
[52]. Petrangeli, M., P.E. Pinto, and V. Ciampi, *Fiber element for cyclic bending and shear of RC structures. I: Theory.* Journal of Engineering Mechanics, 1999. **125**(9): p. 994-1001.
[53]. Martinelli, L. *The behavior of reinforced concrete piers under strong seismic actions*. in *Proceedings of the Twelfth Word Conference on Earthquake Engineering Auckland, New Zealand*. 2000.
[54]. Martinelli, L. *Numerical simulation of cyclic tests of R/C shear walls*. in *The Twelfth European Conference on Earthquake Engineering (12th ECEE)*. 2002.
[55]. Remino, M. and U.d.s.d. Trento, *Shear Modeling of Reinforced Concrete Structures*. 2004.
[56]. Kotronis, P. and J. Mazars, *Simplified modelling strategies to simulate the dynamic behaviour of R/C walls.* Journal of Earthquake Engineering, 2005. **9**(02): p. 285-306.

[57]. Marini, A. and E. Spacone, *Analysis of reinforced concrete elements including shear effects.* ACI Structural Journal, 2006. **103**(5): p. 645.
[58]. Gregori, J.N., et al., *A 3D numerical model for reinforced and prestressed concrete elements subjected to combined axial, bending, shear and torsion loading.* Engineering Structures, 2007. **29**(12): p. 3404-3419.
[59]. Pinho, R., *Nonlinear dynamic analysis of structures subjected to seismic action*, in *Advanced earthquake engineering analysis*. 2007, Springer. p. 63-89.
[60]. Menegotto, M. *Method of analysis for cyclically loaded RC plane frames including changes in geometry and non-elastic behavior of elements under combined normal force and bending*. in *Proc. of IABSE symposium on resistance and ultimate deformability of structures acted on by well defined repeated loads*. 1973.
[61]. Monti, G. and C. Nuti, *Nonlinear cyclic behavior of reinforcing bars including buckling.* Journal of Structural Engineering, 1992. **118**(12): p. 3268-3284.
[62]. Bunni, N., et al., *Stress-strain behavior of concrete confined by overlapping hoops at low and high-strain rates-discussion.* Journal of the American Concrete Institute, 1982. **79**(6): p. 496-498.
[63]. Mander, J.B., M.J. Priestley, and R. Park, *Theoretical stress-strain model for confined concrete.* Journal of structural engineering, 1988. **114**(8): p. 1804-1826.
[64]. Zeris, C.A. and S.A. Mahin, *Behavior of reinforced concrete structures subjected to biaxial excitation.* Journal of structural engineering, 1991. **117**(9): p. 2657-2673.
[65]. Mullapudi, R.S., A. Ayoub, and A. Belarbi. *A fiber beam element with axial, bending and shear interaction for seismic analysis of RC structures*. in *Proceedings of the 14th World Conference on Earthquake Engineering*. 2008.
[66]. Ceresa, P., et al., *A fibre flexure–shear model for seismic analysis of RC-framed structures.* Earthquake Engineering & Structural Dynamics, 2009. **38**(5): p. 565-586.
[67]. Neuenhofer, A. and F.C. Filippou, *Evaluation of nonlinear frame finite-element models.* Journal of structural engineering, 1997. **123**(7): p. 958-966.
[68]. Bazant, Z.P. and P.D. Bhat, *Prediction of hysteresis of reinforced concrete members.* ASCE J STRUCT DIV, 1977. **103**(1): p. 153-167.
[69]. Menegotto, M. and P.E. Pinto, *Slender RC compressed members in biaxial bending.* Journal of the Structural Division, 1977. **103**(3).
[70]. Hellesland, J. and A. Scordelis. *Analysis of RC bridge columns under imposed deformations*. in *IABSE colloquium*. 1981. Delft the Netherlands.
[71]. Sinha, B., K.H. Gerstle, and L.G. Tulin. *Stress-strain relations for concrete under cyclic loading*. in *Journal Proceedings*. 1964.
[72]. Karsan, I.D. and J.O. Jirsa, *Behavior of concrete under compressive loadings.* Journal of the Structural Division, 1969.
[73]. Yankelevsky, D.Z. and H.W. Reinhardt, *Model for cyclic compressive behavior of concrete.* Journal of Structural Engineering, 1987. **113**(2): p. 228-240.
[74]. Popovics, S. *A review of stress-strain relationships for concrete*. in *Journal Proceedings*. 1970.
[75]. Martínez-Rueda, J.E. and A.S. Elnashai, *Confined concrete model under cyclic load.* Materials and structures, 1997. **30**(3): p. 139-147.
[76]. Chang, G. and J.B. Mander, *Seismic energy based fatigue damage analysis of bridge columns: part 1-evaluation of seismic capacity.* 1994.
[77]. Bahn, B.Y. and C.-T.T. Hsu, *Stress-strain behavior of concrete under cyclic loading.* ACI Materials Journal, 1998. **95**: p. 178-193.

[78]. Palermo, D. and F.J. Vecchio, *Compression field modeling of reinforced concrete subjected to reversed loading: formulation.* Structural Journal, 2003. **100**(5): p. 616-625.
[79]. Sakai, J. and K. Kawashima. *An unloading and reloading stress-strain model for concrete confined by tie reinforcements*. in *Proc. 12th WCEE*. 2000.
[80]. Sakai, J.-i., K. Kawashima, and G. Shoji, *A stress-strain model for unloading and reloading of concrete confined by tie reinforcement.* Doboku Gakkai Ronbunshu, 2000. **2000**(654): p. 297-316.
[81]. Sakai, J. and K. Kawashima, *Unloading and reloading stress–strain model for confined concrete.* Journal of Structural Engineering, 2006. **132**(1): p. 112-122.
[82]. Park, R., D.C. Kent, and R.A. Sampson, *Reinforced concrete members with cyclic loading.* Journal of the Structural Division, 1972. **98**(st 7).
[83]. Aktan, A.E., B. Karlsson, and M.A. Sozen, *Stress-strain relationships of reinforcing bars subjected to large strain reversals*. 1973, University of Illinois Engineering Experiment Station. College of ….
[84]. Ma, S.Y.M., V.V. Bertero, and E.P. Popov, *Experimental and analytical studies on the hysteretic behavior of reinforced concrete rectangular and T-beams*. 1976: University of California Berkeley, CA.
[85]. Stanton, J.F. and H.D. McNiven, *The development of a mathematical model to predict the flexural response of reinforced concrete beams to cyclic loads, using system identification*. 1979, University of California, Earthquake Engineering Research Center.
[86]. Filippou, F.C., V.V. Bertero, and E.P. Popov, *Effects of bond deterioration on hysteretic behavior of reinforced concrete joints.* 1983.
[87]. Hoehler, M.S. and J.F. Stanton, *Simple phenomenological model for reinforcing steel under arbitrary load.* Journal of Structural Engineering, 2006. **132**(7): p. 1061-1069.
[88]. Mohd, Y.M., *Nonlinear analysis of prestressed concrete structures under monotonic and cyclic loads.* 1995.

CURRICULUM VITAE

Name	**:** Halmat Ahmed Awla
Nationality	**:** Iraqi
Date of birth	**:** March 10, 1987
Place of Birth	**:** Erbil, Iraq
Gender	**:** Male
Marital Status	**:** Married
Email Address	**:** halmat.awlla@epu.edu.iq
	: halmat.eng87@gmail.com
Phone No.	**:** +9647504725378